NAWCWD TM 8757

LX-10 Explosive Damage Studies

by
A. I. Atwood, I. Purifoy, C. J. Wheeler, E. Woods
Energetics Research Division
Weapons and Energetics Department

MARCH 2015

NAVAL AIR WARFARE CENTER WEAPONS DIVISION
CHINA LAKE, CA 93555-6001

FOREWORD

This report describes a study conducted by the Combustion Sciences Branch to generate and examine the mechanical damage of LX-10 explosive. The study, conducted from May through October 2014, includes a comparison of LX-10 and Composition B explosives. The testing included closed bomb combustion and dry screening of the damaged LX-10 samples and gauged the damage vulnerability of the energetic material to mechanical insult. The work was funded by the Lawrence Livermore National Laboratory. The screened size fractions of the damaged spherical LX-10 samples will be further studied at Lawrence Livermore National Laboratory.

This report was reviewed by the authors for technical accuracy. The findings of this study are preliminary in nature and the report is released at the working level.

J. DAVIS, *Head*
Energetics Research Division
Weapons and Energetics Department
3 March 2015

NAWCWD TM 8757, published by Code 4G0000D,
9 paper, 10 electronic media.

REPORT DOCUMENTATION PAGE

Form Approved
OMB No. 0704-0188

1. REPORT DATE *(DD-MM-YYYY)*	2. REPORT TYPE	3. DATES COVERED (From - To)
03-03-2015	Preliminary Report	1 June – 30 October 2014

4. TITLE AND SUBTITLE
LX-10 Explosive Damage Studies (U)

5a. CONTRACT NUMBER
N/A

5b. GRANT NUMBER
N/A

5c. PROGRAM ELEMENT NUMBER
N/A

6. AUTHOR(S)
A.I. Atwood, I. Purifoy, C. J. Wheeler, E. Woods

5d. PROJECT NUMBER
N/A

5e. TASK NUMBER
N/A

5f. WORK UNIT NUMBER
N/A

7. PERFORMING ORGANIZATION NAME(S) AND ADDRESS(ES)
Naval Air Warfare Center Weapons Division
1 Administration Circle
China Lake, CA 93555-6100

8. PERFORMING ORGANIZATION REPORT NUMBER
NAWCWD TM 8757

9. SPONSORING/MONITORING AGENCY NAME(S) AND ADDRESS(ES)
N/A

10. SPONSOR/MONITOR'S ACRONYM(S)
N/A

11. SPONSOR/MONITOR'S REPORT NUMBER(S)
N/A

12. DISTRIBUTION/AVAILABILITY STATEMENT
DISTRIBUTION STATEMENT A. Approved for public release.

13. SUPPLEMENTARY NOTES
None.

14. ABSTRACT

(U) Cylindrical and spherical explosive geometries were damaged using an 18-millimeter (mm) smooth bore gun. Burning rates of the undamaged LX-10 sample were determined and used to evaluate the change in burn area ratio of the cylindrical samples using the closed bomb. The recovered spherical debris was dry screened with the majority of the sample distribution resulting in fragments in the two coarsest size fractions. The individual size fractions of the explosive were returned to Lawrence Livermore National Laboratory for further analysis.

15. SUBJECT TERMS
CompB, Composition B, cylinders, energetic materials, explosive, LX-10, melt cast, pressed, shotgun/friability testing, spheres

16. SECURITY CLASSIFICATION OF:			17. LIMITATION OF ABSTRACT	18. NUMBER OF PAGES	19a. NAME OF RESPONSIBLE PERSON
a. REPORT	b. ABSTRACT	c. THIS PAGE			Alice Atwood
UNCLASSIFIED	UNCLASSIFIED	UNCLASSIFIED	SAR	128	19b. TELEPHONE NUMBER *(include area code)* (760) 939-0203

CONTENTS

Background 3
Objective 3
Approach 3
Experiment 4
Shotgun 4
Closed Bomb 5
Particle Size Analysis 6
Samples 7
Results 11
Part I – Cylinder 11
Part II – Spheres 16
Summary/Conclusions 27
Cylindrical LX-10 27
Spherical LX-10 27
Further Study 27
References 28

Appendixes:
A. Cylindrical and Spherical LX-10 Samples A-1
B. Cylindrical and Spherical Impact Damaged LX-10 Samples B-1
C. Characterization of Explosive Brittle Fracture/Composition B Burning Rate Studies C-1

Figures:
1. Schematic of the 18-mm Impact Device Used for the CompB Friability Study 4
2. Schematic of the Closed Bomb Data Acquisition System 5
3. Typical Cylindrical LX-10 Friability Sample (mm scale divisions) 10
4. Spherical LX-10 Sample (mm scale) 10
5. 18-mm Arrangement for the LX-10 Friability Samples 11
6. LX-10 Burning Rates Compared to CompB 12
7. Percent Recovered Versus Impact Velocity for Cylindrical Samples 13
8. Cylindrical LX-10 Sample Impact Damaged at 121 ft/s 13

9. Cylindrical LX-10 Sample Impact Damaged at 385 ft/s 14
10. Maximum dp/dt Versus Impact Velocity 14
11. Maximum Burn Area Ratio Versus Impact Velocity for LX-10 Cylinders 15
12. Particle Size Distribution of LX-10 Damaged Cylinders 16
13. Spherical LX-10 Sample Recovered Versus Impact Velocity 16
14. Size Fractions for Spherical LX-10 Samples Impact Damaged at Less Than 200 ft/s 17
15. Spherical LX-10 Sample Impact Damaged at 132 ft/s 18
16. Size Fractions for Spherical CompB Samples Impact Damaged Between 222 and 294 ft/s 18
17. Spherical LX-10 Sample Impact Damaged at 294 ft/s 19
18. Size Fractions for Spherical LX-10 Samples Impact Damaged Between 312 and 416 ft/s 19
19. Spherical LX-10 Sample Impact Damaged at 416 ft/s 20
20. Size Fractions for Spherical LX-10 Samples Impact Damaged Between 434 and 500 ft/s 20
21. Spherical LX-10 Sample Impact Damaged at 435 ft/s 21
22. A Comparison of Spherical LX-10 Samples Impact Damaged at 178 ft/s 21
23. A Comparison of Spherical LX-10 Samples Impact Damaged at 222 ft/s 22
24. A Comparison of Spherical LX-10 Samples Impact Damaged at 416 ft/s 22
25. A Comparison of Spherical LX-10 Samples Impact Damaged at 434 and 435 ft/s 23
26. A Comparison of Impact Damage for Two Explosive Geometries 23
27. A Comparison of Impact Damage for Two Explosive Geometries 24
28. A Comparison of Impact Damage for Two Explosive Geometries 24
29. A Comparison of Impact Damage for Two Explosive Geometries 25
30. A Comparison of Impact Damage for Two Explosive Geometries 25
31. Change in Diameter Greater Than 3,360 μm Size Fraction 26
32. Change in Fine Particles Less Than 106 μm Size Fraction 26

Tables:

1. Undamaged Cylinder Data 8
2. Spherical LX-10 Sample Data 9

BACKGROUND

Shotgun/friability testing is used to examine the damage vulnerability of an energetic material to mechanical insult. The test is used in the evaluation of deflagration-to-detonation transition (DDT) potential (Reference 1) and in hazard classification testing (Reference 2).

Shotgun testing in the United States was originally designed to evaluate the damage thresholds of viscoelastic propellants and their potential to DDT. The test has been used to determine the surface area increase as a function of impact velocity in these materials. Shotgun testing has been extended to the evaluation of explosive formulations more recently (Reference 3).

The successful modeling of mechanically induced brittle fracture is currently under investigation at Lawrence Livermore National Laboratory (LLNL), and this effort will provide data to support the ongoing studies to understand impact fracture and fragmentation.

OBJECTIVE

The objective of this study was to generate and examine the mechanical damage of LX-10 explosive in two geometric configurations for LLNL and to compare the results to those of Composition B (CompB) from an earlier study (Reference 4). The effort was designed to gain insight into the mechanisms of brittle fracture resulting from mechanical insult to the explosive and to provide validation data for ongoing fracture models under development.

APPROACH

This study included a two-part approach and tested cylindrical and spherical LX-10 explosive samples.

Part I of the study was to perform traditional shotgun/friability testing with 18-mm-diameter cylindrical LX-10 samples. The samples were fired from a smooth bore, 18-mm gun against a steel target at various velocities. The resulting debris was

collected and fired in a manometric closed vessel. The pressure-time history was recorded, and an analysis of the data was performed to evaluate both the maximum pressurization rate (dp/dt) and burn area increase as a function of impact velocity.

Part II of the study was performed with 18-mm-diameter spherical LX-10 explosive samples that were again fired from the 18-mm gun at various velocities. The resulting debris was dry screened into size fractions from 3,360 to 106 μm. Selections of damaged LX-10 cylindrical samples were also dry screened then recombined and fired as in Part 1. The damaged spherical samples were returned to LLNL for further study at that facility.

EXPERIMENT

SHOTGUN

A schematic of the Naval Air Warfare Center Weapons Division (NAWCWD) 18-mm high velocity impact device is shown in Figure 1. The device was designed and built by Safety Management Services. The breach of the gun barrel was designed to operate with either powder or gas-driven actuation. The 18-mm barrel was fired using nitrogen in this study. The device incorporates a 2.3-liter accumulator tank with an air actuated ball valve. This enables the operator to vary the propulsion gas pressure and thus the velocity of the explosive sample. Impact velocities of 111 to 500 ft/s (27.13 to 132.59 m/s) were achieved in this study.

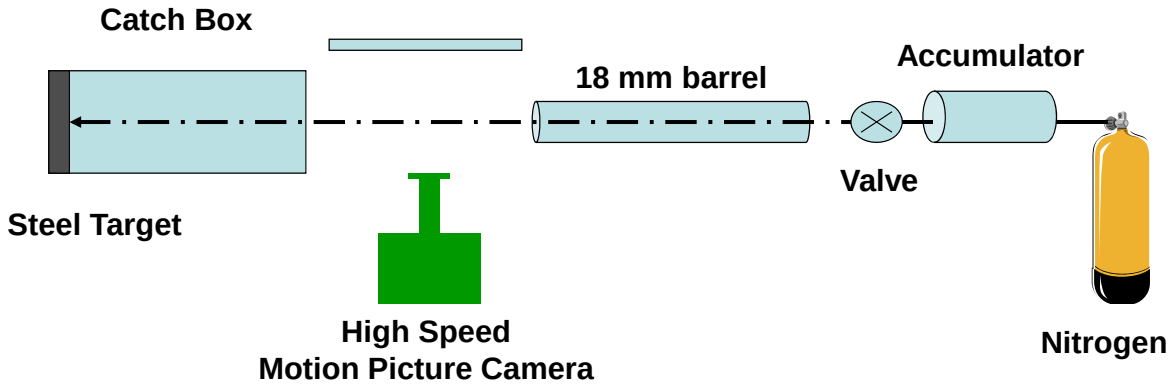

FIGURE 1. Schematic of the 18-mm Impact Device Used for the CompB Friability Study.

CLOSED BOMB

A 200 cm^3 Harwood Engineering powder bomb was sleeved to a volume of 108 cm^3 for this study. Ignition of the sample was by means of a Reynolds air bag squib firing into approximately 1.0 gram of DuPont PB smokeless powder acting as the ignition aid. The squib and aid were packaged in a silk bag, and the entire ignition unit was similarly bagged with the LX-10 samples.

A schematic of the closed bomb data acquisition system is shown in Figure 2. Pressure-time data were acquired using a Kistler model 607C4 pressure transducer. The amplified pressure signal was digitized and recorded on a Nicolet Multipro digital data acquisition system. The pressure-time records obtained from the digital oscilloscope were processed to remove wild points, smoothed using a parametric spline, and differentiated (Reference 5).

It was noted that the number of segments selected in the smoothing process had an effect on the maximum dp/dt determined from the shot. The number of segments selected for the parametric spline was varied until the resulting value of maximum dp/dt did not vary more than five percent to maintain a constant smoothing contribution.

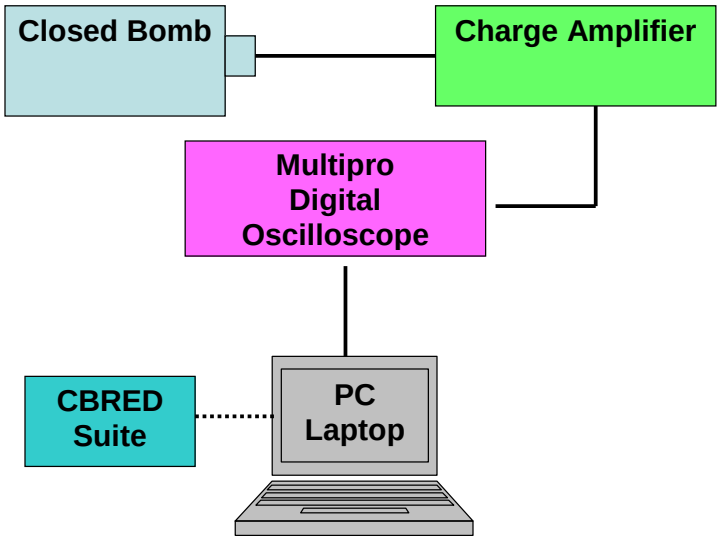

FIGURE 2. Schematic of the Closed Bomb Data Acquisition System.

The Closed Bomb Data Reduction Program (CBRED) II was used to reduce the closed bomb data obtained in this study (Reference 6). Closed bomb reduction transforms a measured pressure-time history into a mass regression rate through application of an equation of state. The CBRED II code used the Noble-Abel co-volume equation of state (Equation 1):

$$P(V_s - nw_e) = w_pF \quad (1)$$

where

P = System pressure
V_s = System volume
n = Covolume
w_e = Weight of explosive burned
F = Impetus, f(temperature, molecular weight)
w_p = Initial weight of explosive

The measured pressure-time history from a closed bomb firing is converted to a mass regression rate based on thermochemistry, as determined from a thermochemical equilibrium code (BLAKE in this study) (Reference 7). The mass burning rate ($\dot{m}$) of an energetic is the product of the surface area (A_b), the sample density (ρ), and the linear burning rate (r) (Equation 2).

$$\dot{m} = \rho r A_b \tag{2}$$

The density and initial burn area are known or calculated for the undamaged sample, and the linear burning rate as a function of pressure can be determined. Once the linear burning rate has been determined for a formulation, it can then be used as input into the CBRED II program for the damaged sample evaluation. The pressure-time history for the closed bomb firing of the damaged sample is again converted to mass burning rate-time in the program. Referring again to Equation 2 for the damaged sample, the density (assumed to be unchanged) and linear burning rate are known, and the burn area as a function of time and distance burned can be determined. The surface-to-volume ratio (S/V) of the damaged sample can also be calculated from the burn area data by multiplying the original S/V of the sample by the maximum burn area ratio.

The discussion above indicates that the closed bomb analysis relies on a sample with good combustion properties. Equilibrium thermochemistry is employed and gaseous combustion products are assumed for the optimal application of the analysis. Sample integrity (no flaws from manufacturing or deconsolidation during combustion) and uniformity are key to optimal data reduction.

PARTICLE SIZE ANALYSIS

The recovered damaged spherical samples and five of the cylindrical samples were dry screened to obtain an understanding of the particle size distribution of the fragments as a function of impact velocity. The damaged samples were dry screened from 3,360 to 106 μm using a set of 14 screens.

The final development of the screening technique included sending the entire damaged sample first through the 355 μm mesh screen. The sample remaining on top of the 355 μm screen was then sent through the 3,360-, 1,000-, 840-, 590-, 500-, and

420-μm mesh screens. The sample smaller than 355 μm was sent through the 250-, 212-, and 180-μm screens, and the less than 180-μm fraction was sent through the 150-, 125-, and 106-μm mesh screens. (Note: the 150-μm screen was replaced by a 149-μm screen for the damaged cylinders and spheres 26 through 29.) The testing showed that the size fractions below 200 μm required a large amount of agitation in order to achieve particle separation. An alternate method for particle size analysis should be employed to obtain the size fractions below 106 μm.

A shortfall of most size analysis methods, including screening, is that they are based on a spherical particle. The size analysis error will increase as the length-to-diameter ratio increases in the fragments generated upon impact. The assumption is that microscopy will be applied to the size fractions at LLNL in order to evaluate the particle morphology.

SAMPLES

Cylindrical and spherical samples of LX-10 were received from LLNL for this study. The cylindrical samples (ID B253, 122013.75) were used in Part I of the study, and the spherical samples (ID B253, 111113.75) were used in Part II.

The LX-10 explosive is a pressed explosive containing 95 weight percent 1,3,5,7-Tetranitro-1,3,5,7-Tetraazacyclooctane, Cyclotetramethylene Tetranitramine (HMX), and 5 weight percent Viton. A density of 1.85 gm/cm^3 for the explosive was used in the closed bomb analysis.

The cylinders and spheres were weighed, measured, and photographed upon receipt prior to testing. A summary of these data can be found in Tables 1 and 2, respectively. Photographs of the undamaged LX-10 samples can be found in Appendix A.

TABLE 1. Undamaged Cylinder Data.

LX-10, B253, cylinders ID = 122013.75			
Part No.	Weight, g	Diameter, mm	Length, mm
1	9.8505	18.01	21.05
3	9.8793	18.01	21.04
5	9.8923	18.01	21.15
6	9.9263	18.02	21.13
7	9.9126	18.02	21.03
8	9.9098	18.02	21.09
9	9.9351	18.02	21.01
10	9.9029	18.02	21.01
11	9.9173	18.02	21.02
12	9.9231	18.02	21.01
13	9.9324	18.02	21.07
14	9.9103	18.03	21.00
16	9.9111	18.02	21.09
17	9.9010	18.02	21.08
18	9.9049	18.02	21.02
19	9.9070	18.01	21.03
20	9.9113	18.01	21.09
21	9.9003	18.02	21.04
22	9.9186	18.01	21.06
24	9.8973	18.01	21.16
25	9.9024	18.01	21.06
26	9.9159	18.02	21.01
27	9.9048	18.02	21.04
31	9.8944	18.00	21.01
32	9.9042	18.01	21.01
33	9.9119	18.01	21.07
34	9.9144	18.01	21.01
35	9.9139	18.01	20.99
36	9.9253	18.02	21.04
37	9.9041	18.01	21.05
38	9.9100	18.02	21.04
39	9.9113	18.01	21.01

TABLE 2. Spherical LX-10 Sample Data.

LX-10, B253, spheres ID = 111113.75		
Part No.	Weight, g	Diameter, mm
1	5.7002	18.01
2	5.6918	18.02
3	5.6794	18.01
4	5.6742	18.01
5	5.6747	18.00
6	5.6795	18.01
7	5.6884	18.02
8	5.6866	18.02
9	5.6758	18.01
10	5.6767	18.00
11	5.6768	18.01
12	5.6780	18.01
13	5.6761	18.01
14	5.6756	18.01
15	5.6744	18.01
16	5.6776	18.01
17	5.6714	18.01
18	5.6741	18.01
19	5.6766	18.01
21	5.6815	18.01
22	5.6792	18.02
23	5.6710	18.01
24	5.6715	18.01
25	5.6763	18.02
26	5.6744	18.01
27	5.6734	18.01
28	5.6700	18.01
29	5.6726	18.02
30	5.6724	18.01
31	5.6753	18.02
32	5.6789	18.03
33	5.6847	18.03
34	5.6810	18.01
35	5.6784	18.01
36	5.6851	18.02

The LX-10 friability cylinders averaged 18.015 mm ± 0.006 mm in diameter and 21.048 ± 043 mm in length. The cylinders weighed 9.908 ± 0.016 grams. A typical sample is shown in Figure 3.

FIGURE 3. Typical Cylindrical LX-10 Friability Sample (mm Scale Divisions).

The LX-10 friability spheres averaged 18.013 mm ± 0.007 mm in diameter and weighed 5.678 ± 0.006 grams. A typical sample is shown in Figure 4.

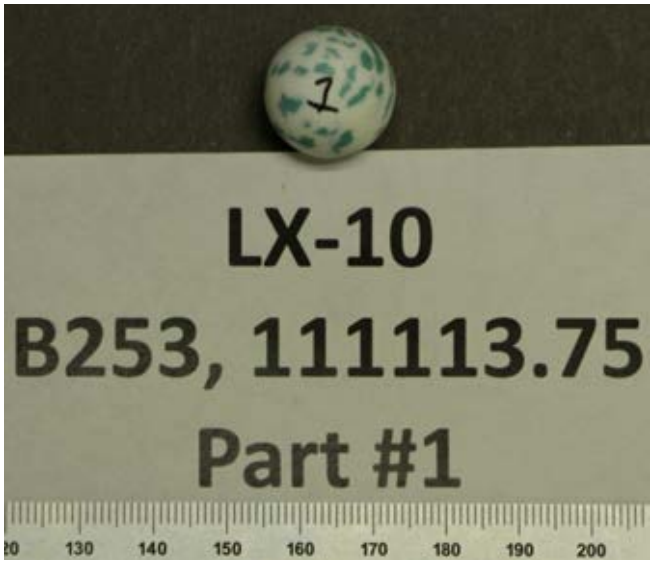

FIGURE 4. Spherical LX-10 Sample (mm scale).

A modified 12-gauge shotgun wad was used as a sabot for the LX-10 cylinders and spheres in the 18-mm damage tests. The sample arrangement is shown in Figure 5.

FIGURE 5. 18-mm Arrangement for the LX-10 Friability Samples.

RESULTS

PART I CYLINDER

Two undamaged LX-10 cylinders, Parts 37 and 39, (closed bomb ID 140604-2 and 140604-3) were burned in the closed bomb in order to obtain the linear burning rate of the LX-10 explosive. The burning rate is needed as input for determining the change in burning surface of the damaged explosive. The burning rate versus pressure is plotted in Figure 6. The burning rates for CompB, from Reference 4, are included in the plot for comparison. The LX-10 burning rates were more reproducible than those of CompB and overall lower in value.

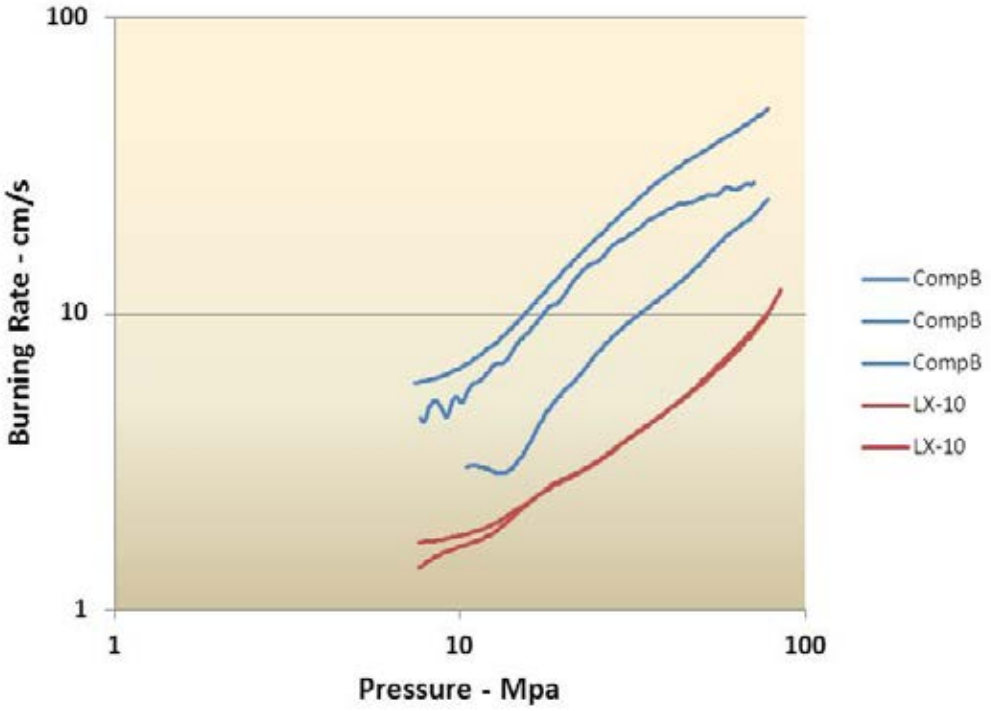

FIGURE 6. LX-10 Burning Rates Compared to CompB.

The variability observed in the CompB samples has been attributed to the contribution of trinitrotoluene, which is not present in the LX-10 formulation. The manufacturing process, pressed versus melt-cast, is also a contributing factor to the differences in burning rate reproducibility.

Twenty eight cylindrical LX-10 samples were impact damaged at velocities from 121 to 500 ft/s (36.88 to 152.40 m/s). The percent recovered versus impact velocity is compared to the CompB samples in Figure 7. The recovered percentage decreased as the impact velocity increased. Tabular data and photographs of the damaged LX-10 cylinders are summarized in Appendix B.

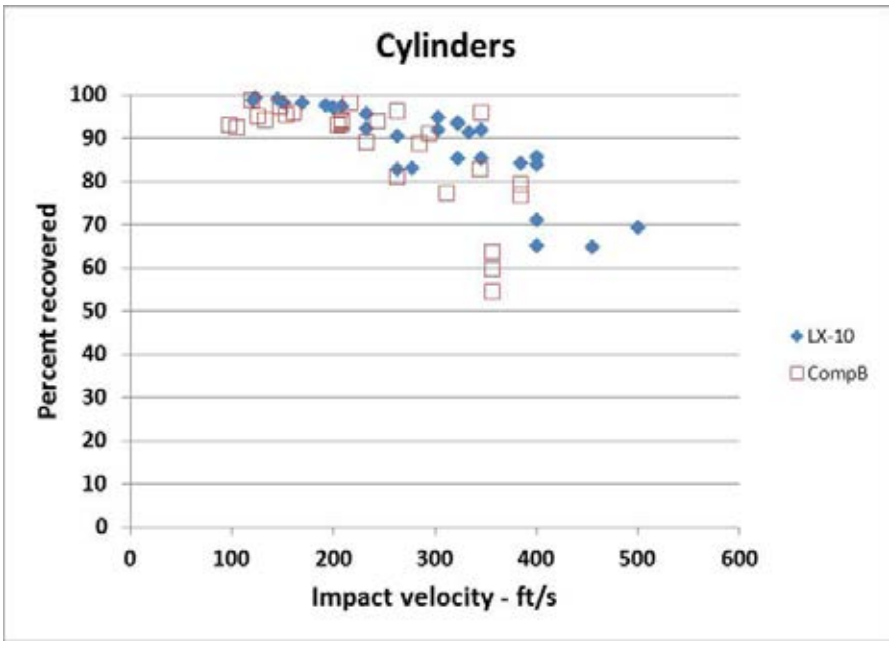

FIGURE 7. Percent Recovered Versus Impact Velocity for Cylindrical Samples.

Cylindrical LX-10 samples impact damaged at 105 and 385 ft/s can be seen in Figures 8 and 9, respectively. The increased damage with increasing velocity is visible with the decreased large fragments and increased amounts of fine powder.

FIGURE 8. Cylindrical LX-10 Sample Impact Damaged at 121 ft/s.

FIGURE 9. Cylindrical LX-10 Sample Impact Damaged at 385 ft/s.

The maximum dp/dt versus impact velocity is plotted for the cylindrical LX-10 samples with CompB in Figure 10. A difference in burning rate cannot be attributed to the scatter observed in the LX-10. The LX-10 data points in Figure 10 with the black outline are those that were dry screened and recombined prior to burning.

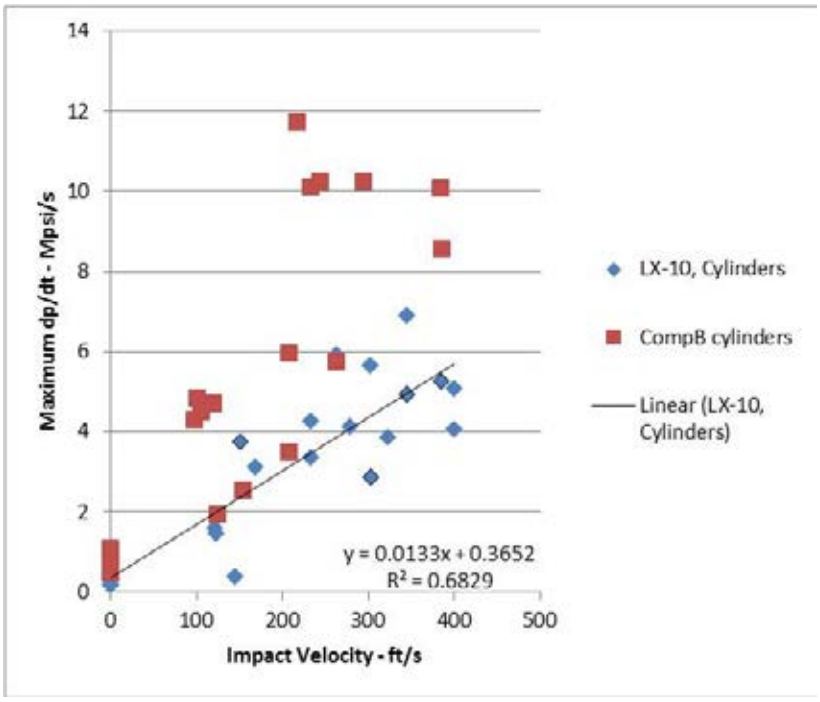

FIGURE 10. Maximum dp/dt Versus Impact Velocity.

A CBRED analysis of the damaged samples was performed with the measured LX-10 burning rates, and the maximum change in burning area versus impact velocity is plotted in Figure 11. The LX-10 data points in the figure with the red outline are those that were dry screened and recombined prior to burning.

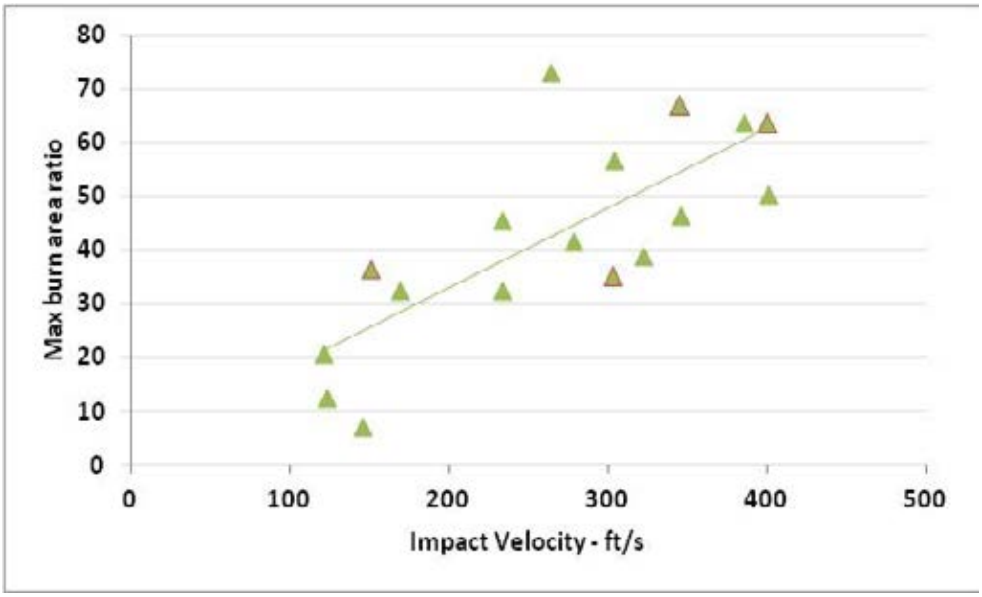

FIGURE 11. Maximum Burn Area Ratio Versus Impact Velocity for LX-10 Cylinders.

Five additional cylindrical LX-10 samples were impact damaged and subjected to dry screening. Samples were damaged at 151, 263, 303, 345, and 385 ft/s. The percent of recovered mass versus particle size data are plotted in Figure 12. The majority of damaged fragments remain larger than 1,000 μm with a small fraction (<10 percent) at less than 106 μm. The increase in the finest fraction (<106 μm) with a decrease in the coarse (>3,360 μm) as impact velocity increases is evident.

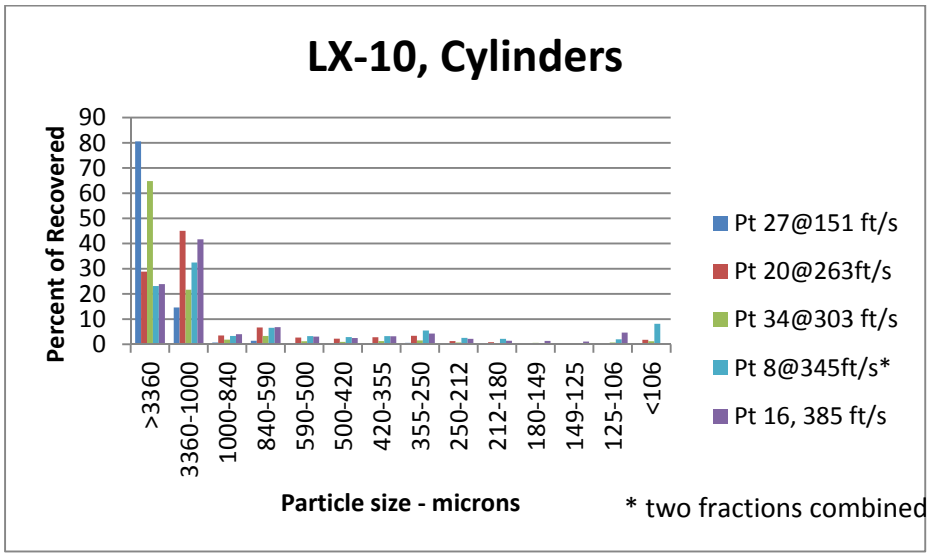

FIGURE 12. Particle Size Distribution of LX-10 Damaged Cylinders.

PART II – SPHERES

Twenty four spherical LX-10 samples were impact damaged at velocities from 111 to 500 ft/s (33.8 to 152.4 m/s). The percent recovered versus impact velocity is plotted in Figure 13 for the LX-10 spheres. The recovered percentage decreased as the impact velocity increased due to the increase in fines and their aerosolization at impact. Tabular data and photos of the damaged samples are summarized in Appendix B.

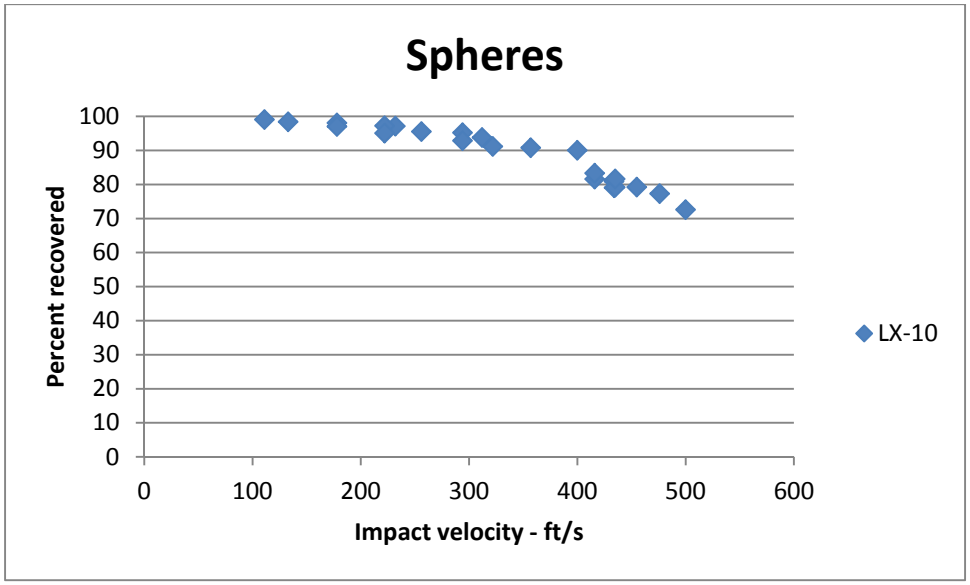

FIGURE 13. Spherical LX-10 Sample Recovered Versus Impact Velocity.

Screened weights for each of the 24 damaged spherical LX-10 samples are summarized in Appendix B. Percentages of the individual size fractions were calculated based on the total mass of the individual fractions. Sample losses due to screening were about 3 percent. A plot of the percent of the individual fractions is given in Figures 14, 16, 18, and 20. The plots have been grouped by increasing velocity for clarity.

The majority of the recovered material was greater than 1,000 μm at impact velocities less than 178 ft/s (54 m/s) (Figure 14). The remaining size fractions were less than 5 percent of the screened total. The finest fraction (<106 μm) was absent at the two lowest impact velocities, 111 and 132 ft/s. A photo of an LX-10 spherical sample impact damaged at 132 ft/s is shown in Figure 15.

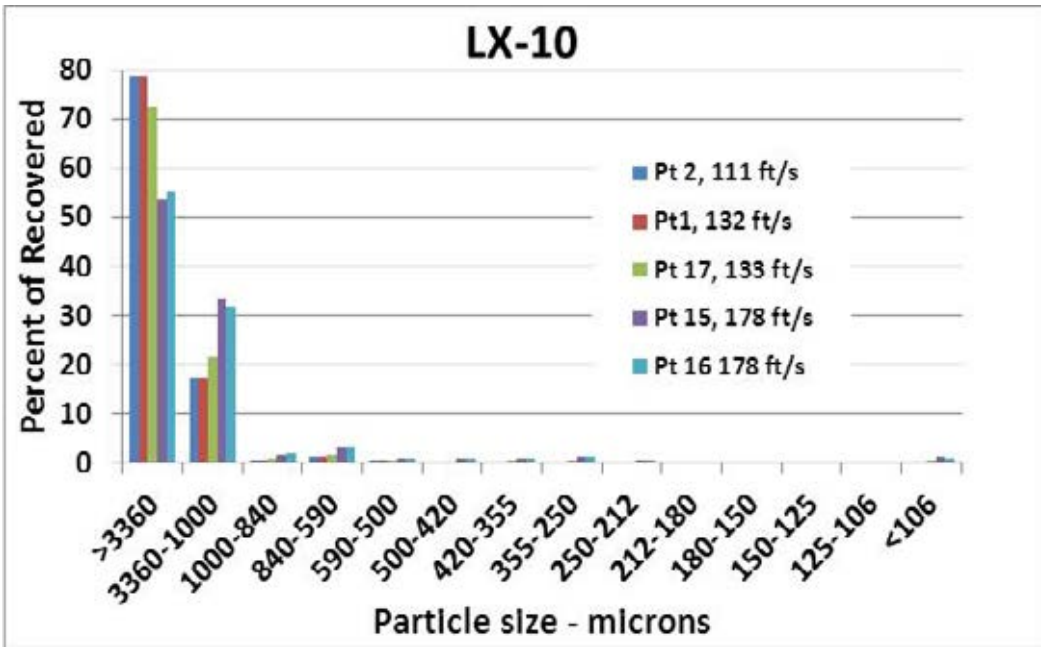

FIGURE 14. Size Fractions for Spherical LX-10 Samples
Impact Damaged at Less Than 200 ft/s.

FIGURE 15. Spherical LX-10 Sample Impact Damaged at 132 ft/s.

The size fraction less than 3,360 μm decreased with an increase in the 3,360 to 1,000 μm fraction in the LX-10 samples impact damaged at velocities between 222 and 294 ft/s (Figure 16). The less than 106 μm fraction increased slightly to about 2 percent. The fraction 1,000 to 3,360 μm increased to about 35 weight percent of total sample collected. A spherical LX-10 sample impact damaged at 232 ft/s is shown in Figure 17.

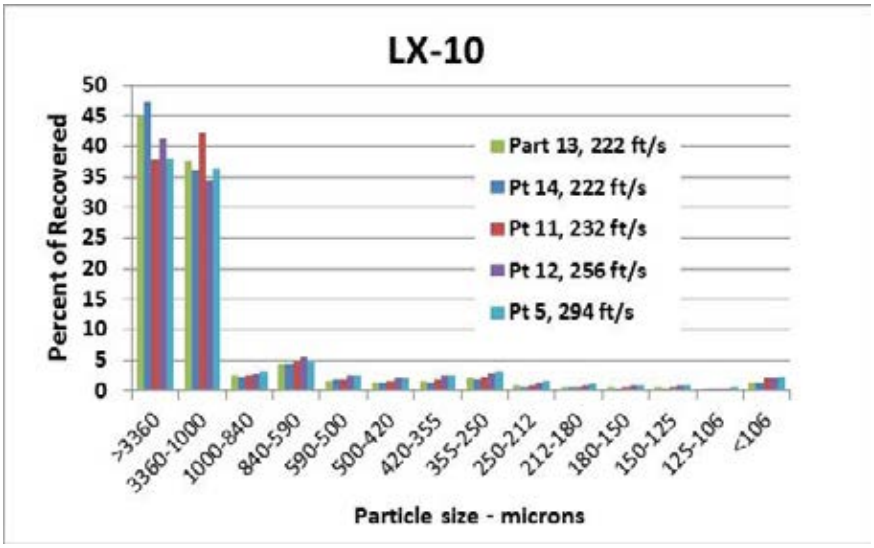

FIGURE 16. Size Fractions for Spherical CompB Samples Impact Damaged Between 222 and 294 ft/s.

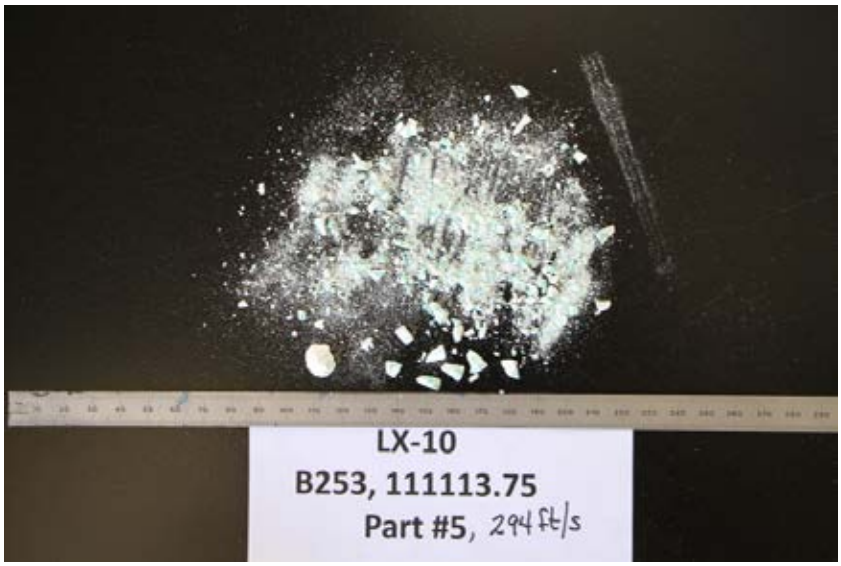

FIGURE 17. Spherical LX-10 Sample Impact Damaged at 294 ft/s.

The size fraction greater than 3,360 µm decreased to below 20 weight percent and 3,360 to 1,000 µm increased to about 40 weight percent in the LX-10 samples impact damaged at velocities between 312 and 416 ft/s (Figure 18) with a minor increase in all of the finer fractions. A spherical LX-10 sample impact damaged at 416 ft/s is shown in Figure 19.

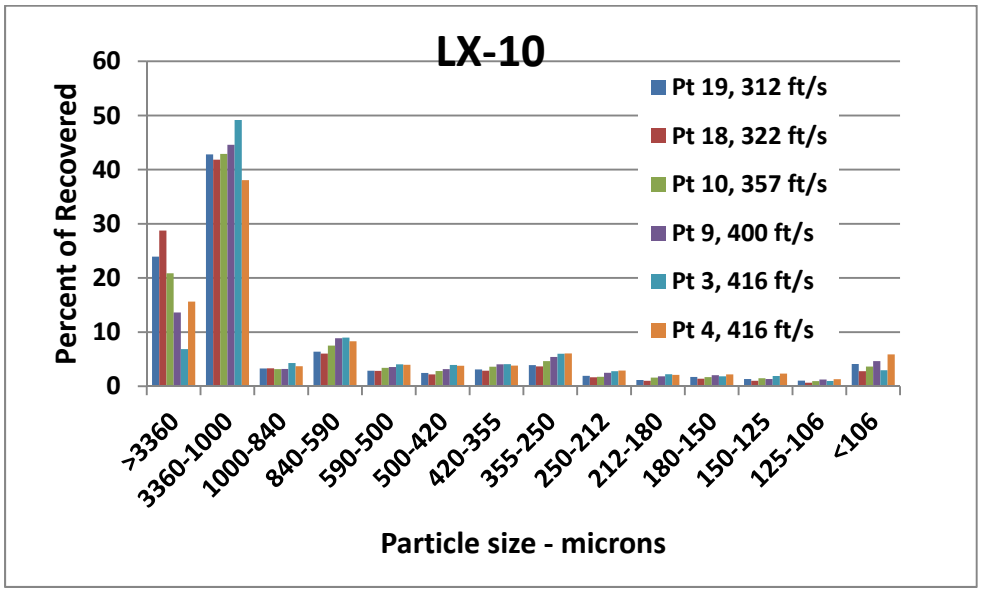

FIGURE 18. Size Fractions for Spherical LX-10 Samples Impact Damaged Between 312 and 416 ft/s.

FIGURE 19. Spherical LX-10 Sample Impact Damaged at 416 ft/s.

The size fraction greater than 3,360 μm decreased to about 10 weight percent in the LX-10 samples impact damaged at velocities between 434 and 500 ft/s (Figure 20) with an increase in the less than 106 μm fraction to about 10 percent. The fraction 3,360 to 1,000 μm remained relatively constant. A spherical LX-10 sample impact damaged at 435 ft/s is shown in Figure 21.

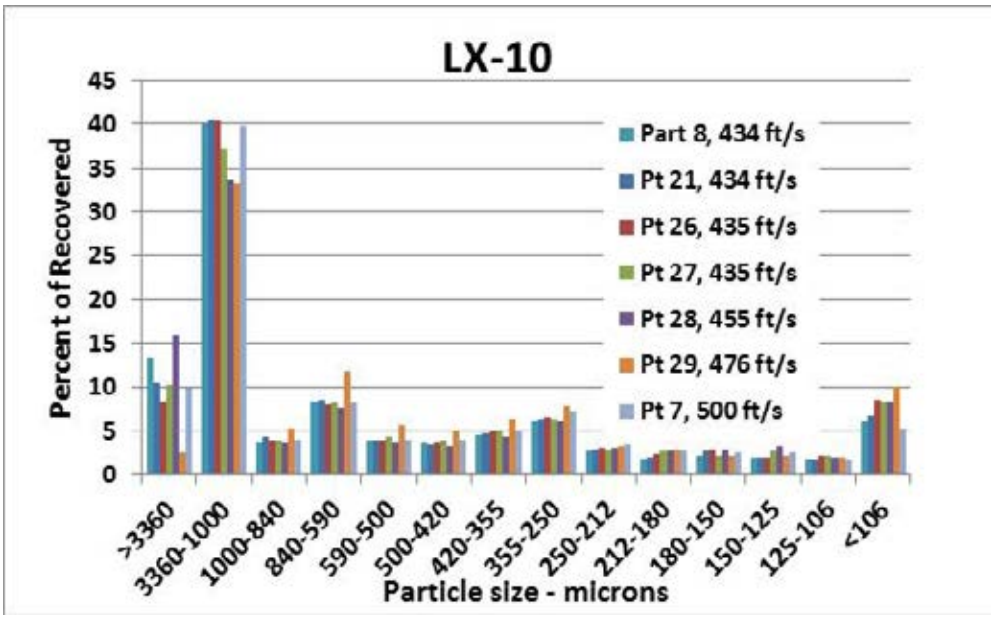

FIGURE 20. Size Fractions for Spherical LX-10 Samples Impact Damaged Between 434 and 500 ft/s.

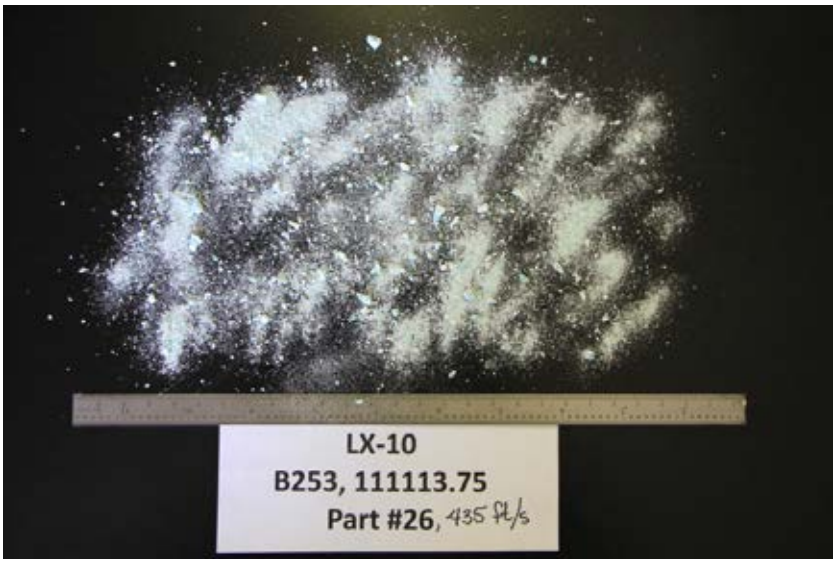

FIGURE 21. Spherical LX-10 Sample Impact Damaged at 435 ft/s.

Sample reproducibility can be examined for spherical LX-10 samples impact damaged at 178, 222, 416, 434, and 435 ft/s in Figures 22 through 25, respectively. The majority of the recovered samples fall into the coarsest fractions. The lowest impact velocities of 178 and 222 ft/s were the most reproducible with about 10 percent variation in fractions 500 to 420 and greater than 106 μm in the samples damaged at 179 ft/s and about 15 percent variation in the fraction 126 to 106 μm in the samples damaged at 222 ft/s. The largest variation was 39 percent in the greater than 3,360 μm fraction in the sample damaged at 416 ft/s.

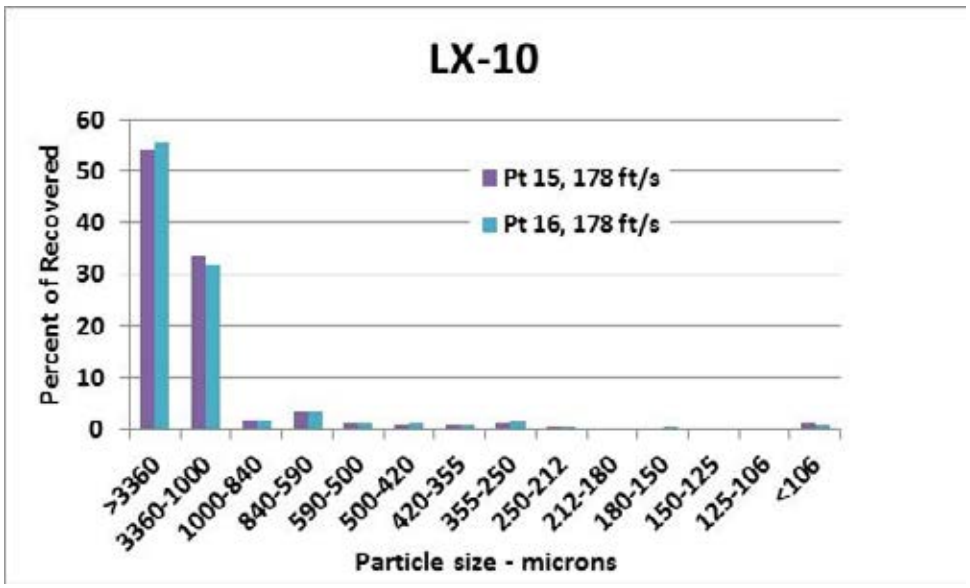

FIGURE 22. A Comparison of Spherical LX-10 Samples Impact Damaged at 178 ft/s.

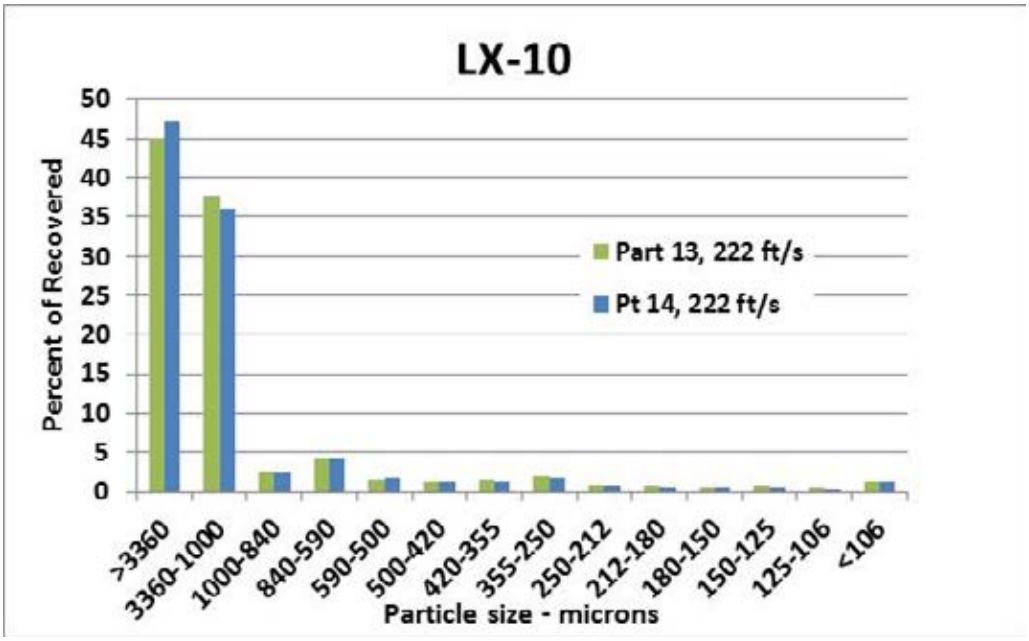

FIGURE 23. A Comparison of Spherical LX-10 Samples Impact Damaged at 222 ft/s.

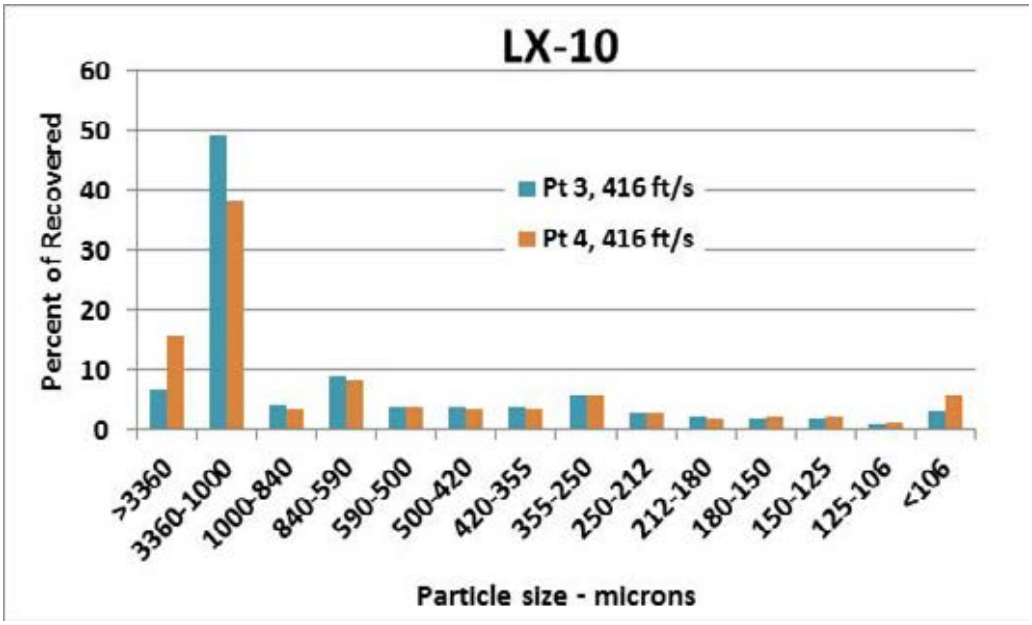

FIGURE 24. A Comparison of Spherical LX-10 Samples Impact Damaged at 416 ft/s.

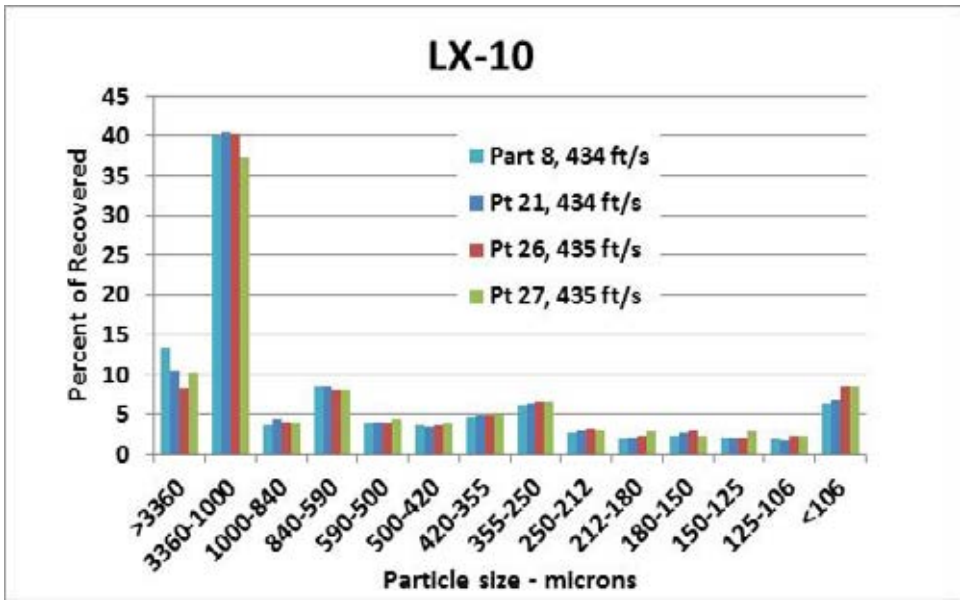

FIGURE 25. A Comparison of Spherical LX-10 Samples Impact Damaged at 434 and 435 ft/s.

A direct comparison of the particle size distribution data for damaged cylindrical and spherical LX-10 samples is difficult as they were not damaged at exactly the same velocity. A comparison of the closest spherical and cylindrical impact velocities is made in Figures 26 through 30. These figures show that the fracture behavior, based on the resulting particle size distribution, is similar for the two geometries; however, more data are needed at equivalent impact velocities coupled with microscopic evaluation of the resulting fractions in order to make a decisive conclusion.

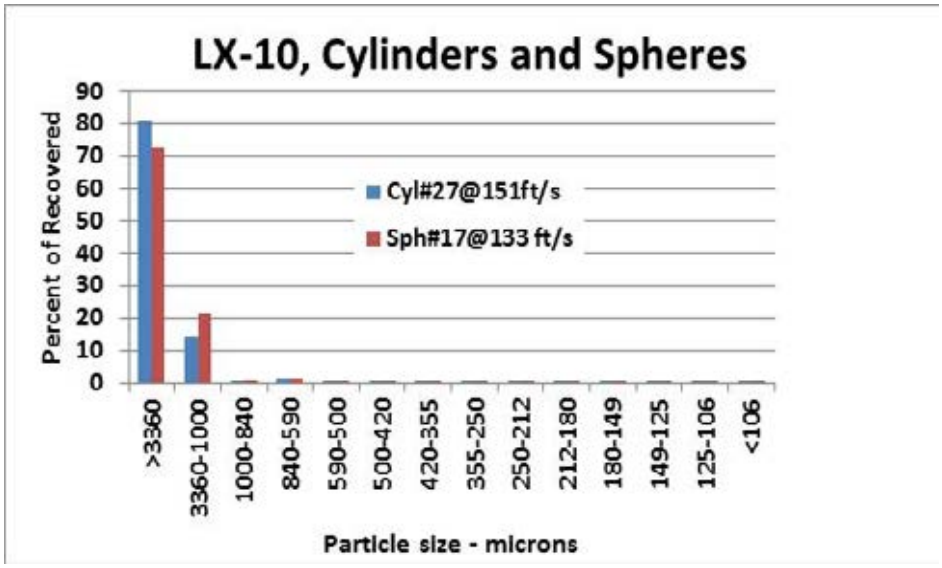

FIGURE 26. A Comparison of Impact Damage for Two Explosive Geometries.

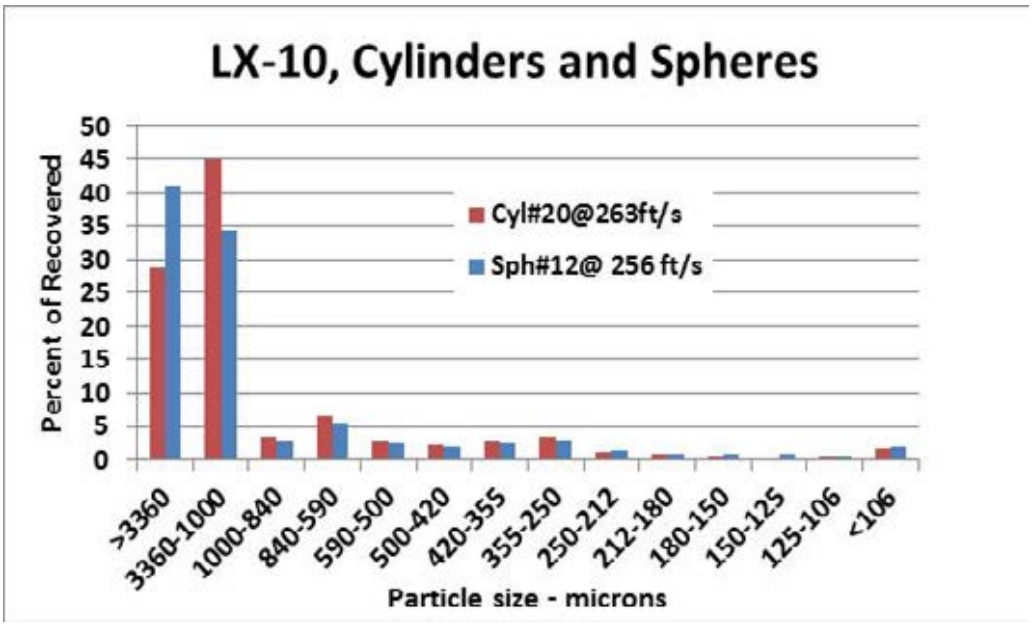

FIGURE 27. A Comparison of Impact Damage for Two Explosive Geometries.

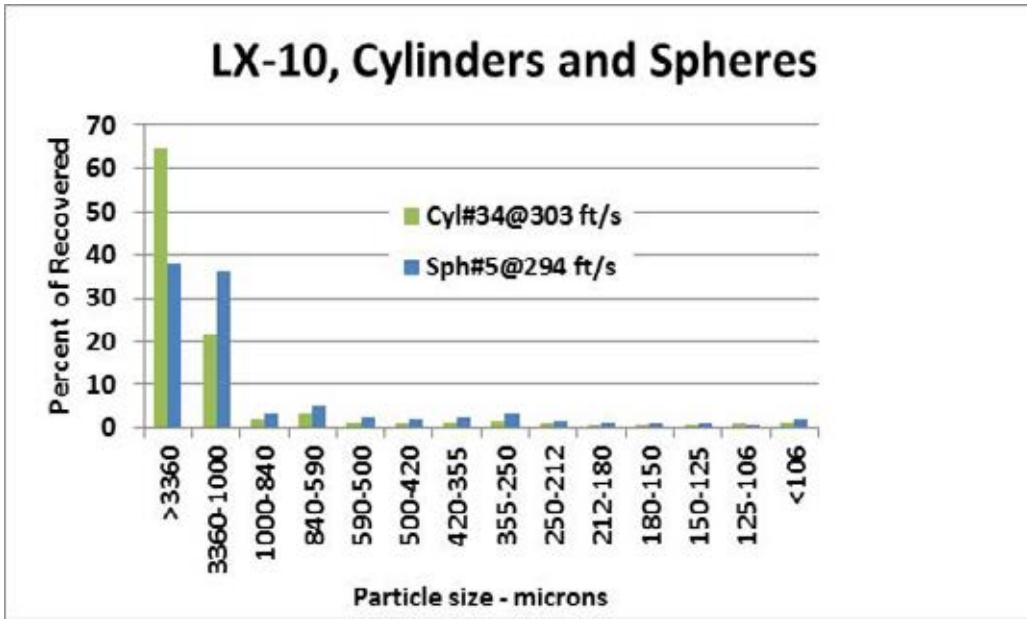

FIGURE 28. A Comparison of Impact Damage for Two Explosive Geometries.

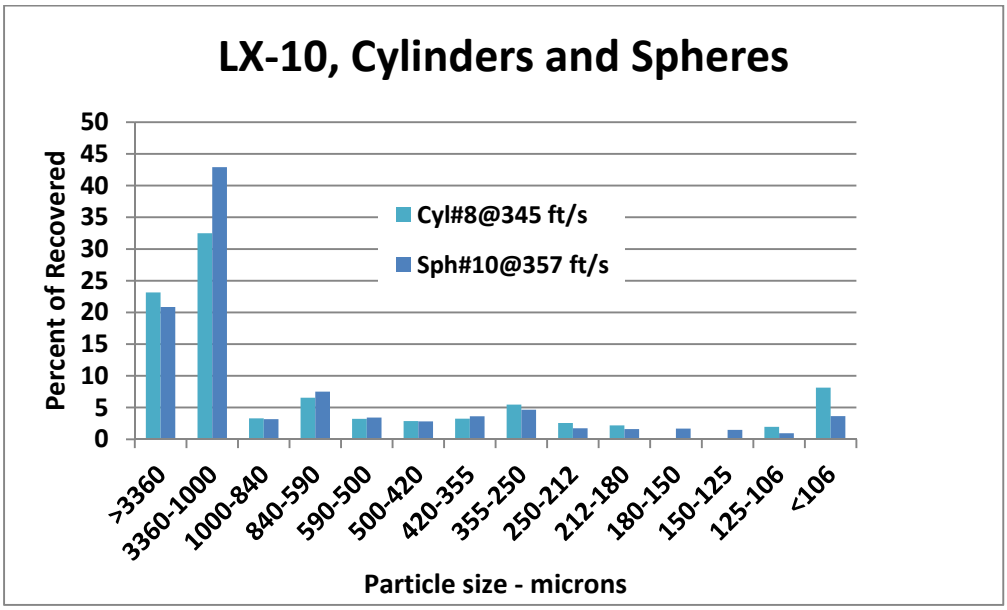

FIGURE 29. A Comparison of Impact Damage for Two Explosive Geometries.

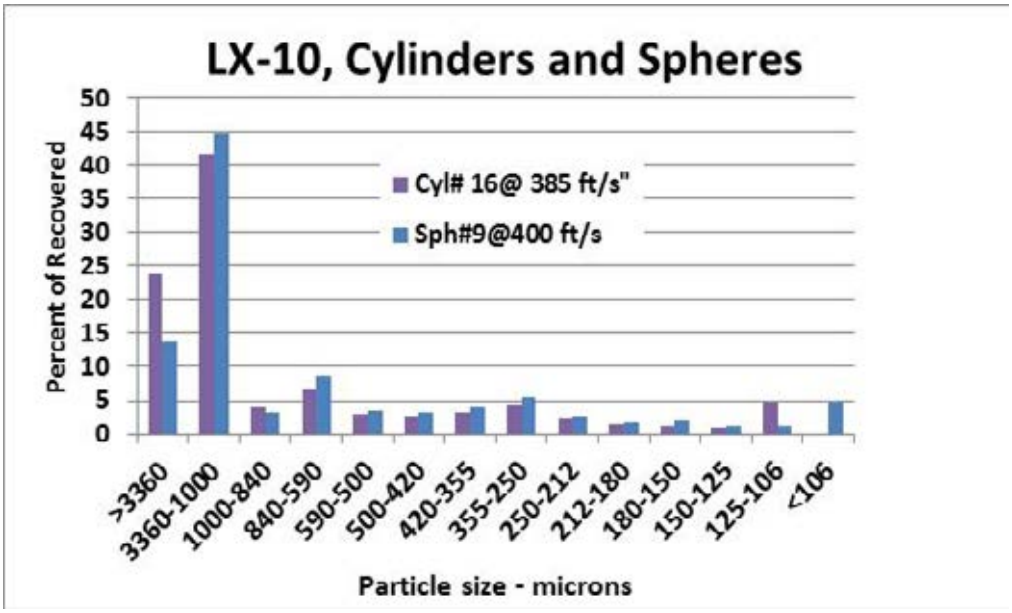

FIGURE 30. A Comparison of Impact Damage for Two Explosive Geometries.

The decrease in large fragments with increasing velocity can be seen in the plot of the fraction greater than 3,360 μm versus impact velocity for both LX-10 and CompB in Figure 31. The CompB fraction is less than the LX-10 fraction in all cases, indicating the generation of a larger fraction of fine material under equivalent impact conditions.

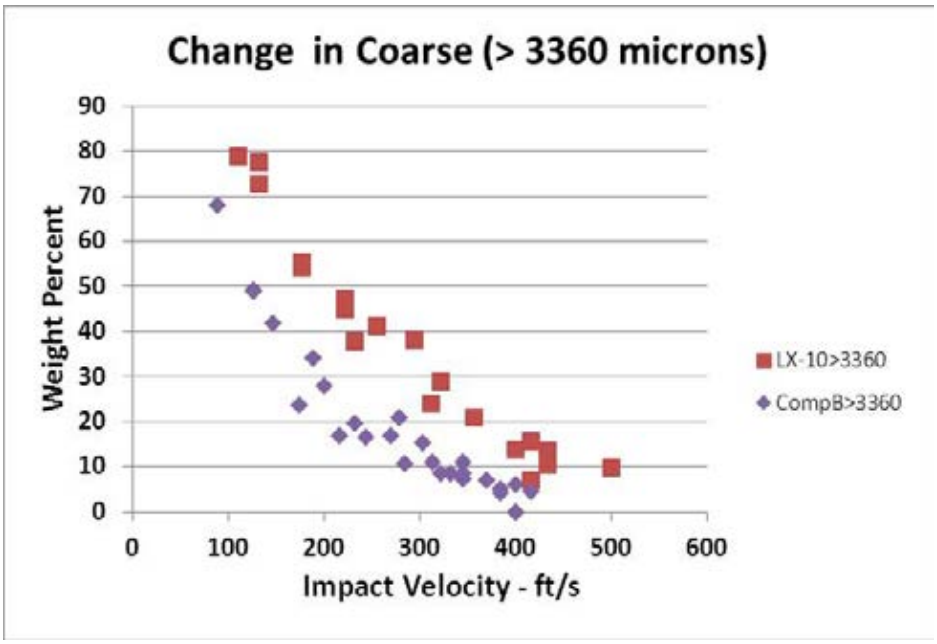

FIGURE 31. Change in Diameter Greater Than 3,360 μm Size Fraction.

The increase in fine particles with increasing velocity can be seen in the plot of the fraction less than 106 μm versus impact velocity for both LX-10 and CompB in Figure 32. The CompB fraction is greater than the LX-10 fraction in all cases, indicative of a higher level of damage at similar impact conditions.

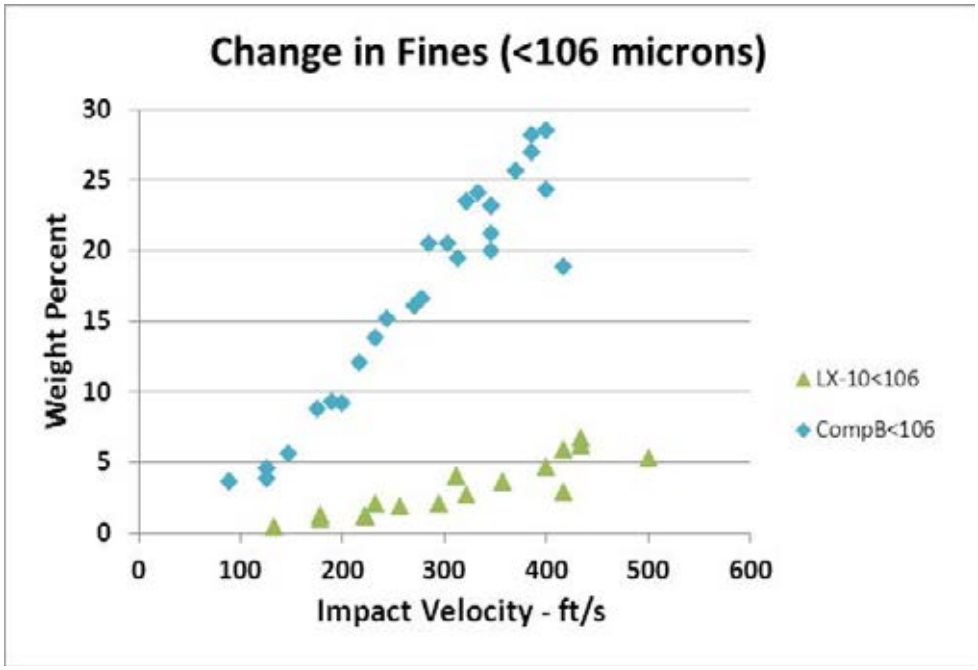

FIGURE 32. Change in Fine Particles Less Than 106 μm Size Fraction.

SUMMARY/CONCLUSIONS

The friability work on LX-10 and CompB resulted in the production of two Joint, Army, Navy, NASA, and Air Force (JANNAF) papers that were presented at the 2014 JANNAF Propulsion Systems Hazards Subcommittee Meeting held in Albuquerque, New Mexico, December 2014. The papers can be found in Appendix C.

CYLINDRICAL LX-10

Sample non-uniformity observed in the undamaged CompB burning rate evaluations was not observed in the LX-10 cylindrical burning tests. The cause of the scatter observed in the LX-10 maximum dp/dt data is not known. Screening of the cylindrical samples revealed a particle distribution with the majority of the damage falling into the two coarsest (diameter >1,000 μm) size fractions.

SPHERICAL LX-10

Dry screening of the highly damaged LX-10 samples required a great deal of agitation to produce an adequate particle separation. A bimodal distribution observed for CompB was not observed for LX-10. Damage, based on particle size distribution was similar for the spherical and cylindrical LX-10 samples. Most of the damage resulted in particles in the greater than 3,360 and the 1,000 to 3,360 μm fractions. The finest size fraction increased with increasing impact velocity, while the fraction greater than 3,360 μm decreased.

FURTHER STUDY

The screened LX-10 size fractions were returned to LLNL for further study. It is recommended that they be submitted to microscopy to ascertain the morphology of the individual particles and that further size analysis be performed on the less than 106 μm fractions.

A comparison of the LX-10 and CompB friability data should be made to that of a viscoelastic explosive in order to compare their damage behavior. High rate mechanical properties measurements of these materials should also be reviewed and compared to the damage results.

REFERENCES

1. J. Isler. "Contribution du Mode de Combustion des Explosifs Compacts au Processus de la Transition Combustion-Deflagration-Detonation," *Proceedings of the 19th International Annual Conference of ICT, 29 June–1 July 1988, Karlsruhe, Federal Republic of Germany*, translation by T. S. Laker, Energetics Research Division, NAWCWD. (publication UNCLASSIFIED.)

2. United Nations. *Recommendations on the Transport of Dangerous Goods*, Manual of Tests and Criteria, United Nations, New York, 2007. (ST/SG/AC.10/11/REV.4/ Amend.2, document UNCLASSIFIED.)

3. A. I. Atwood, K. P. Ford, D. T. Bui, P. O. Curran, and T. M. Lyle. "Assessment of Mechanically Induced Damage in Solid Energetic Materials," presented at the Seventh International Symposium on Special Topics in Chemical Propulsion (7-ISICP) Advancements in Energetic Materials and Chemical Propulsion, Kyoto, Japan, September 2007. Paper UNCLASSIFIED. (Also published in *International Journal of Energetic Materials and Chemical Propulsion*, Begell House, Redding, CT, Vol. 8, No. 5, pp. 391–410, December 2009.)

4. Naval Air Warfare Center Weapons Division. *Composition B Damage Studies*, by A.I. Atwood, K.P. Ford, I Purifoy, C.J. Wheeler, E. Woods. China Lake, CA, NAWCWD, March 2014. (NAWCWD TM 8740, publication UNCLASSIFIED.)

5. Army Ballistic Research Laboratory. "A Versatile User-Oriented Closed Bomb Data Reduction Program (CBRED)," by C. F. Price and A. Juhasz. Aberdeen Proving Ground, MD, BRL, September 1977. (BRL R2018, publication UNCLASSIFIED.)

6. C. F. Price and A. I. Atwood. "CBRED II: A Versatile Tool for the Characterization of Damaged Propellants," *Proceedings of the 1991 JANNAF Propulsion Systems Hazards Subcommittee Meeting, 18-22 March 1991, Albuquerque, NM*. Laurel, MD, Chemical Propulsion Information Agency. CPIA Publication No. 562, pp. 425-432, 1991. Paper UNCLASSIFIED; publication UNCLASSIFIED.

7. Army Ballistic Research Laboratory. *BLAKE – A Thermodynamics Code Based on TIGER: User's Guide and Manual*, by E. Freedman. Aberdeen Proving Ground, MD, BRL, July 1982. (BRL-TR-02411, publication UNCLASSIFIED.)

Appendix A

CYLINDRICAL AND SPHERICAL LX-10 SAMPLES

This page intentionally left blank.

Undamaged Cylinders

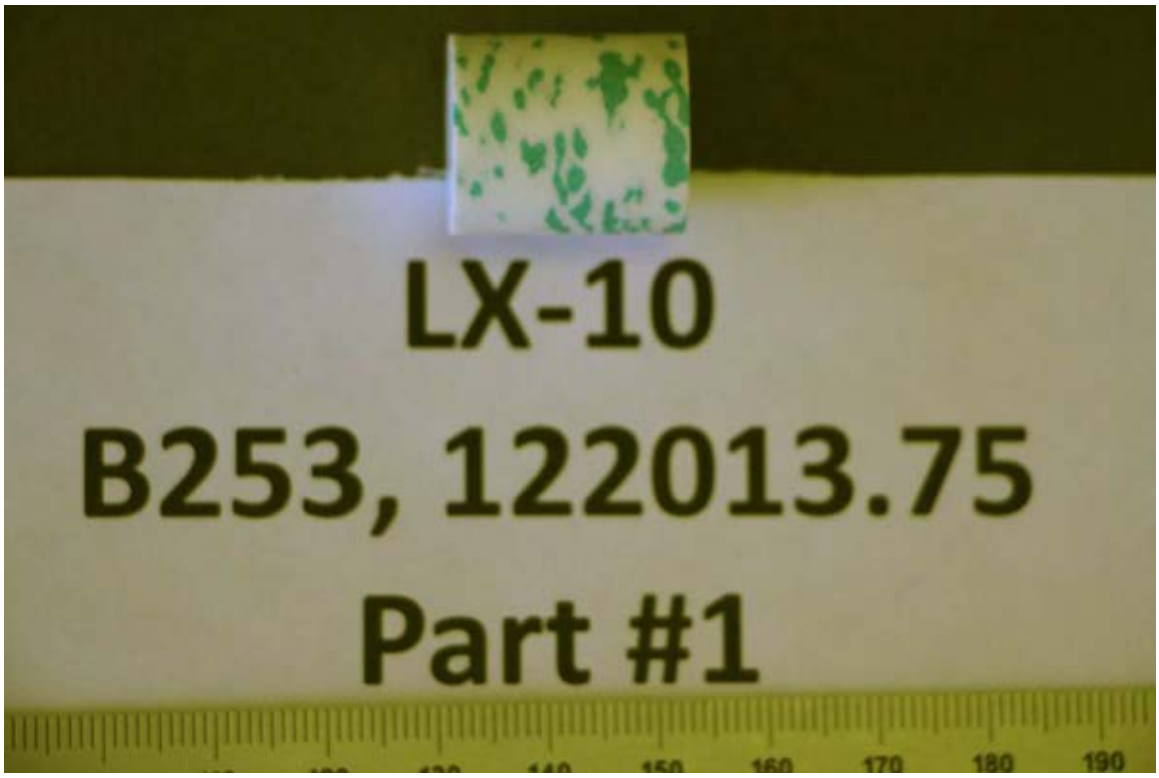

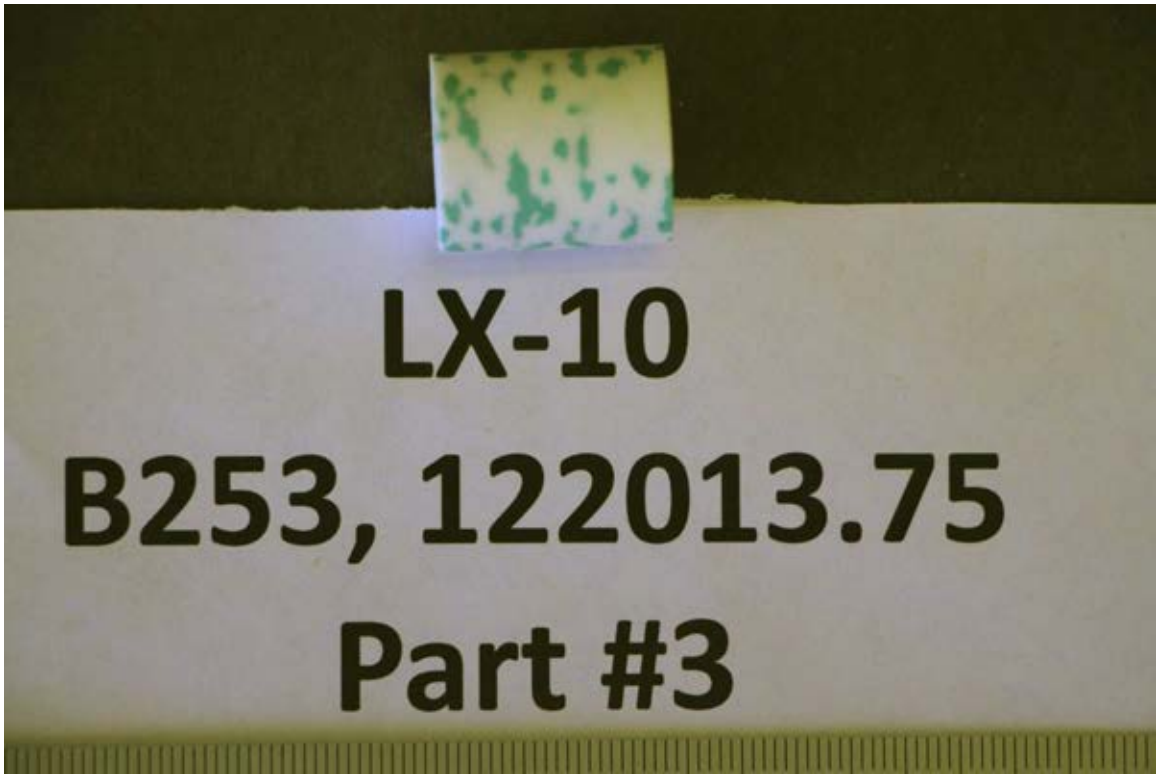

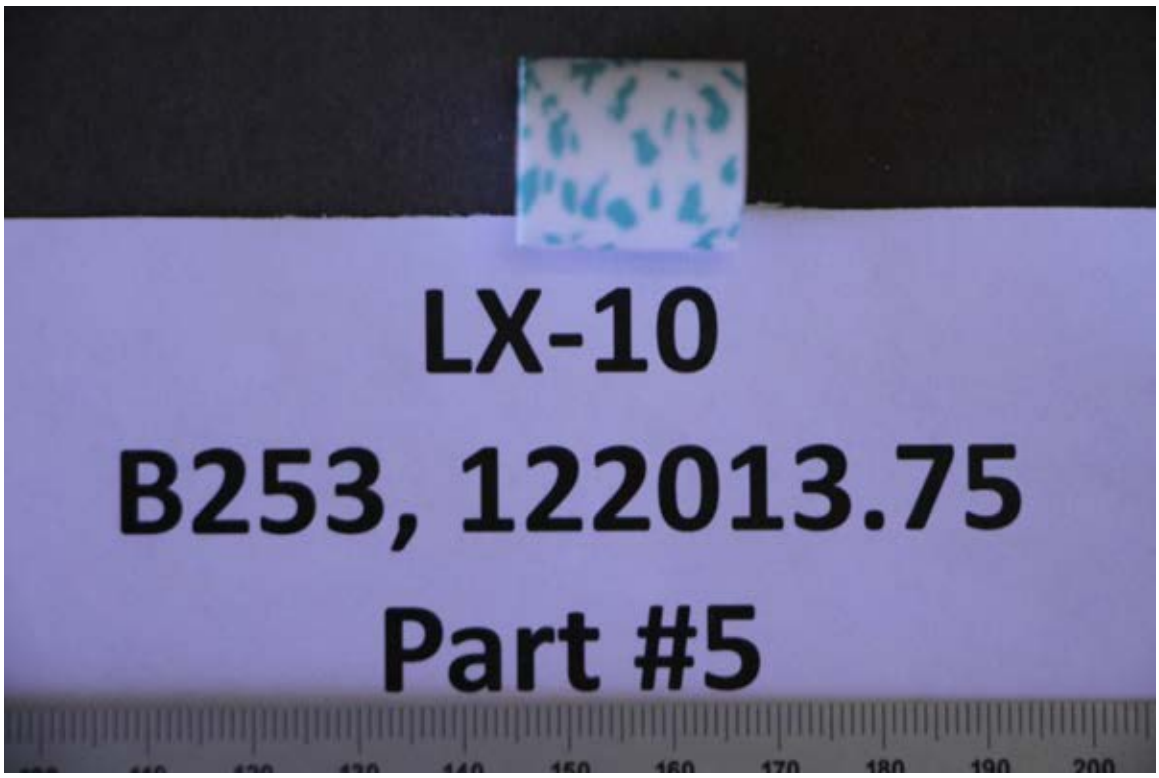
LX-10
B253, 122013.75
Part #5

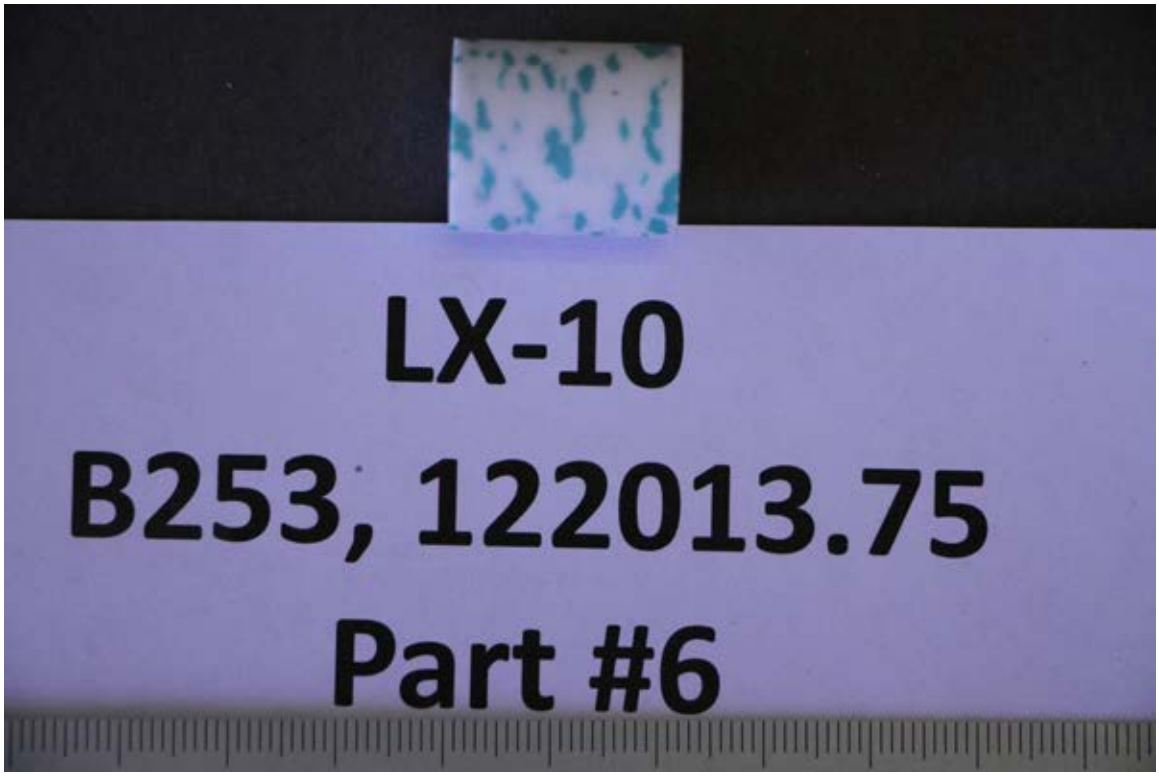
LX-10
B253, 122013.75
Part #6

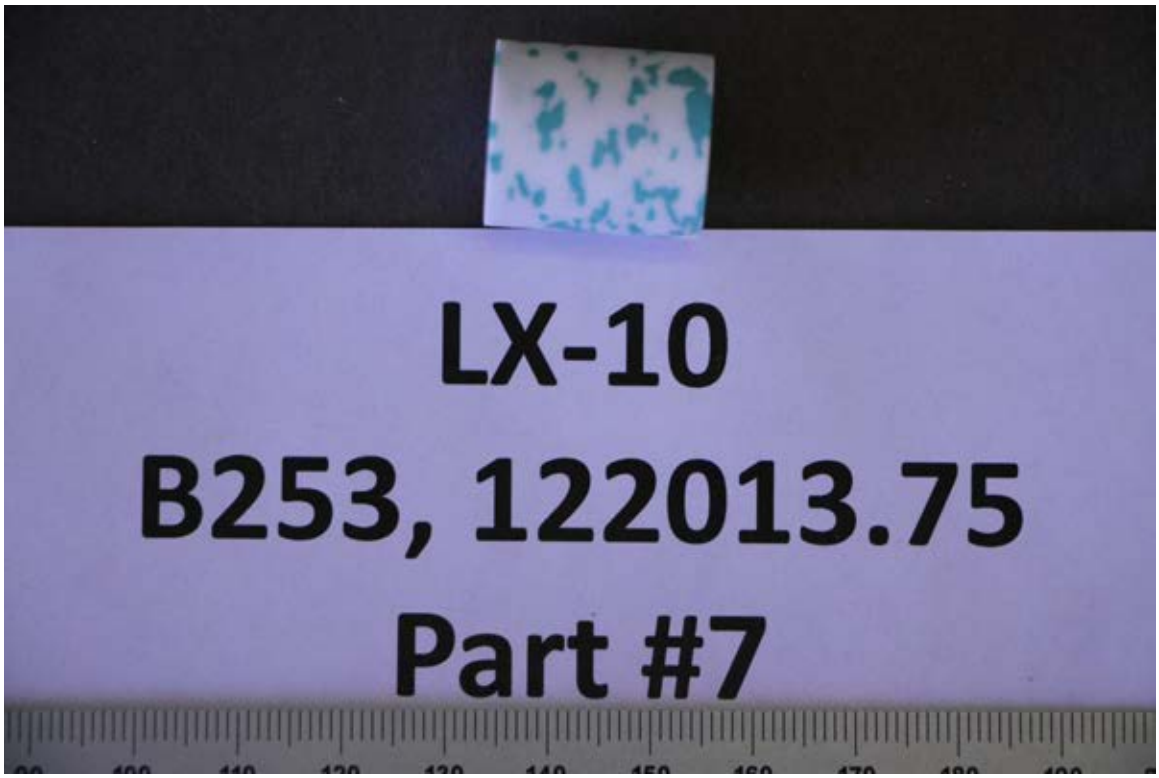
LX-10
B253, 122013.75
Part #7

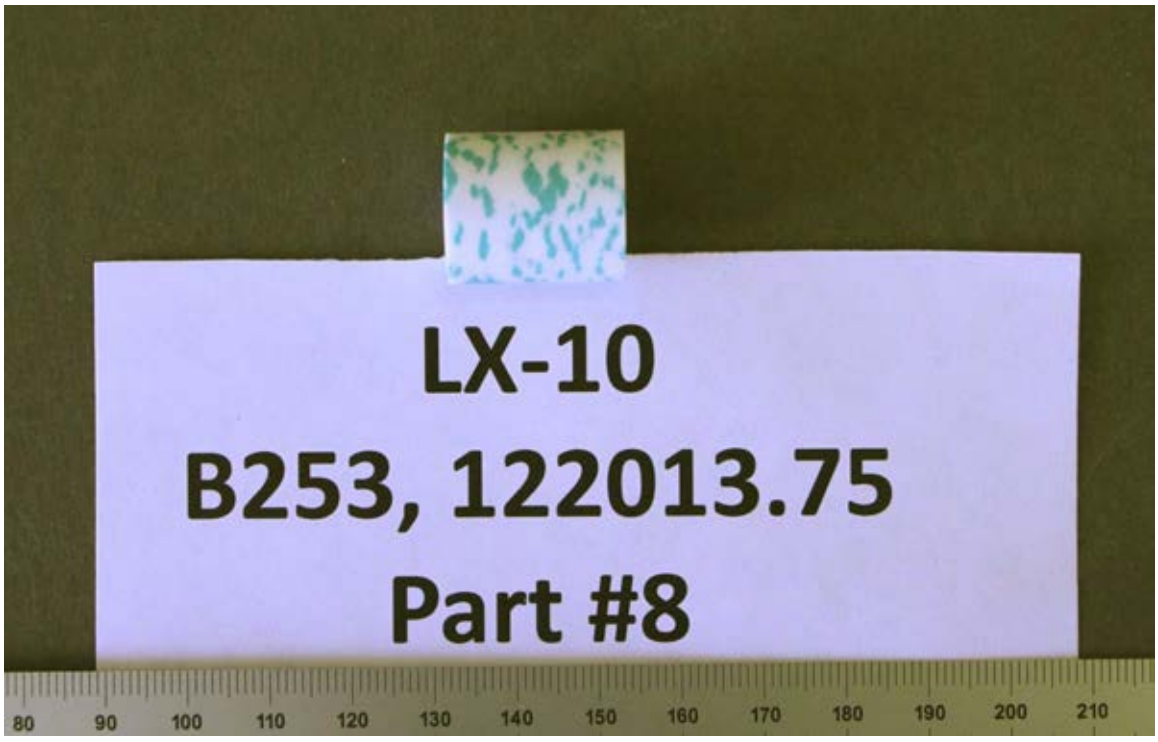
LX-10
B253, 122013.75
Part #8
80 90 100 110 120 130 140 150 160 170 180 190 200 210

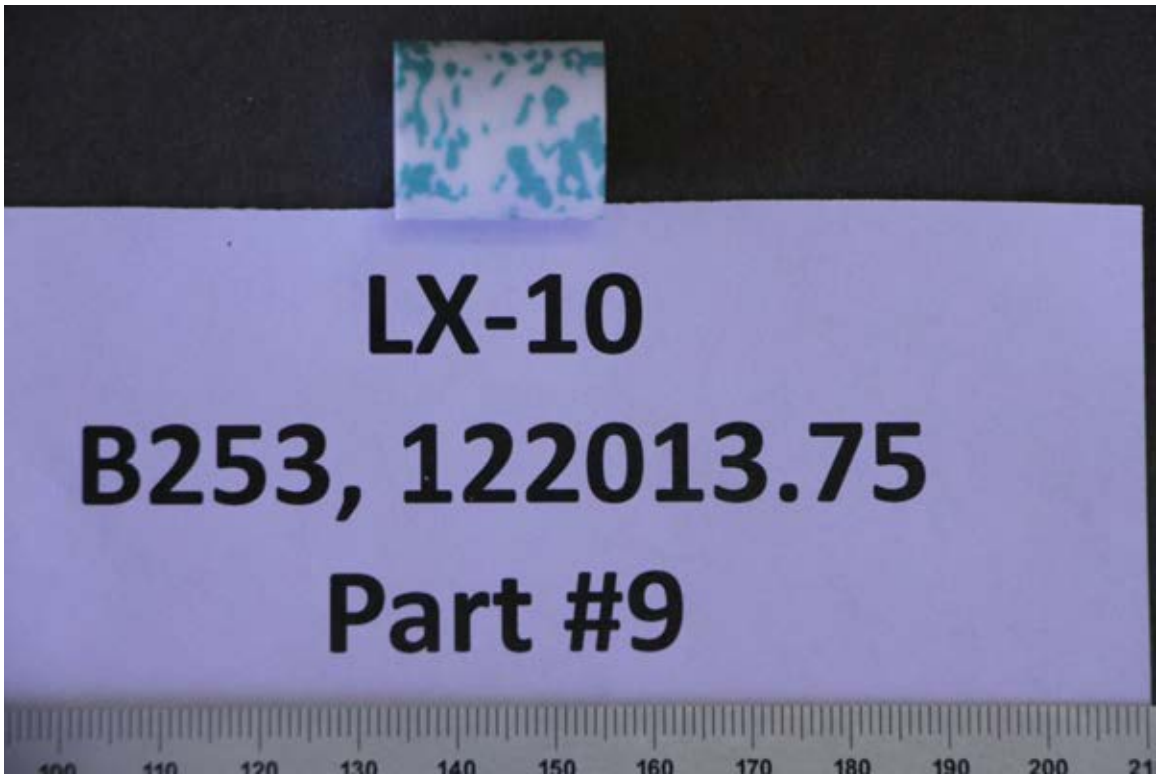
LX-10
B253, 122013.75
Part #9

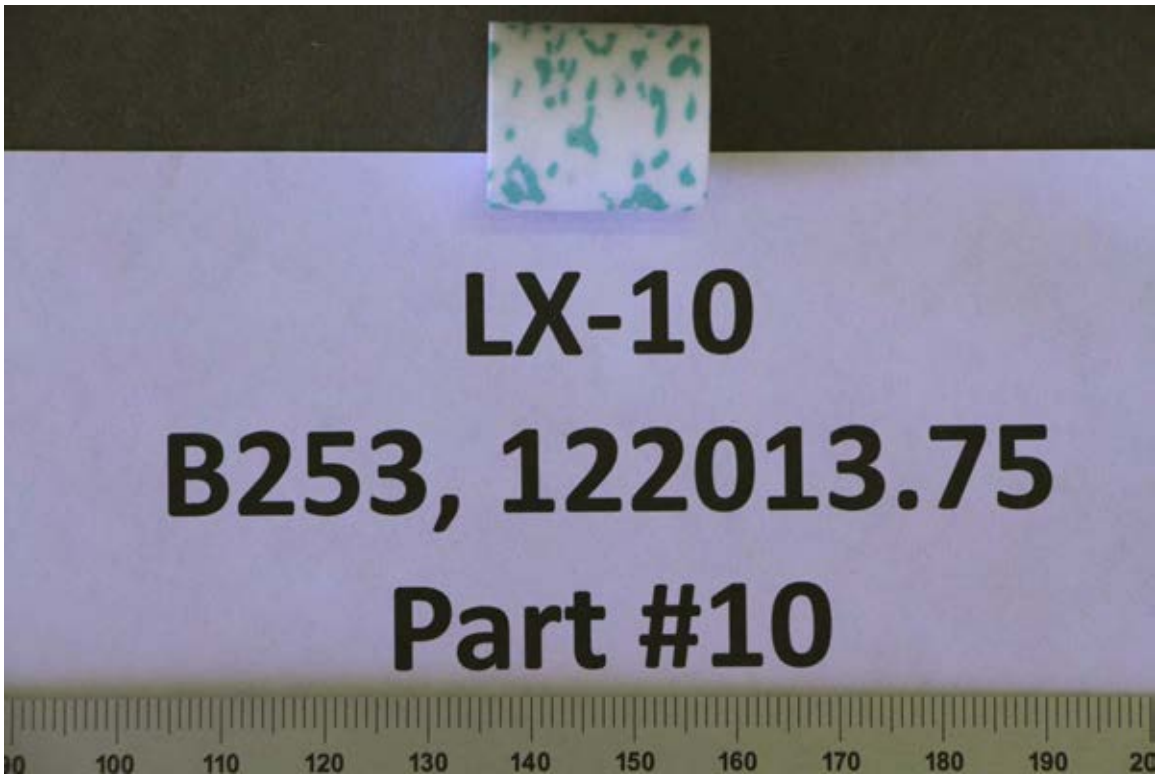
LX-10
B253, 122013.75
Part #10
100
110
120
130
140
150
160
170
180
190

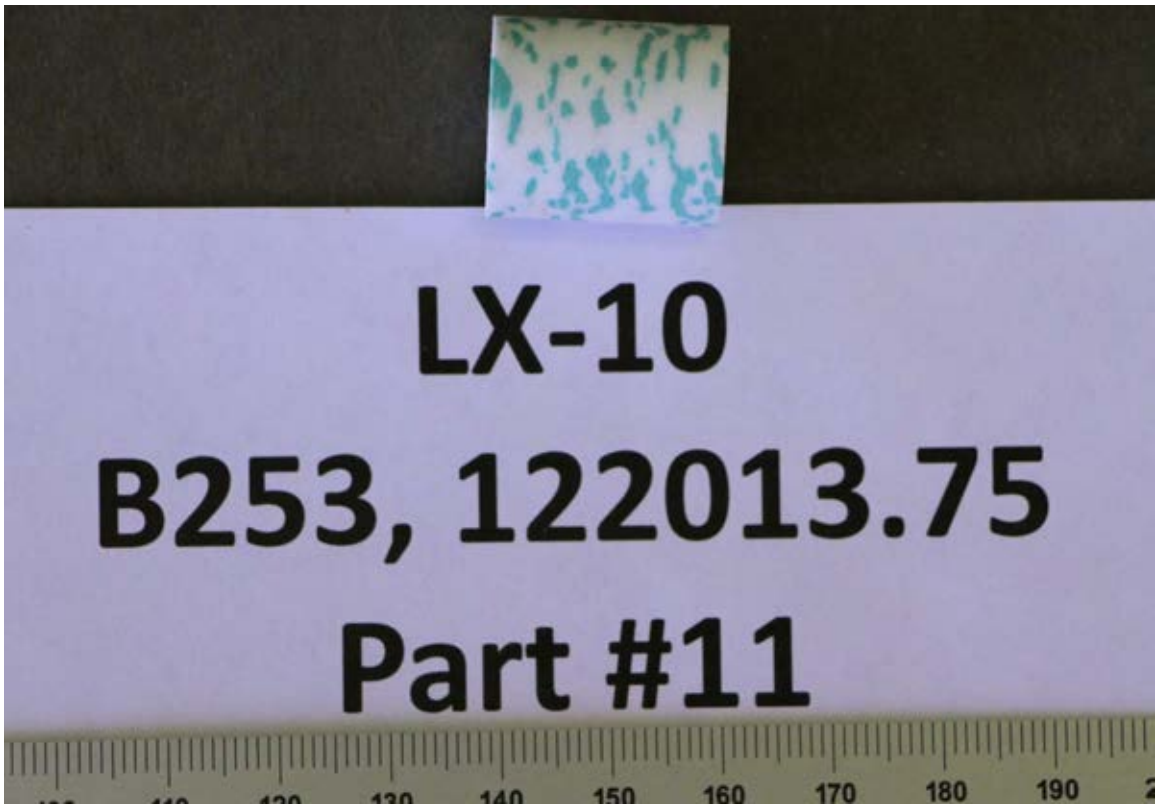
LX-10
B253, 122013.75
Part #11

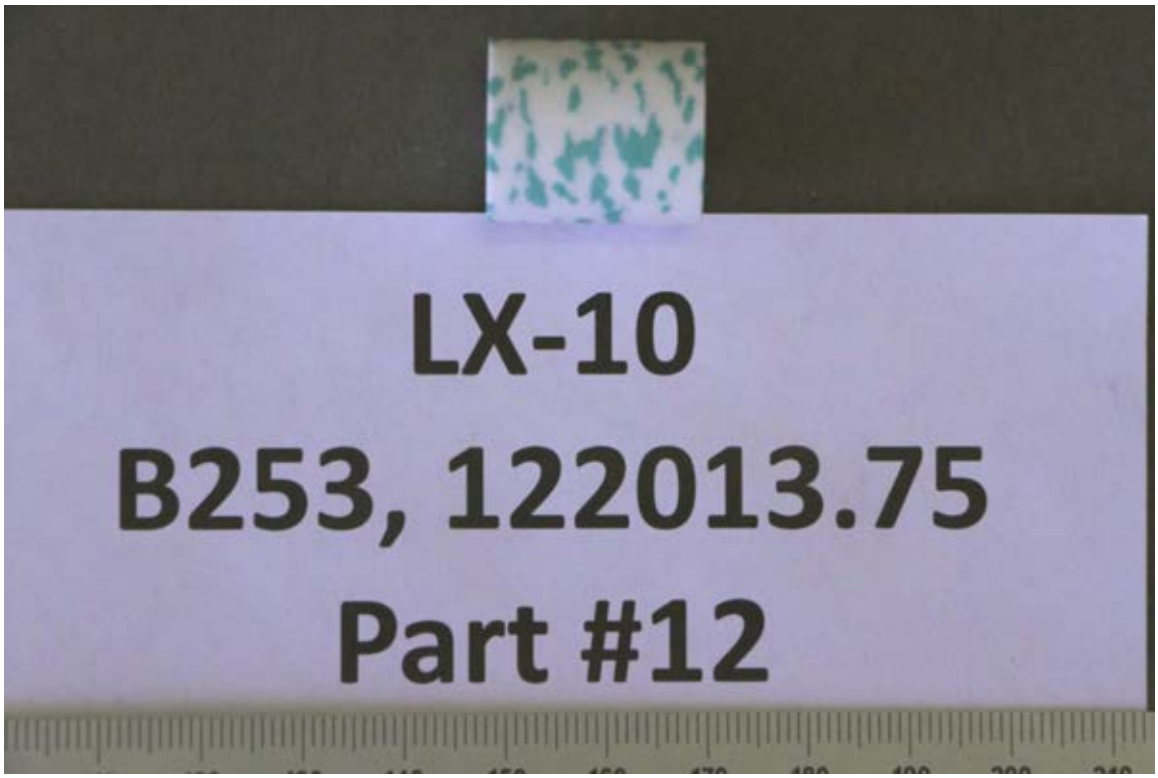
LX-10
B253, 122013.75
Part #12

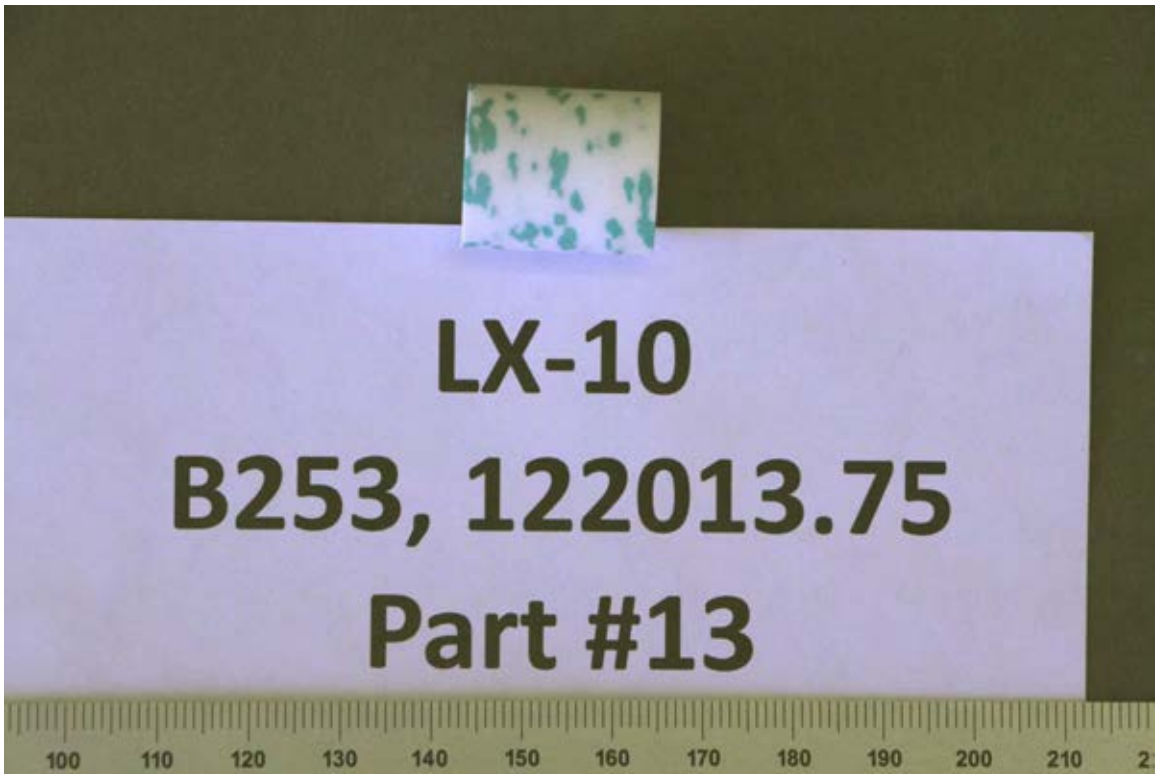
LX-10
B253, 122013.75
Part #13
100 110 120 130 140 150 160 170 180 190 200 210

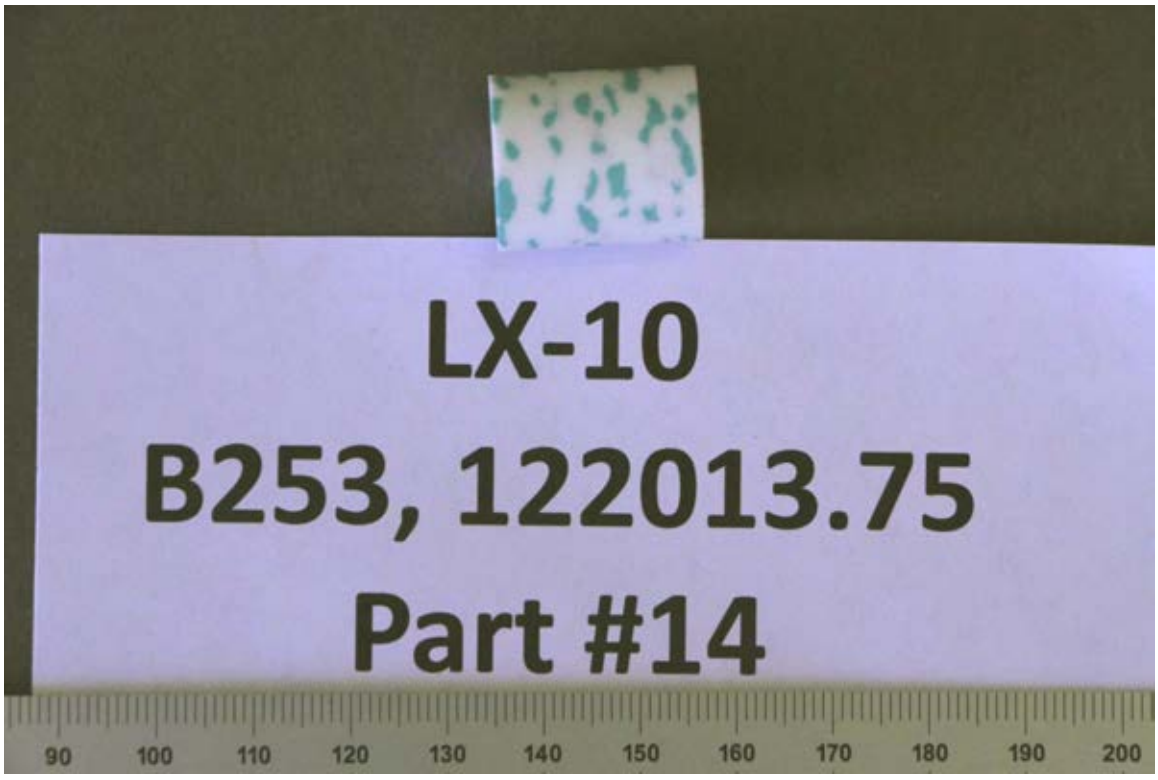
LX-10
B253, 122013.75
Part #14
90 100 110 120 130 140 150 160 170 180 190 200

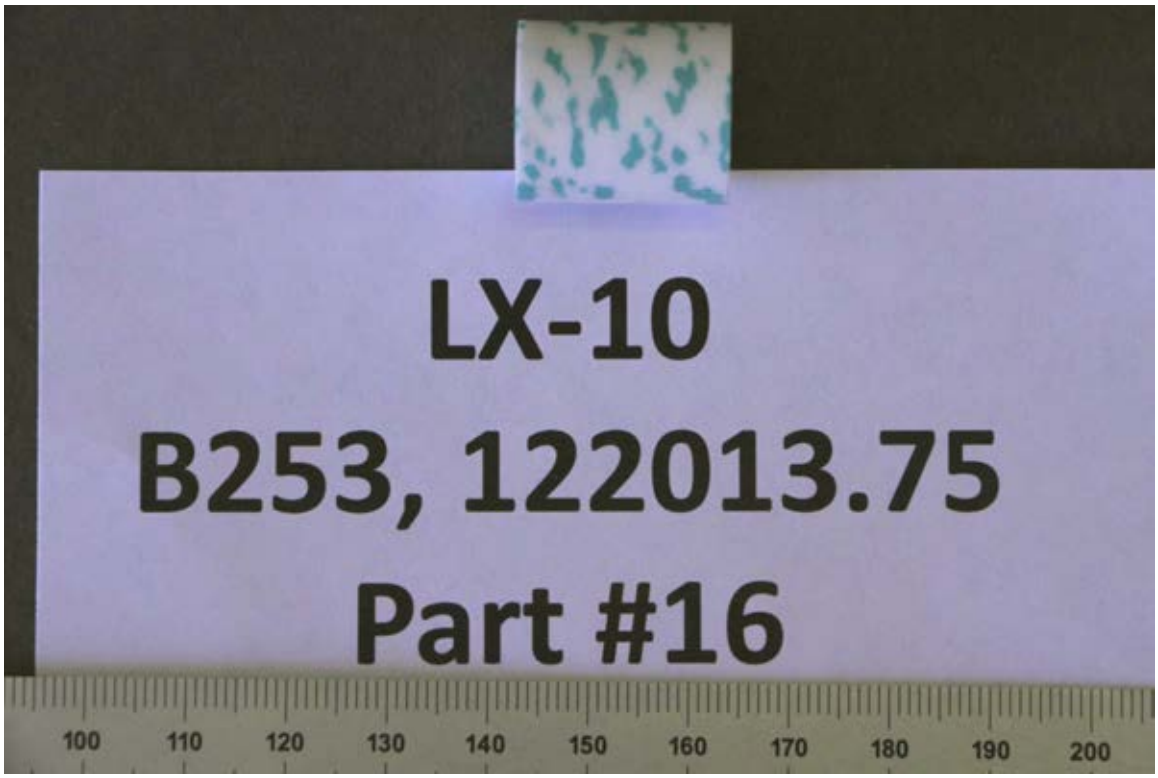
LX-10
B253, 122013.75
Part #16
100 110 120 130 140 150 160 170 180 190 200

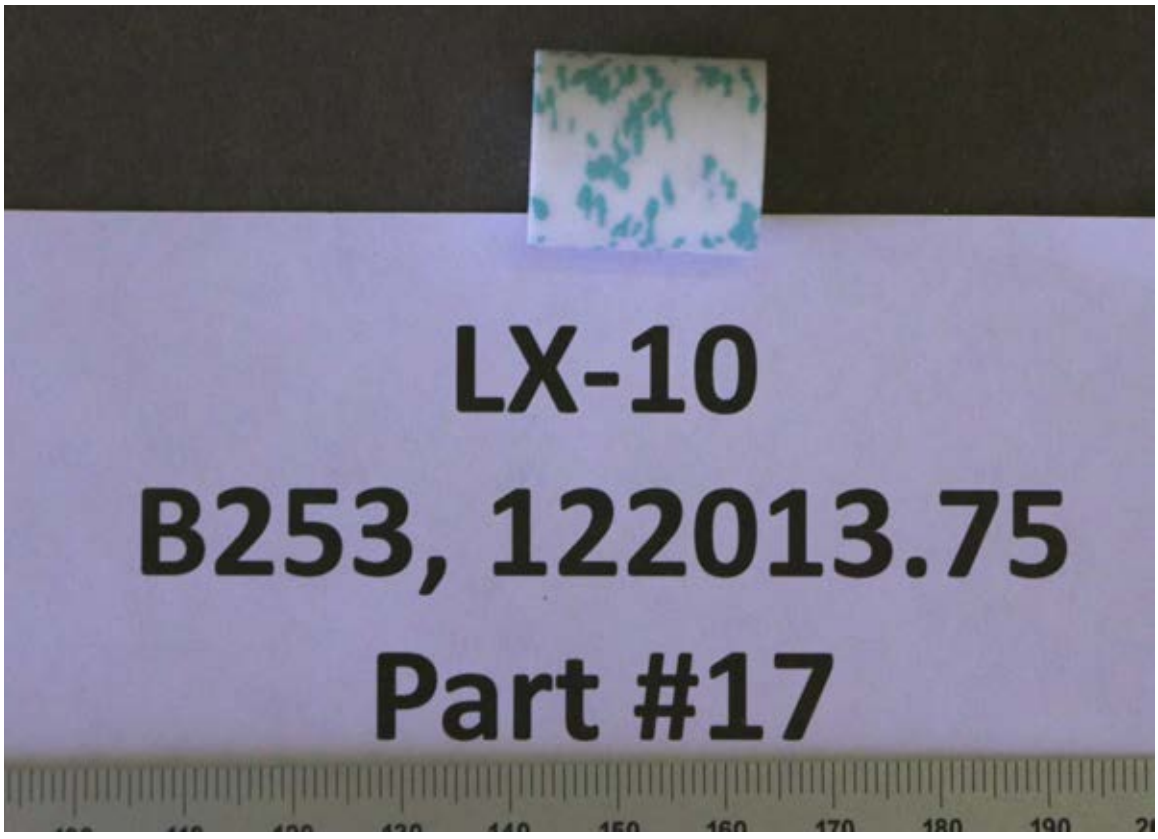
LX-10
B253, 122013.75
Part #17

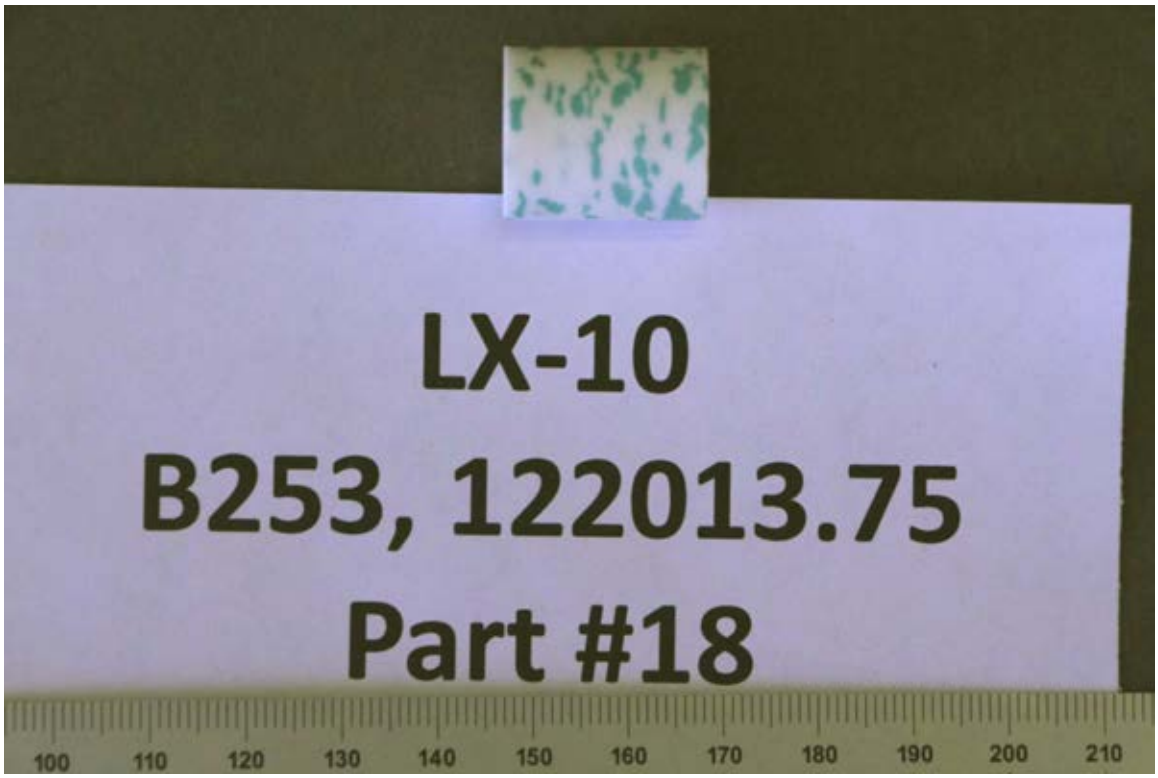
LX-10
B253, 122013.75
Part #18
100 110 120 130 140 150 160 170 180 190 200 210

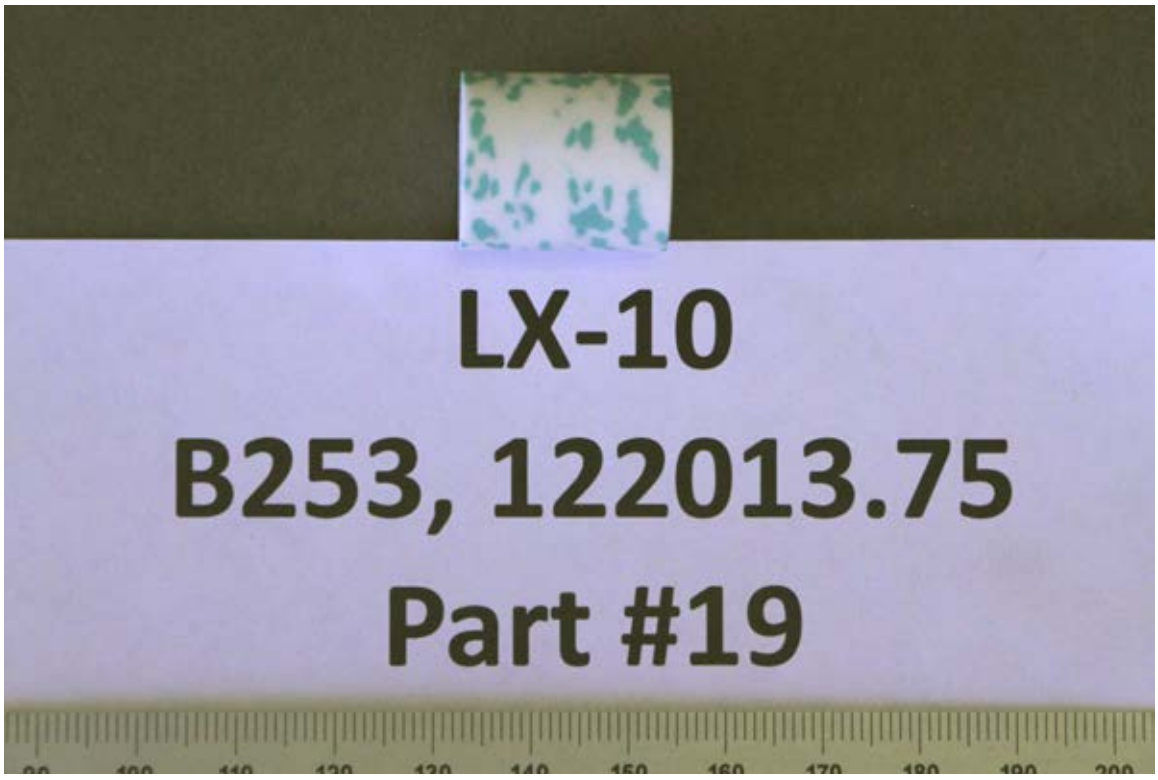
LX-10
B253, 122013.75
Part #19

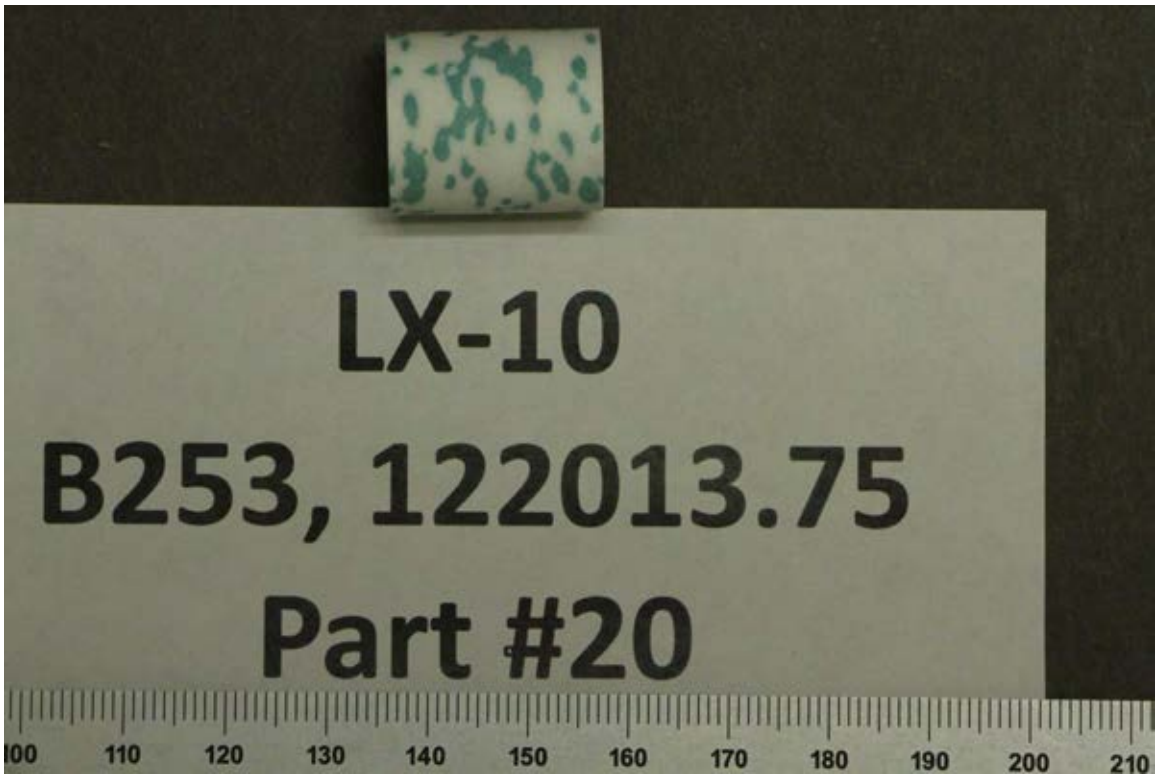
LX-10
B253, 122013.75
Part #20
100 110 120 130 140 150 160 170 180 190 200 210

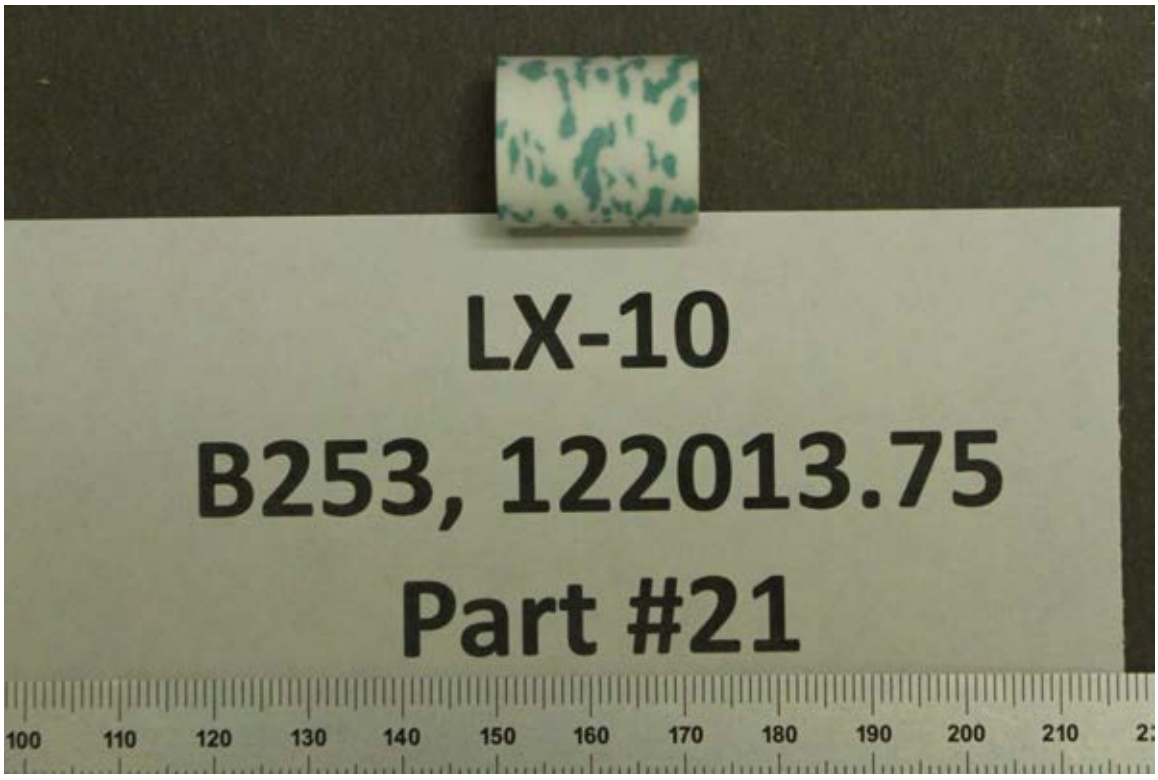
LX-10
B253, 122013.75
Part #21
100 110 120 130 140 150 160 170 180 190 200 210

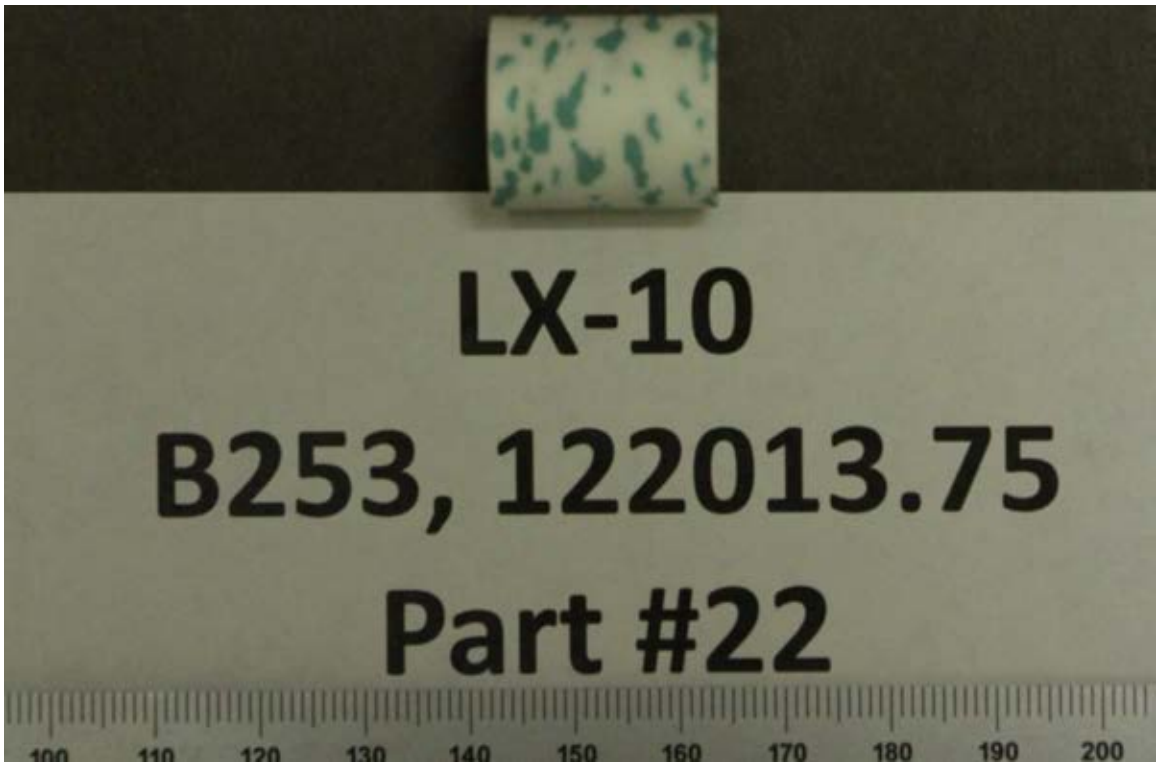
LX-10
B253, 122013.75
Part #22
100 110 120 130 140 150 160 170 180 190 200

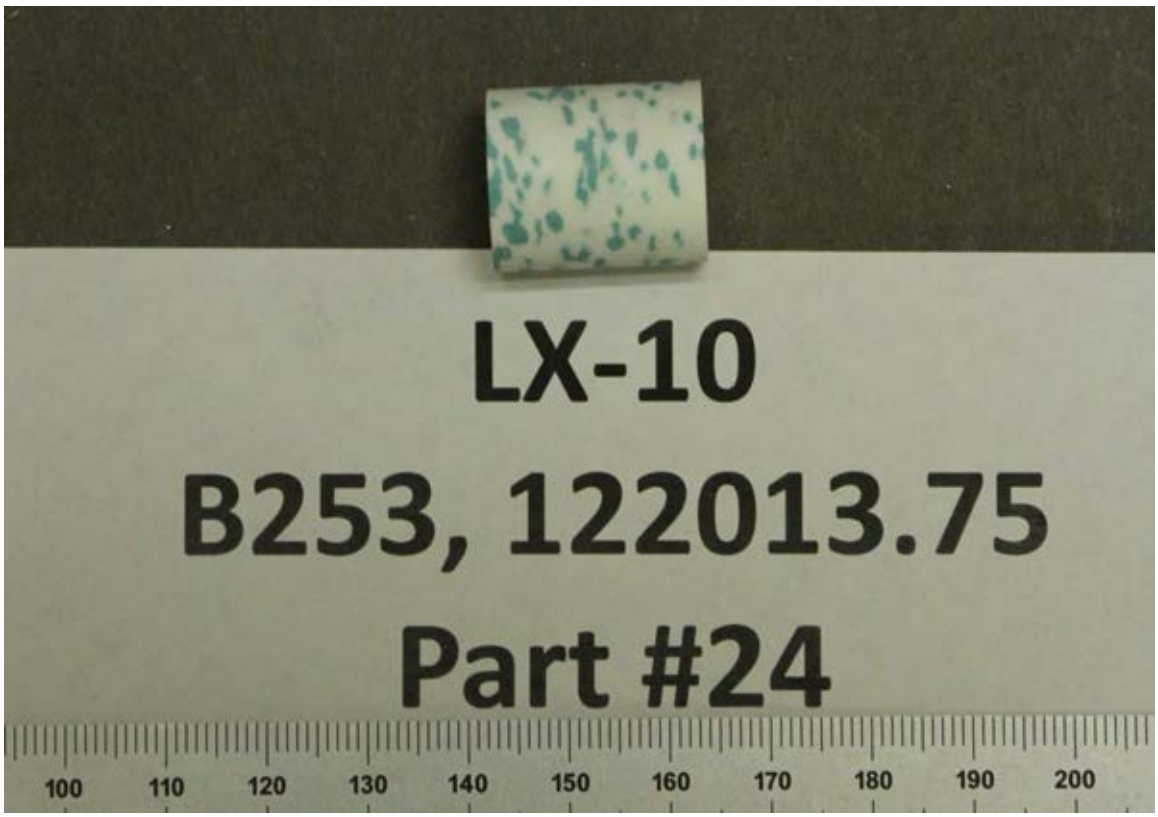
LX-10
B253, 122013.75
Part #24
100 110 120 130 140 150 160 170 180 190 200

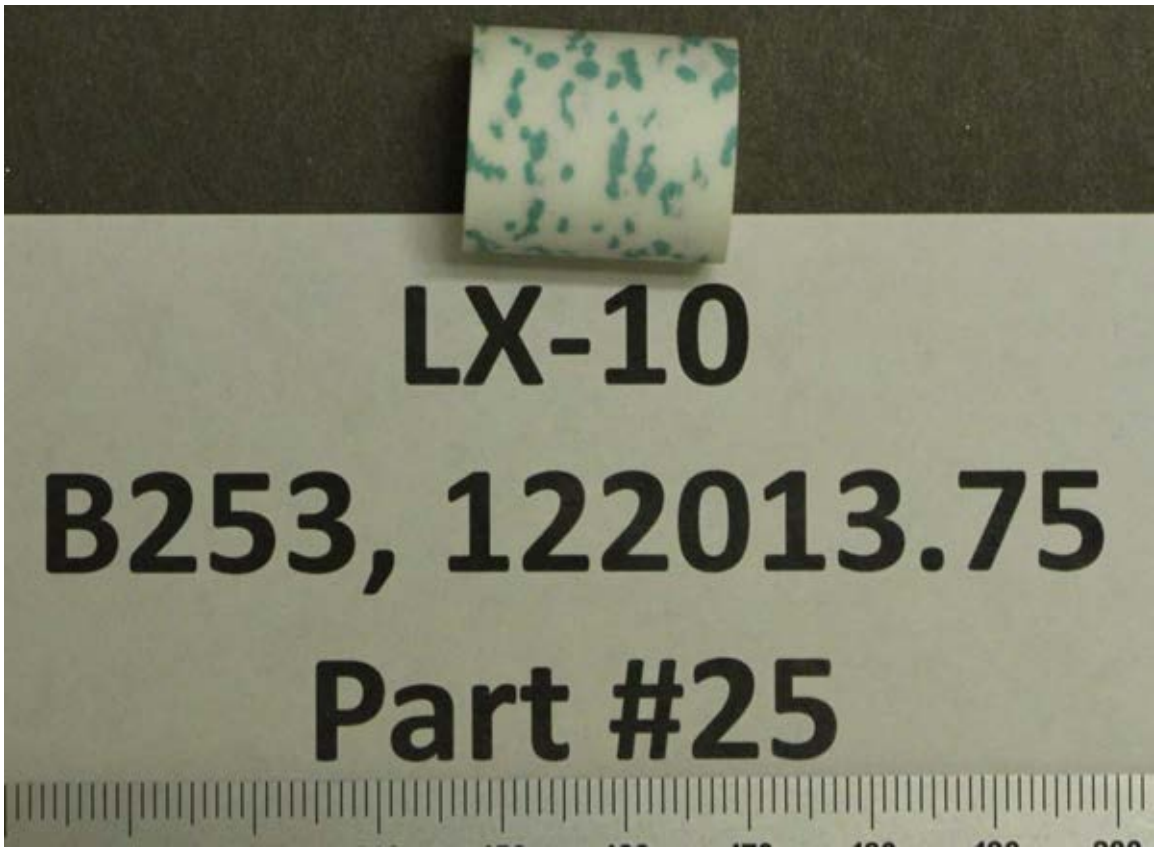
LX-10
B253, 122013.75
Part #25

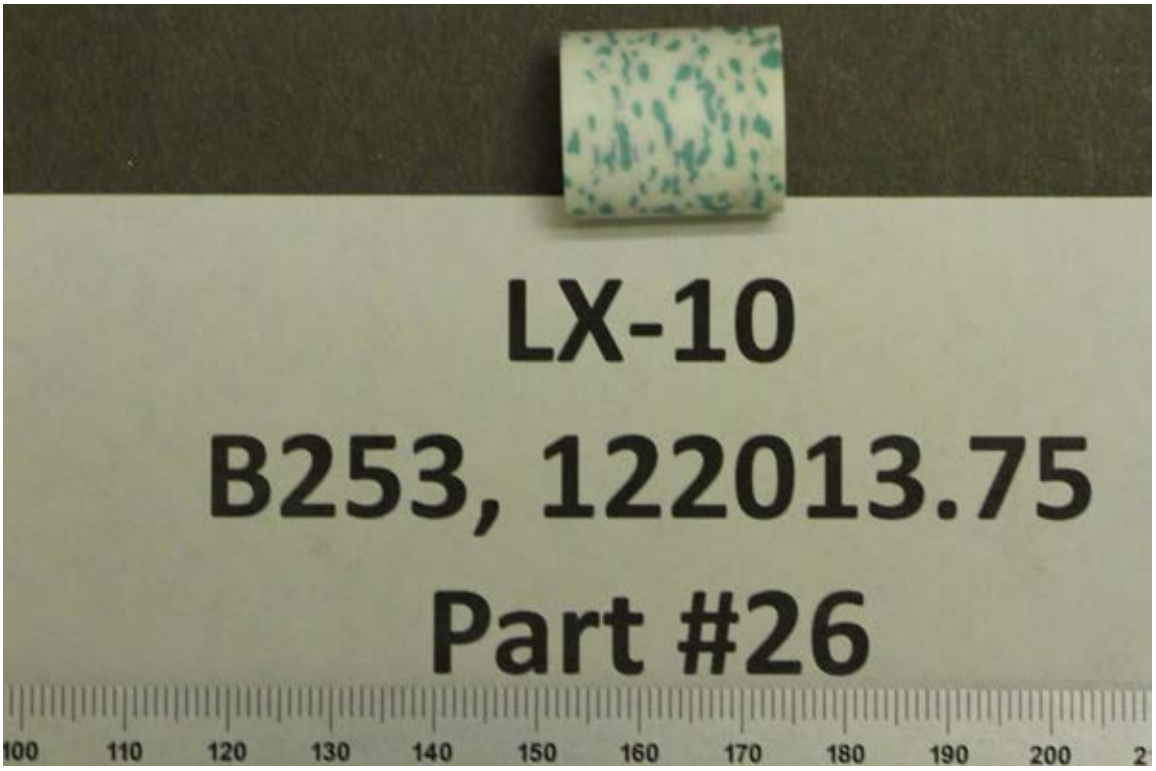
LX-10
B253, 122013.75
Part #26
100 110 120 130 140 150 160 170 180 190 200


LX-10
B253, 122013.75
Part #27
120 130 140 150 160 170 180 190 200

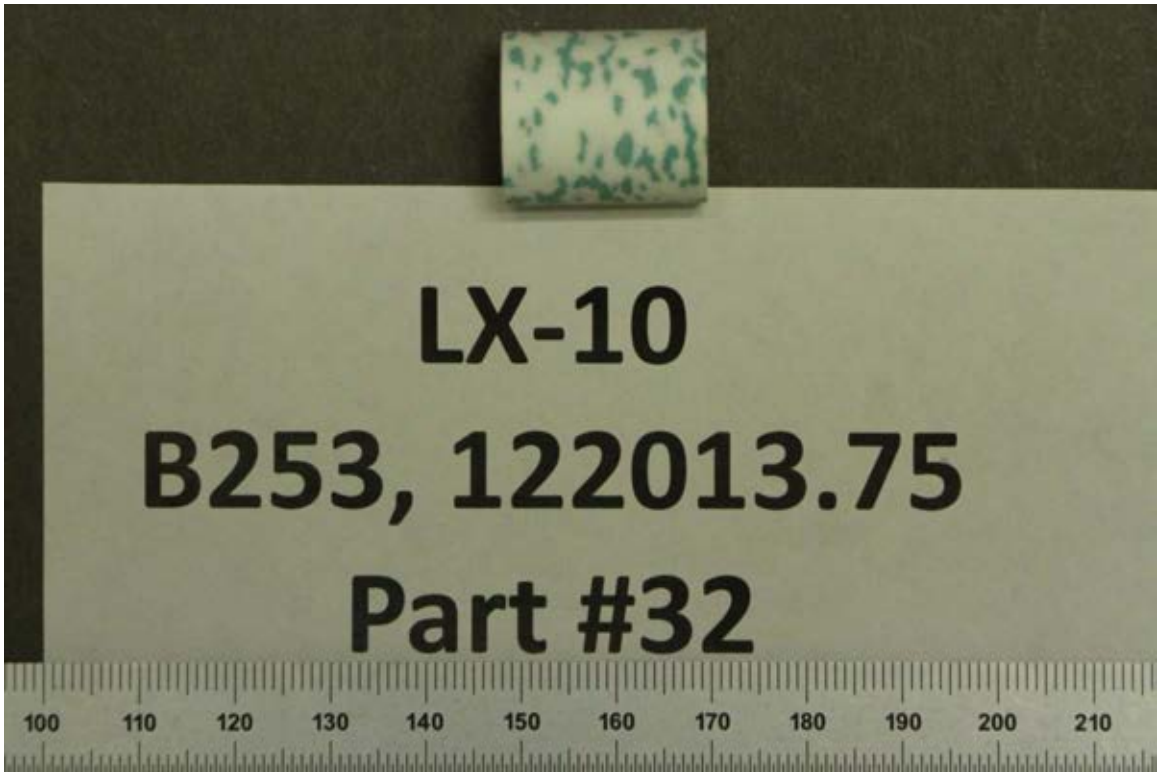
LX-10
B253, 122013.75
Part #32
100 110 120 130 140 150 160 170 180 190 200 210

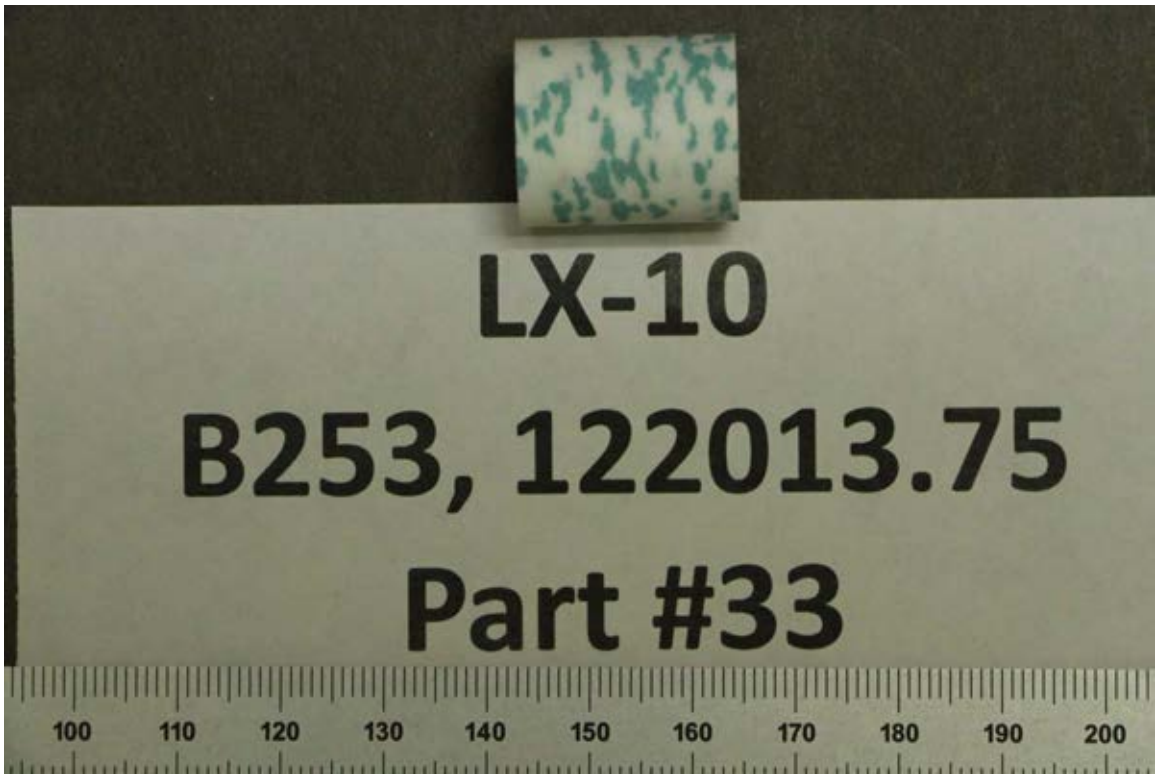
LX-10
B253, 122013.75
Part #33
100 110 120 130 140 150 160 170 180 190 200

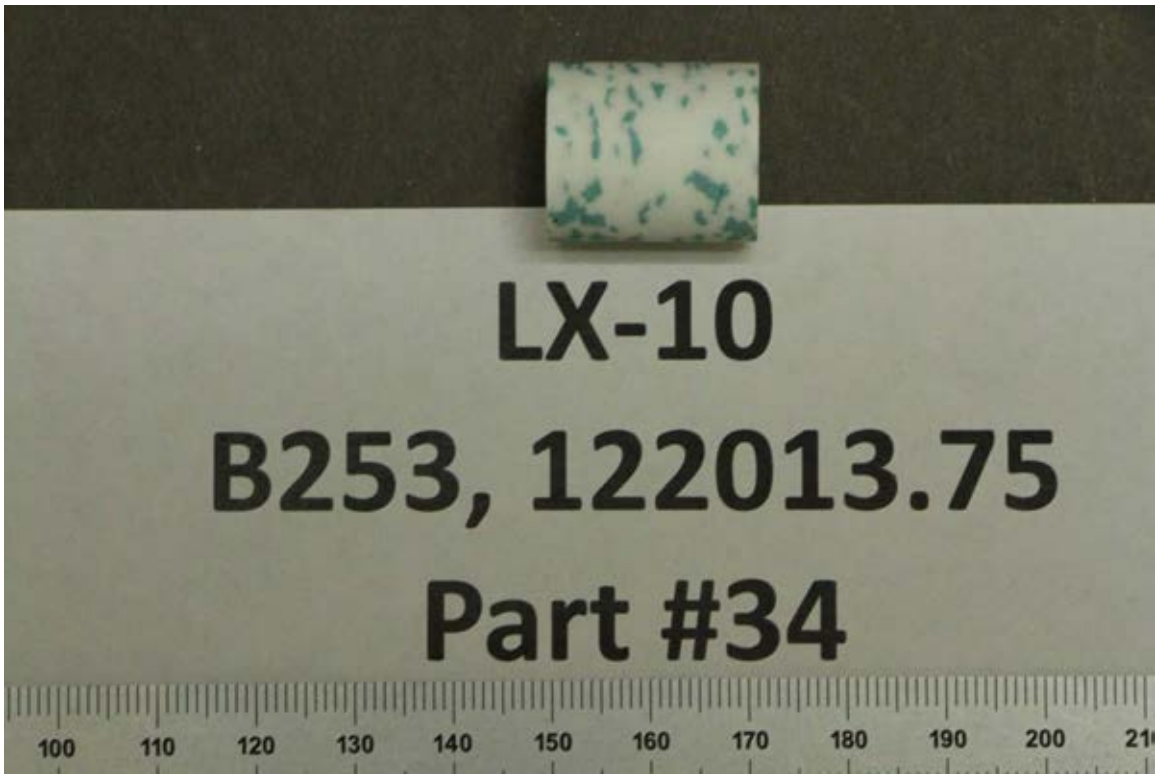
LX-10
B253, 122013.75
Part #34
100 110 120 130 140 150 160 170 180 190 200

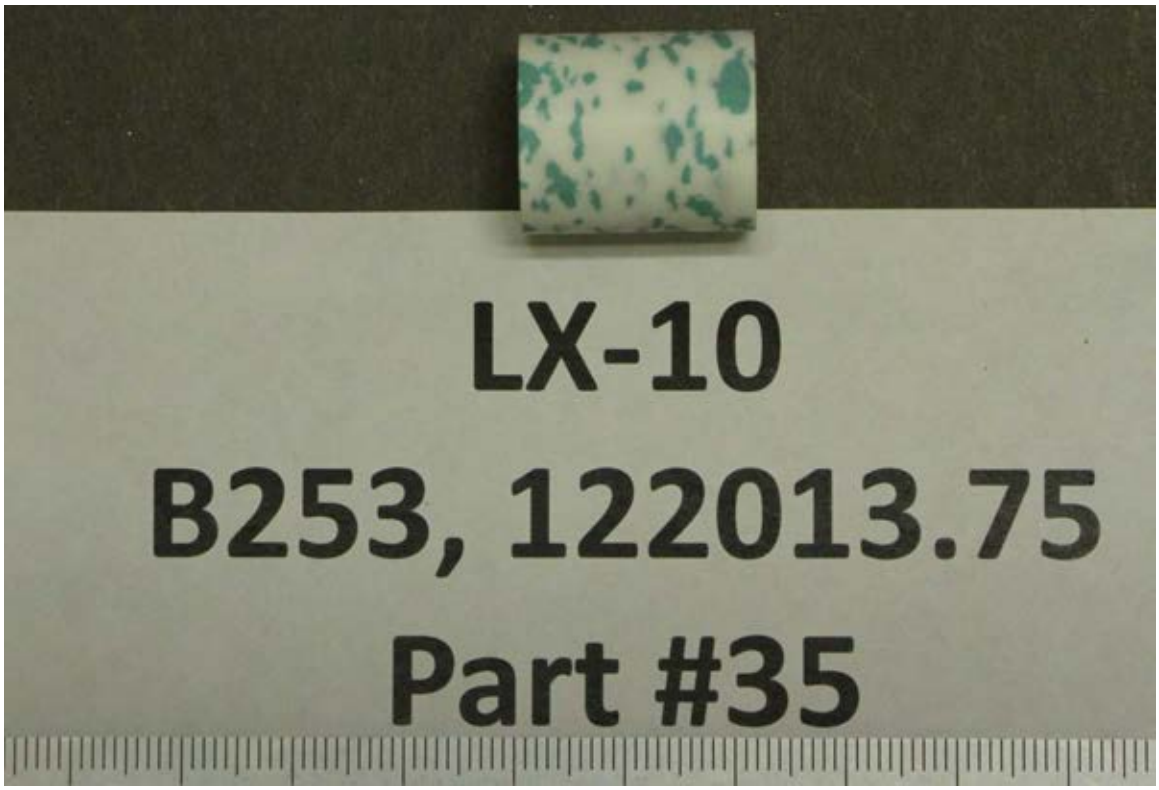
LX-10
B253, 122013.75
Part #35

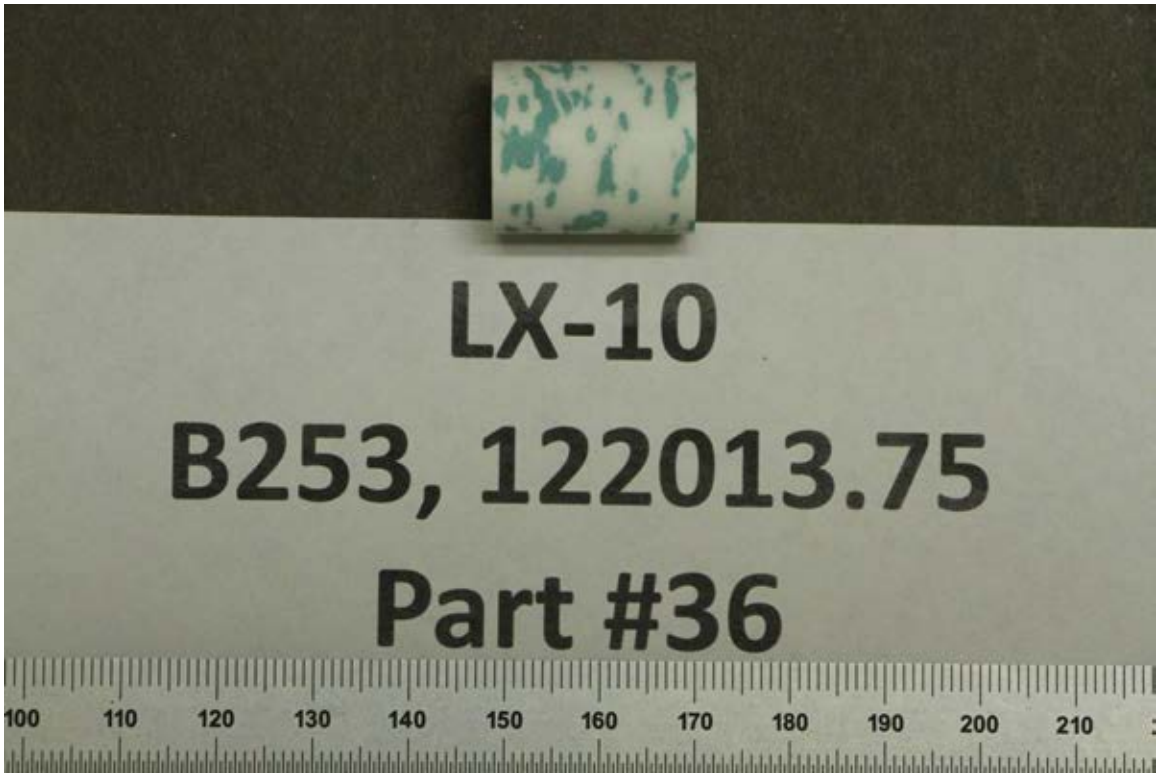
LX-10
B253, 122013.75
Part #36
100
110
120
130
140
150
160
170
180
190
200
210


LX-10
B253, 122013.75
Part #37
100 110 120 130 140 150 160 170 180 190 200

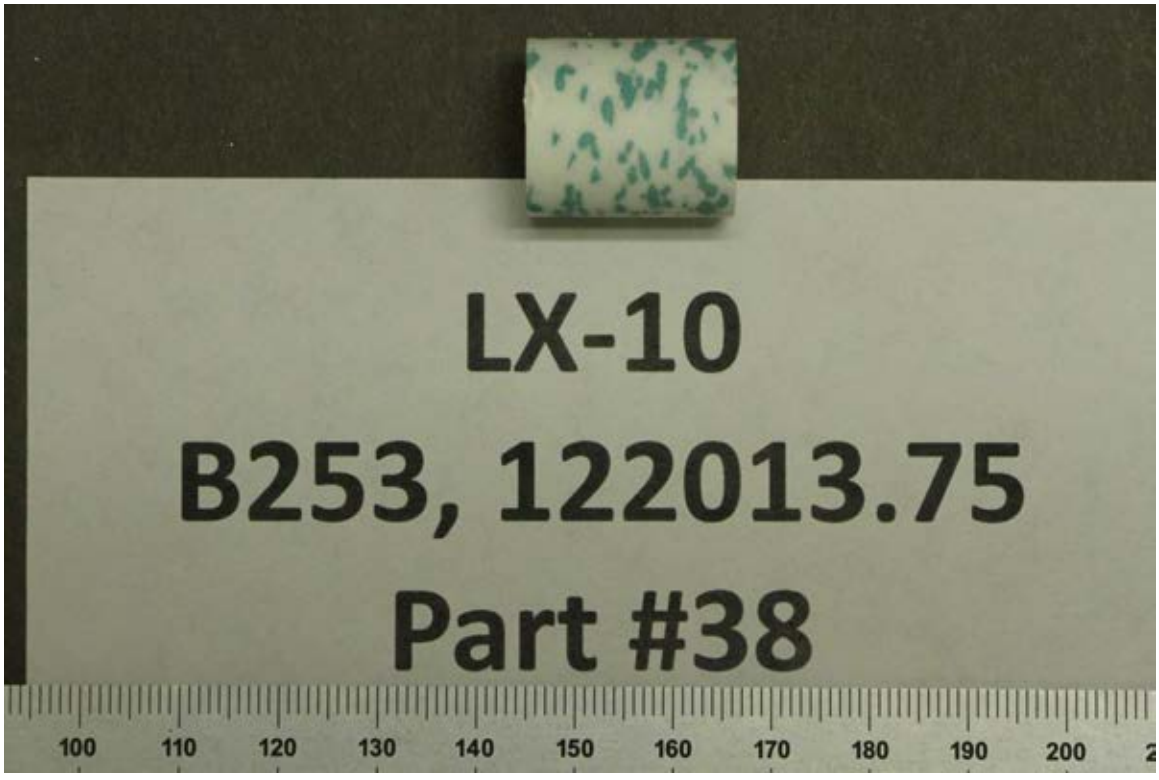
LX-10
B253, 122013.75
Part #38
100 110 120 130 140 150 160 170 180 190 200

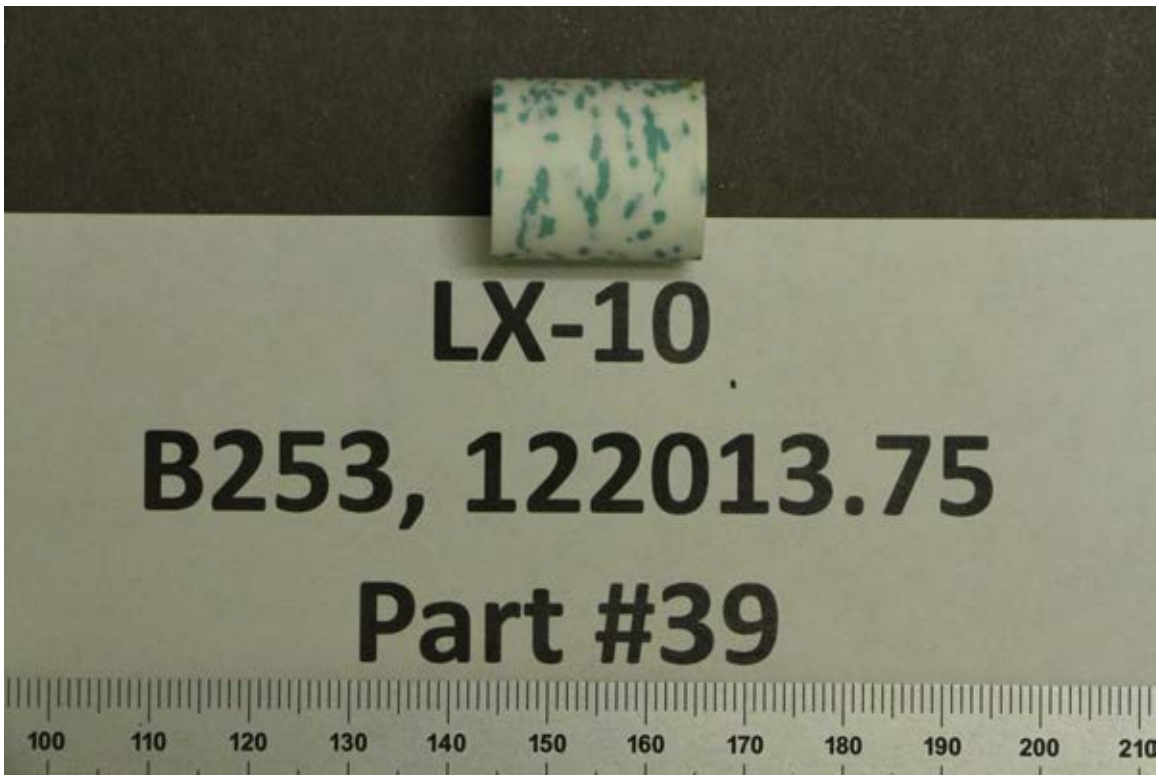
LX-10
B253, 122013.75
Part #39
100 110 120 130 140 150 160 170 180 190 200 210

Undamaged Spheres

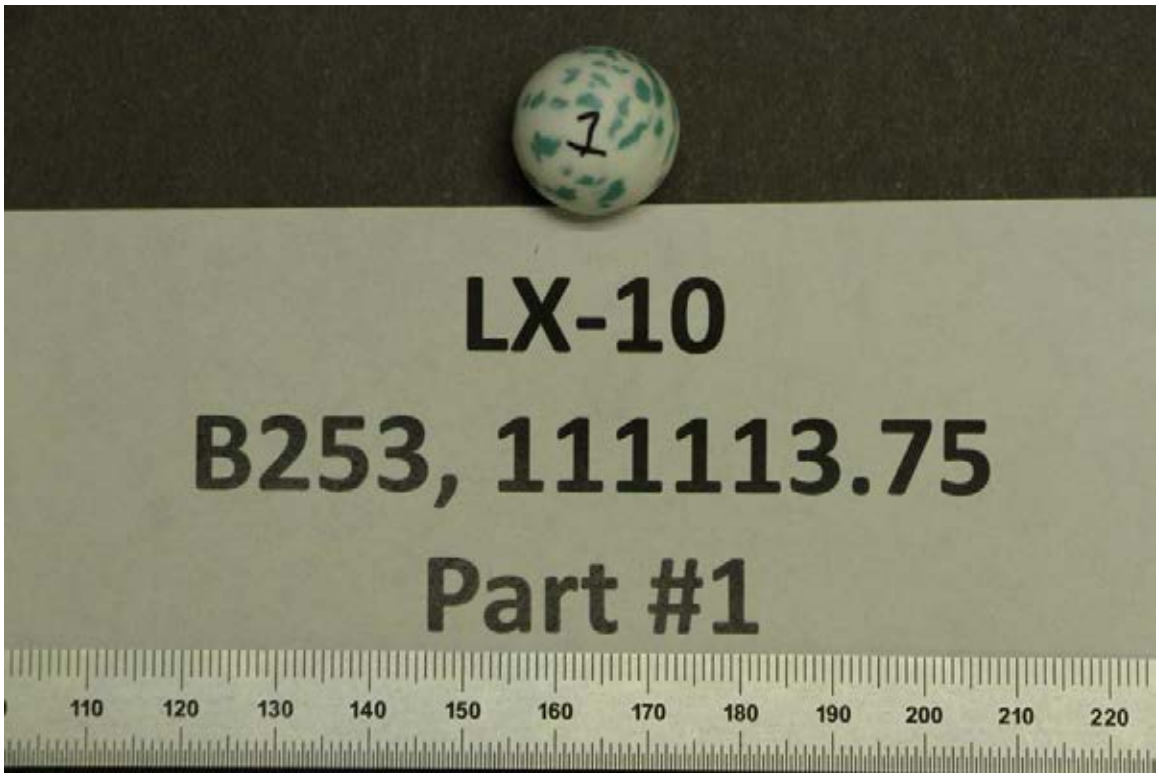

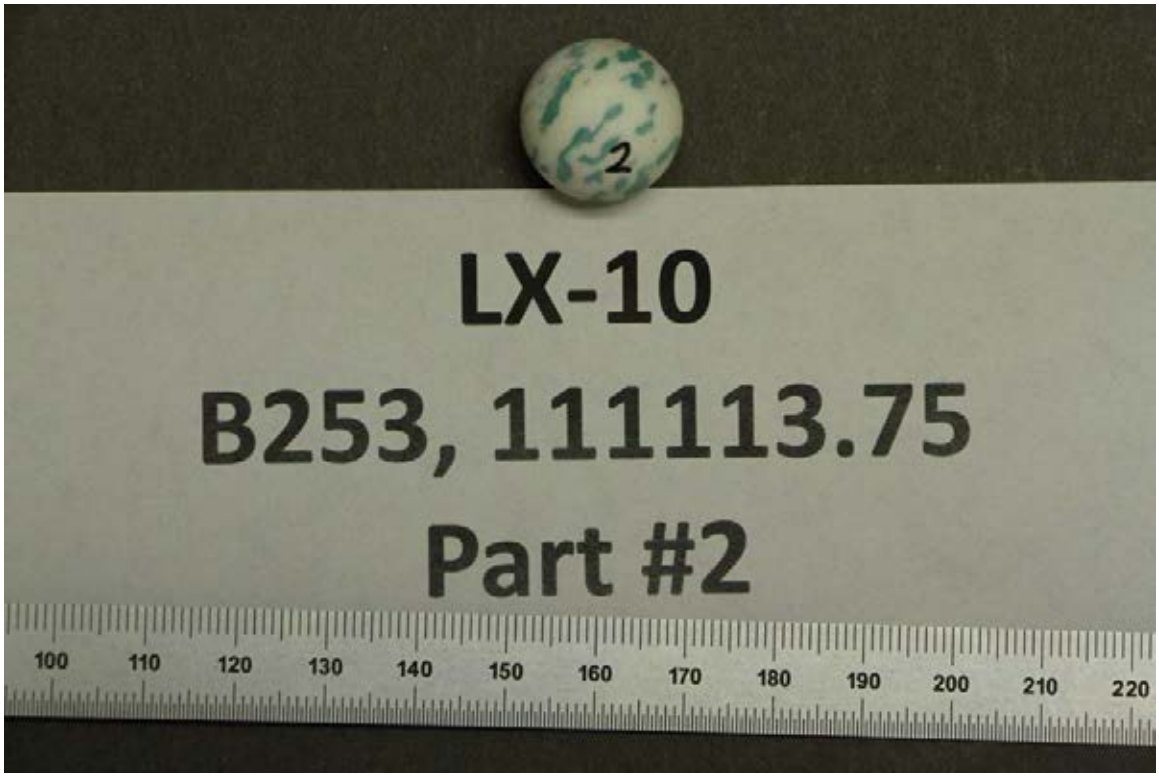


LX-10
B253, 111113.75
Part #3
00 110 120 130 140 150 160 170 180 190 200 210 220


LX-10
B253, 111113.75
Part #4
0 100 110 120 130 140 150 160 170 180 190 20


5
LX-10
B253, 111113.75
Part #5
70 80 90 100 110 120 130 140 150 160 170


6
LX-10
B253, 111113.75
Part #6
110 120 130 140 150 160 170 180 190 200 210


LX-10
B253, 111113.75
Part #7
90 100 110 120 130 140 150 160 170 180 190


8
LX-10
B253, 111113.75
Part #8
90 100 110 120 130 140 150 160 170 180 190 200 210

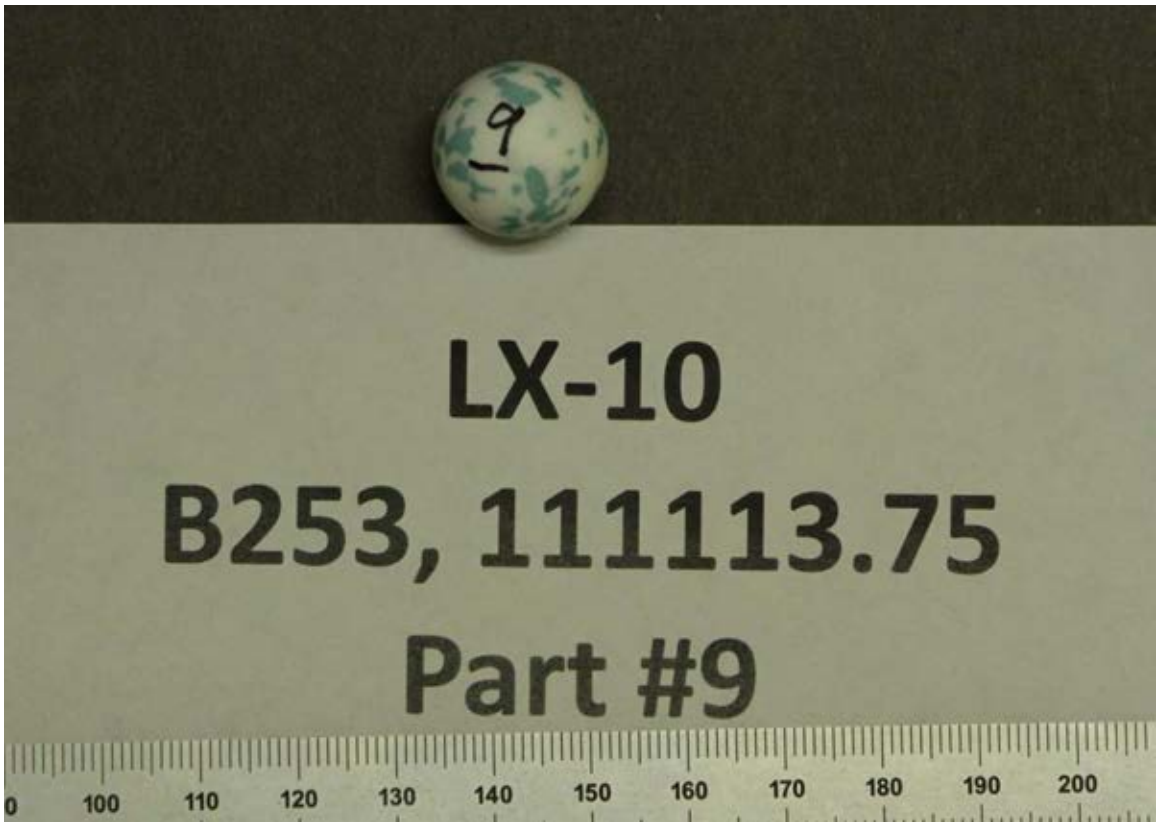
9
LX-10
B253, 111113.75
Part #9
0 100 110 120 130 140 150 160 170 180 190 200


10
LX-10
B253, 111113.75
Part #10
90 100 110 120 130 140 150 160 170 180 190 200 210 220

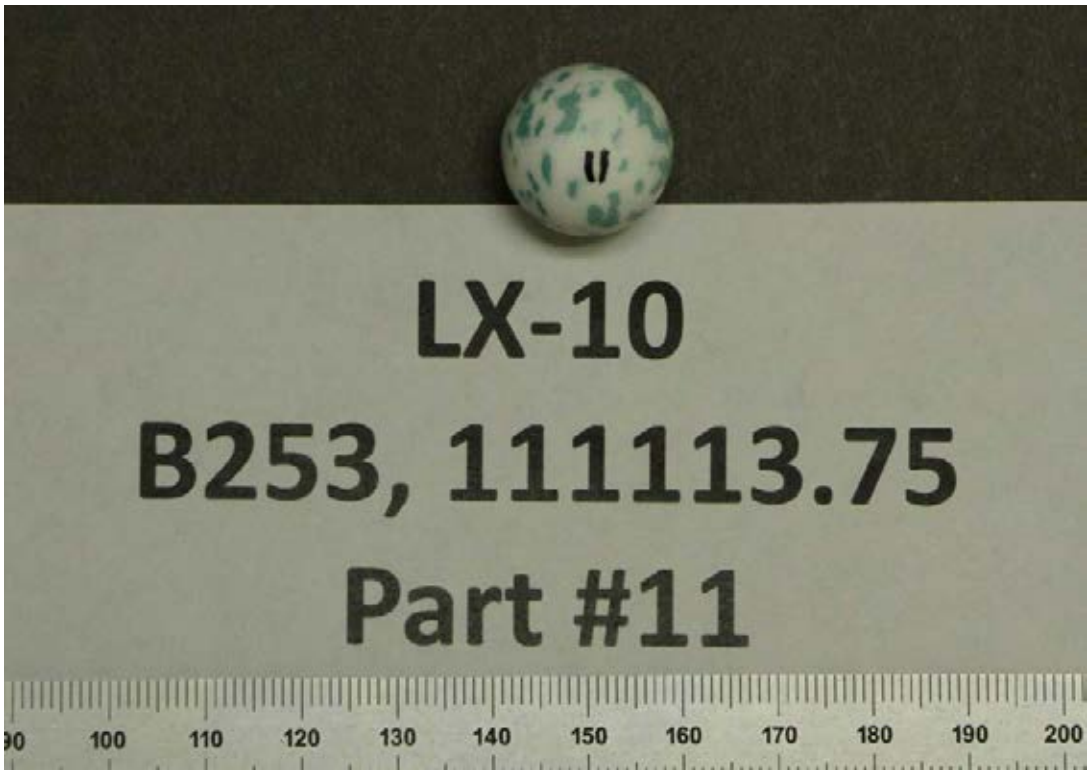
11
LX-10
B253, 111113.75
Part #11
100 110 120 130 140 150 160 170 180 190 200

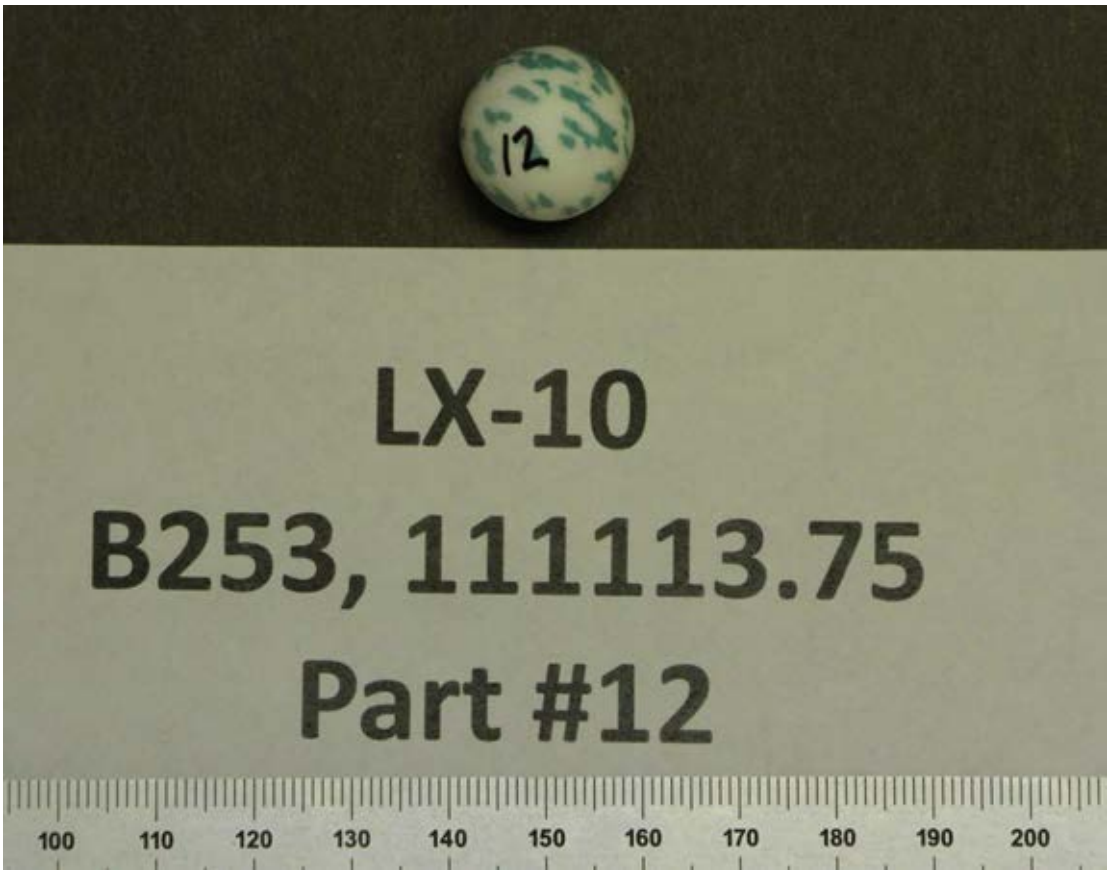
12
LX-10
B253, 111113.75
Part #12
100 110 120 130 140 150 160 170 180 190 200

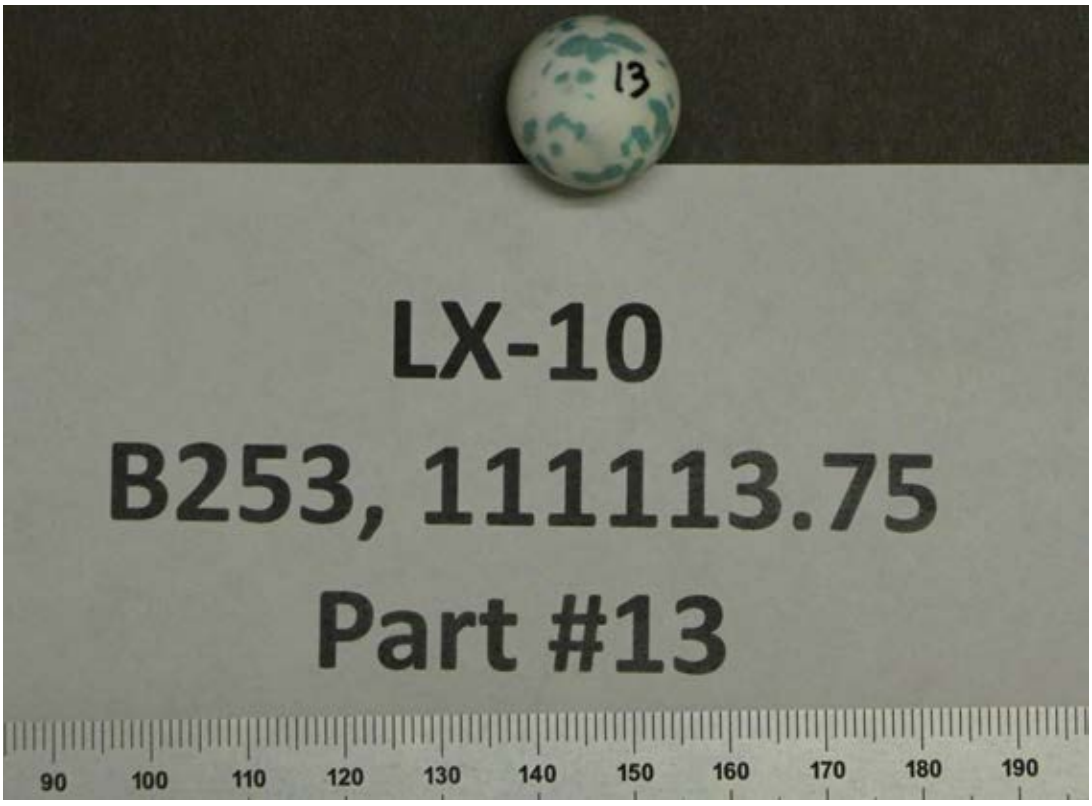
13
LX-10
B253, 111113.75
Part #13
90 100 110 120 130 140 150 160 170 180 190

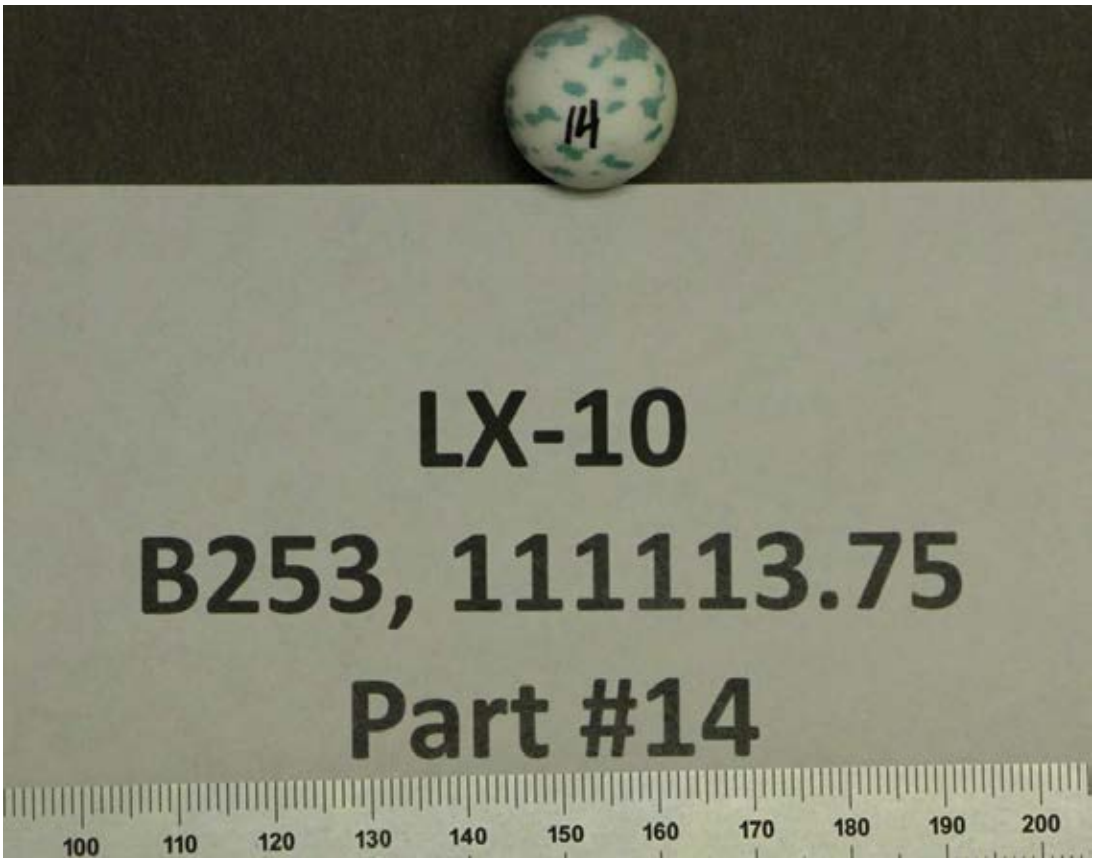
14
LX-10
B253, 111113.75
Part #14
100 110 120 130 140 150 160 170 180 190 200

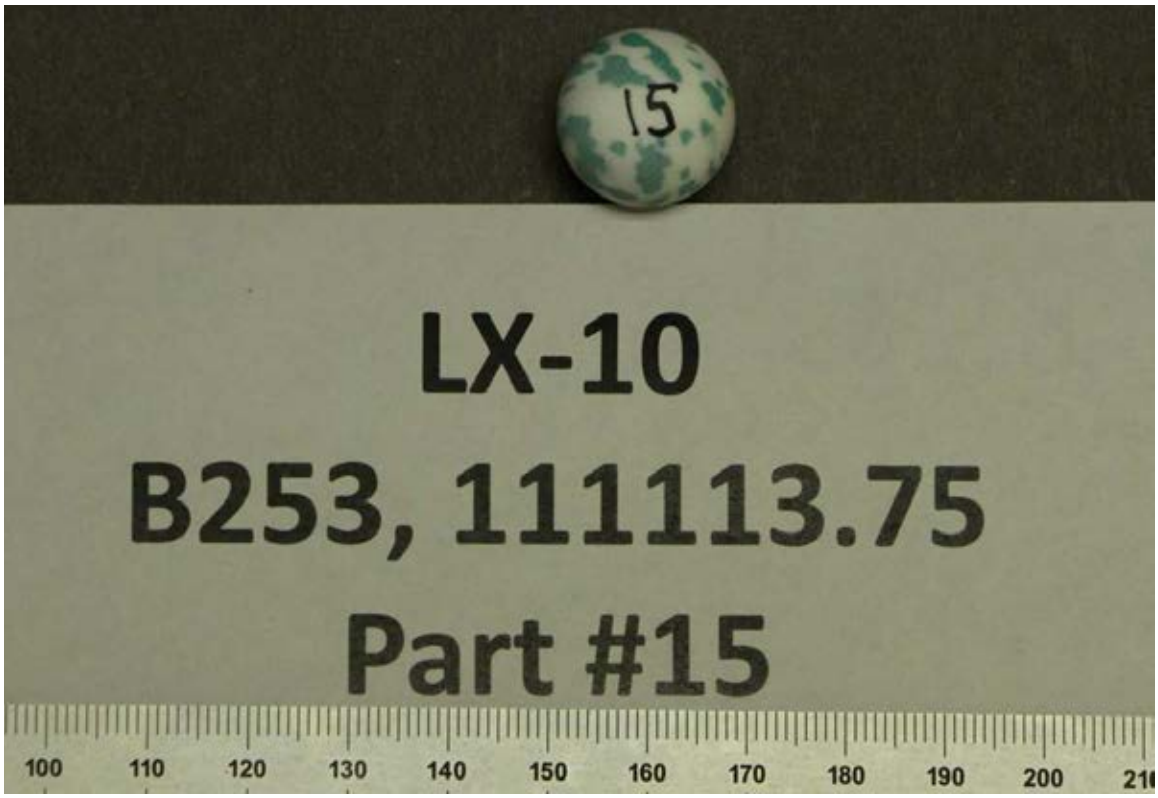
15
LX-10
B253, 111113.75
Part #15
100 110 120 130 140 150 160 170 180 190 200

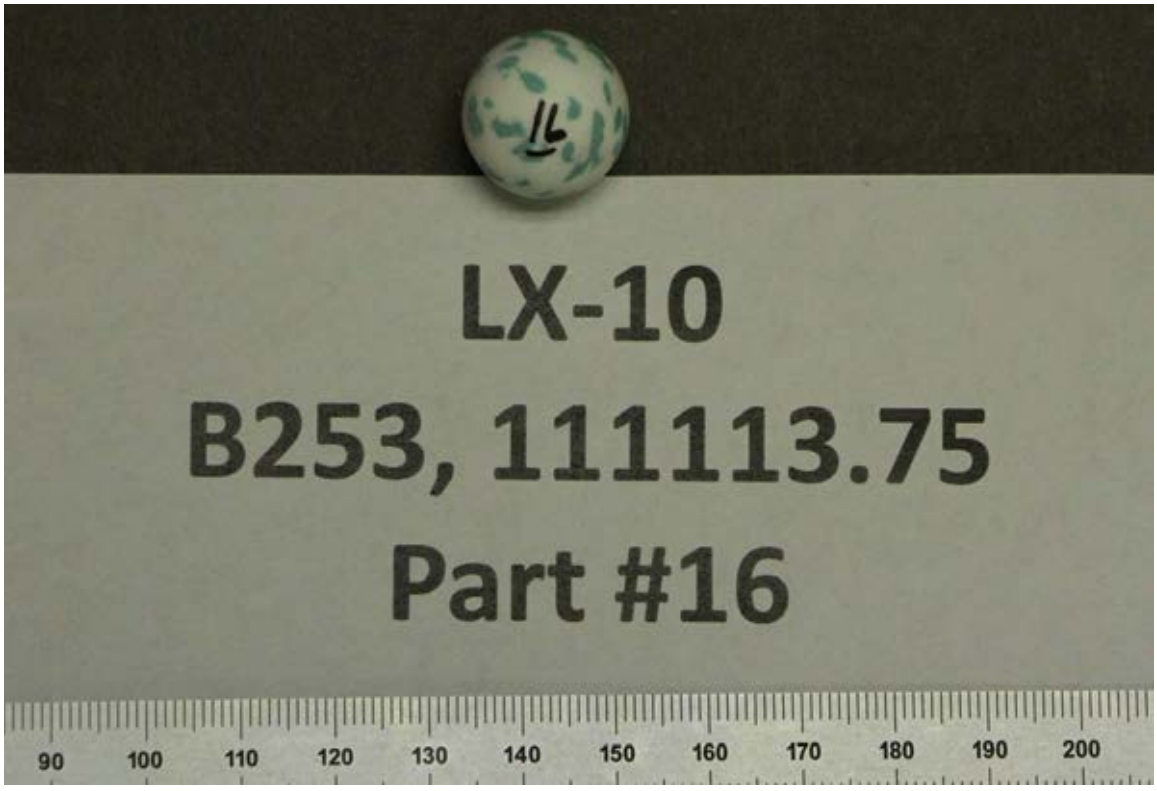
16
LX-10
B253, 111113.75
Part #16
90 100 110 120 130 140 150 160 170 180 190 200

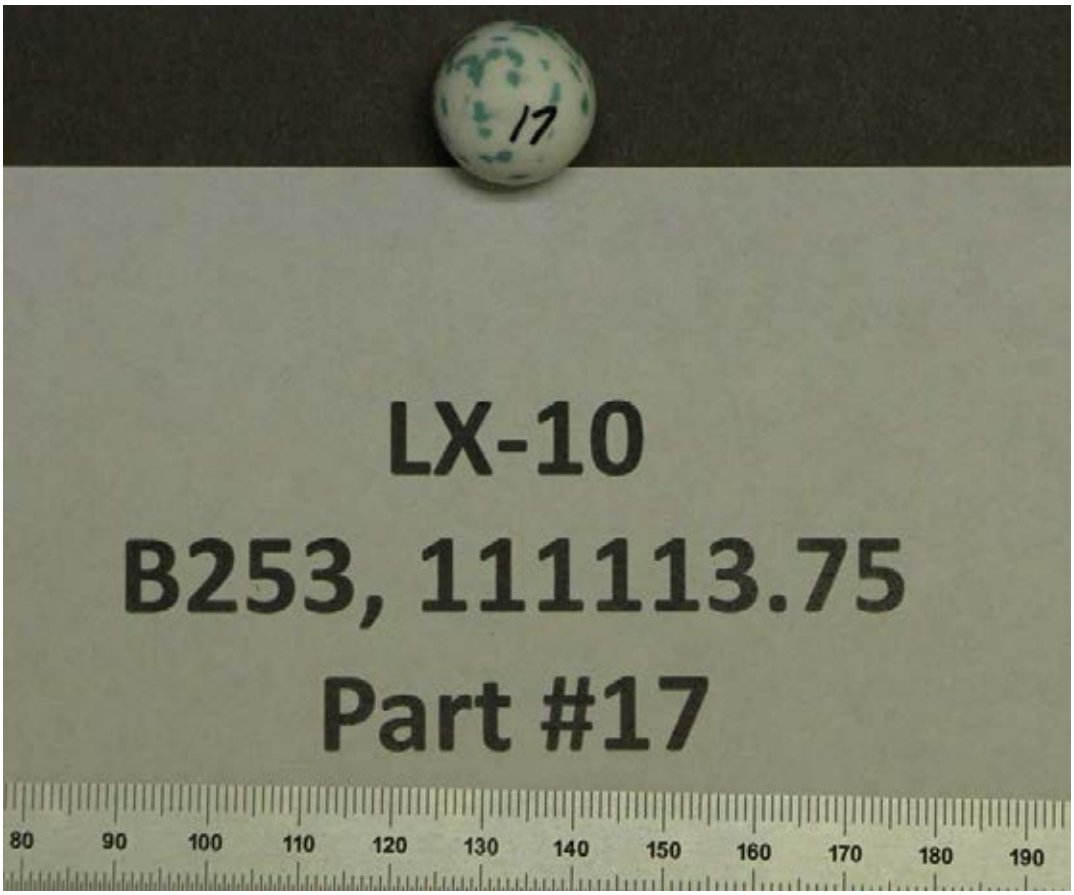
17
LX-10
B253, 111113.75
Part #17
80 90 100 110 120 130 140 150 160 170 180 190

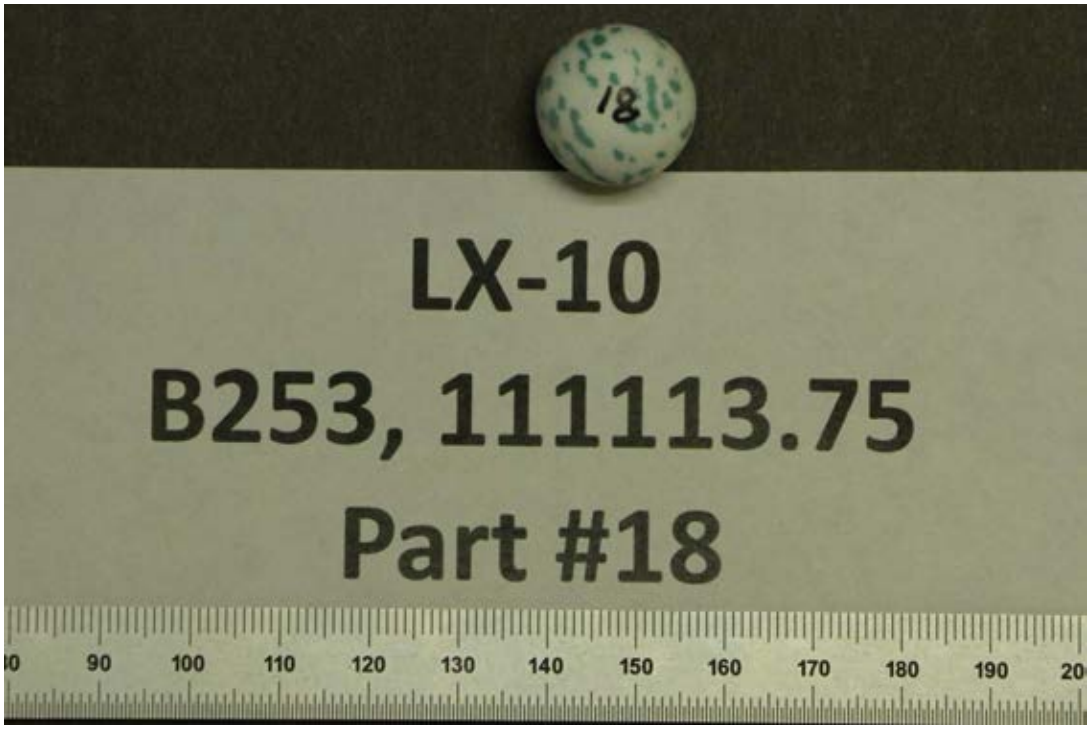
18
LX-10
B253, 111113.75
Part #18
90 100 110 120 130 140 150 160 170 180 190

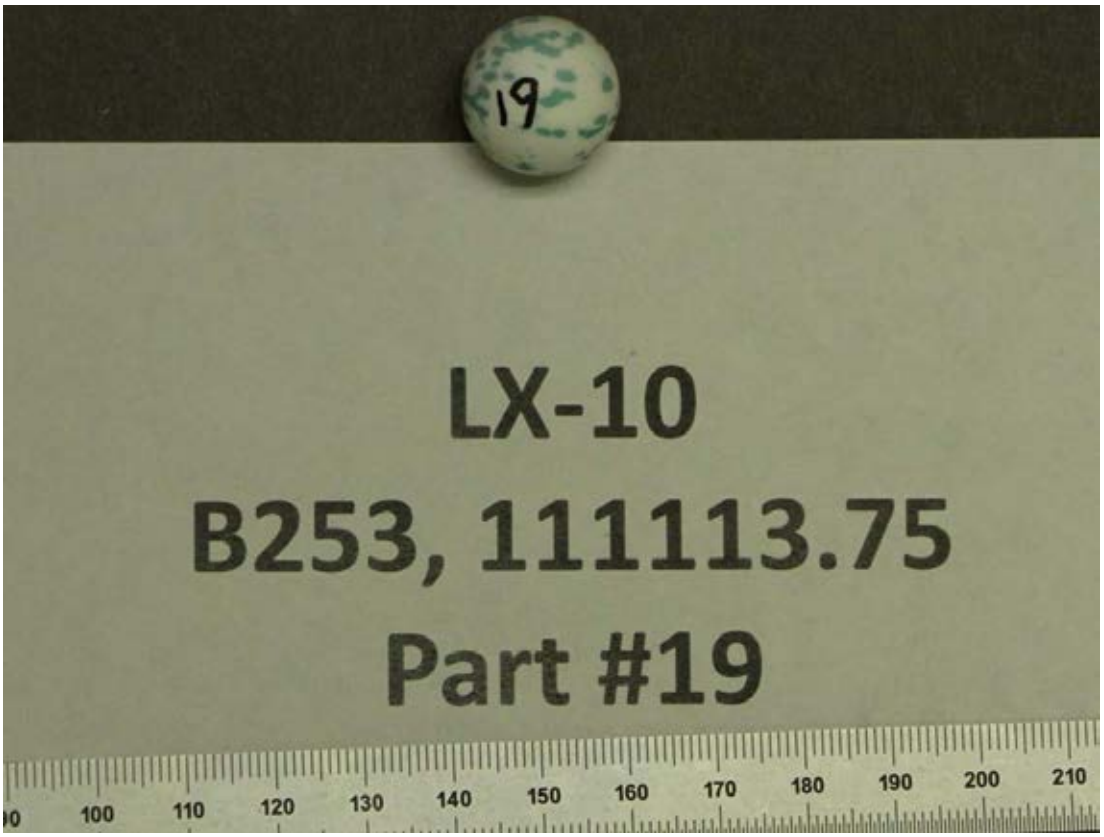
19
LX-10
B253, 111113.75
Part #19
100
110
120
130
140
150
160
170
180
190
200
210


21
LX-10
B253, 111113.75
Part #21
90
100
110
120
130
140
150
160
170
180
190

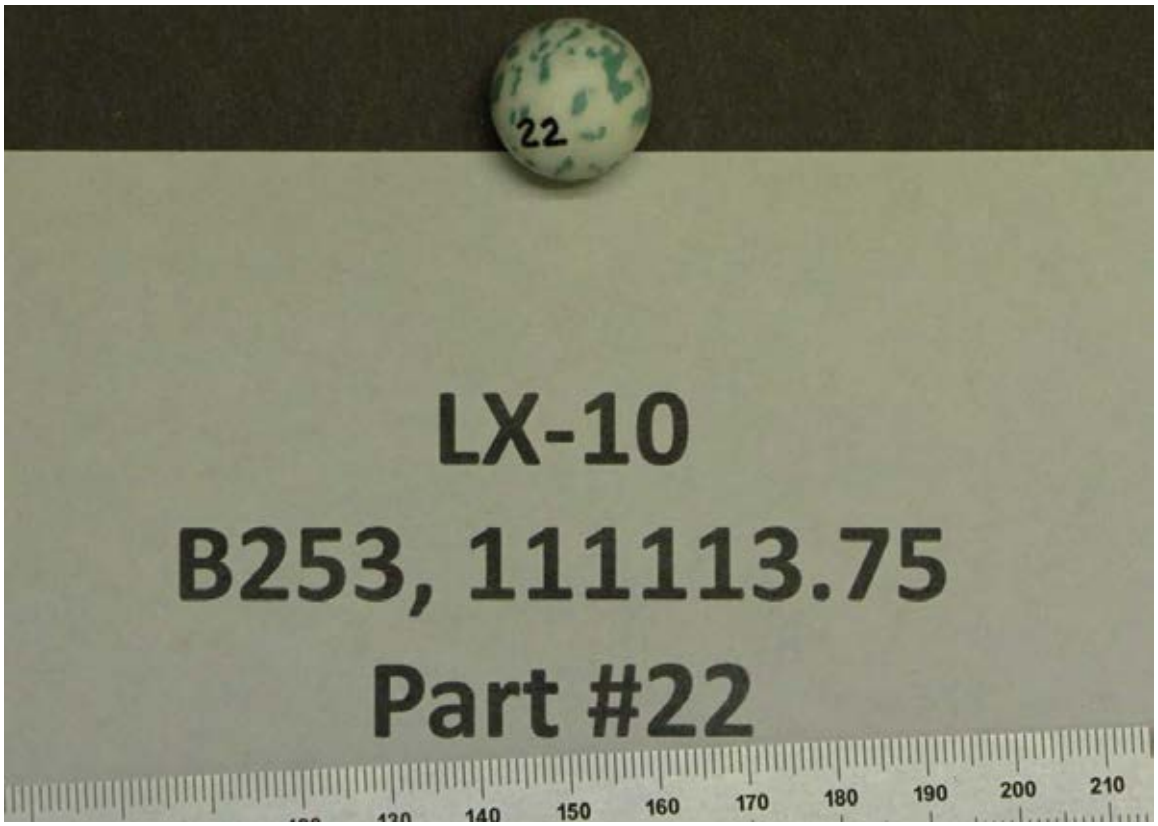
22
LX-10
B253, 111113.75
Part #22
140
150
160
170
180
190
200
210


23
LX-10
B253, 111113.75
Part #23
80
90
100
110
120
130
140
150
160
170
180
190

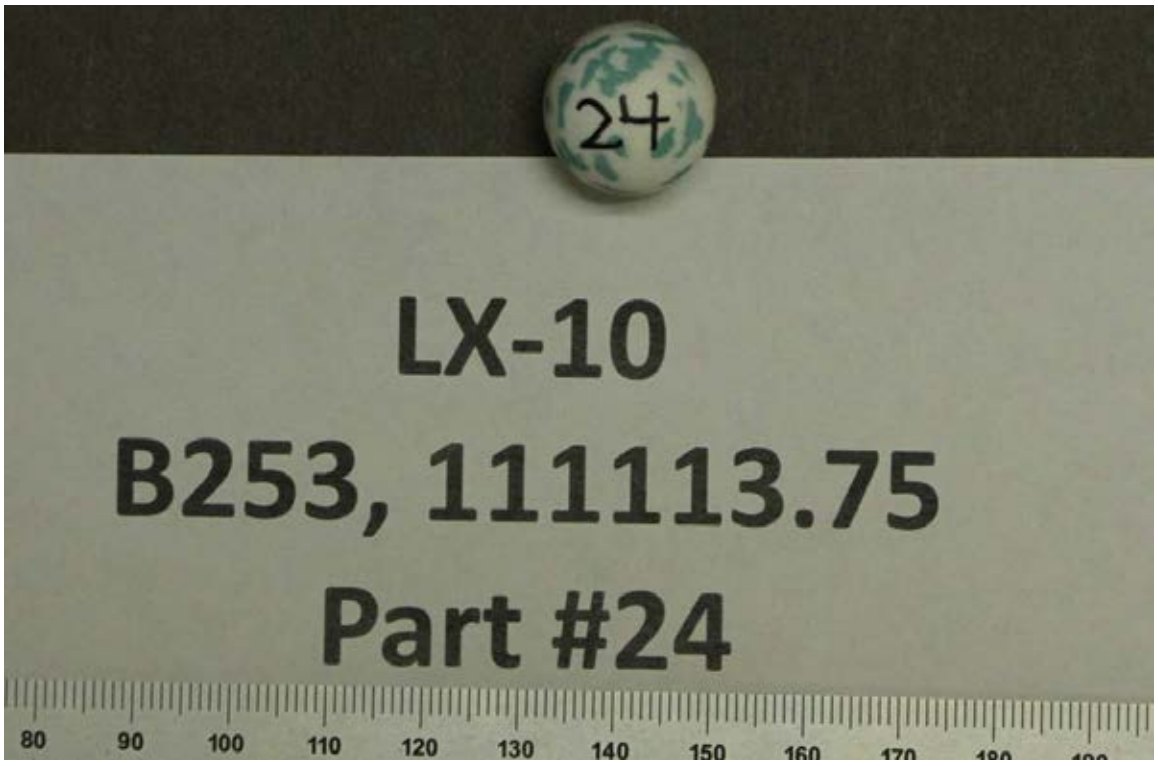
24
LX-10
B253, 111113.75
Part #24
80 90 100 110 120 130 140 150 160 170

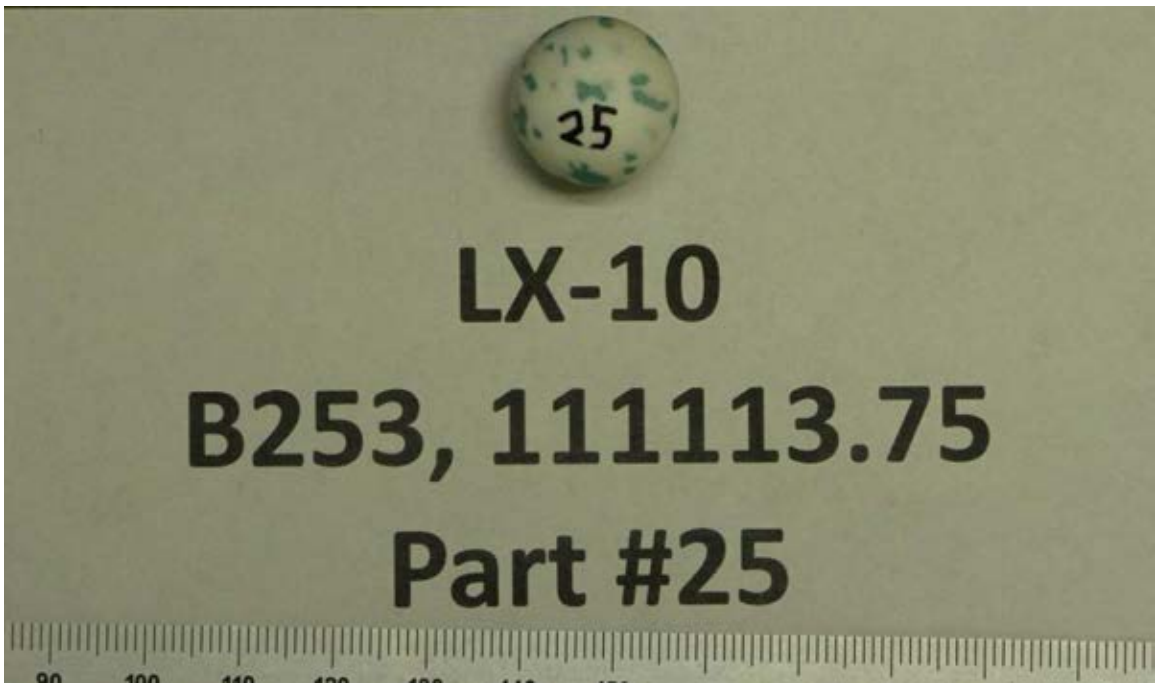
25
LX-10
B253, 111113.75
Part #25

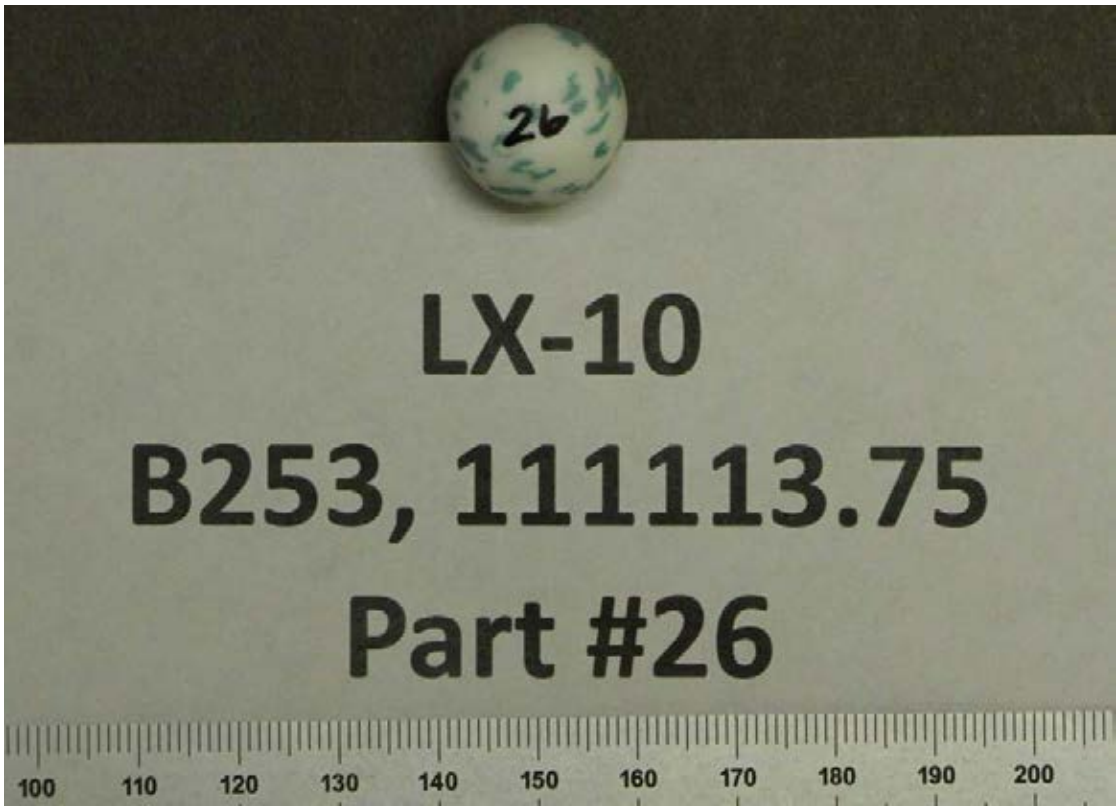
26
LX-10
B253, 111113.75
Part #26
100 110 120 130 140 150 160 170 180 190 200

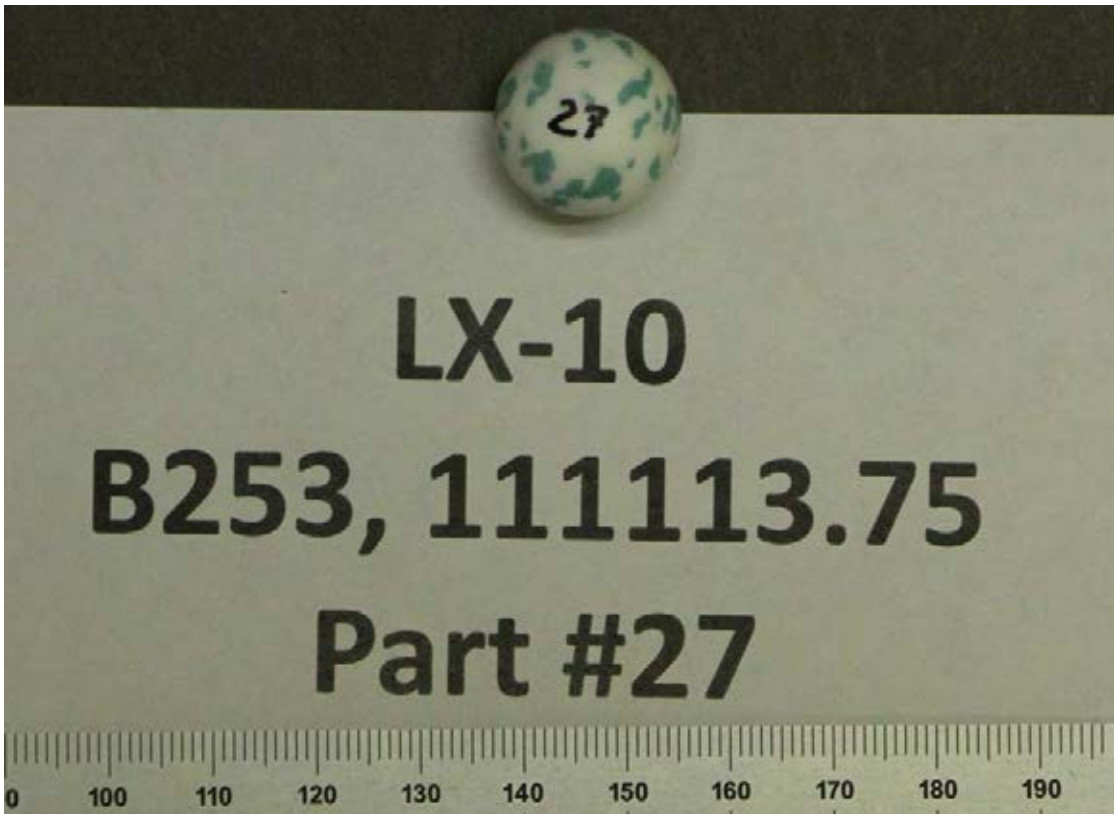
27
LX-10
B253, 111113.75
Part #27
0 100 110 120 130 140 150 160 170 180 190

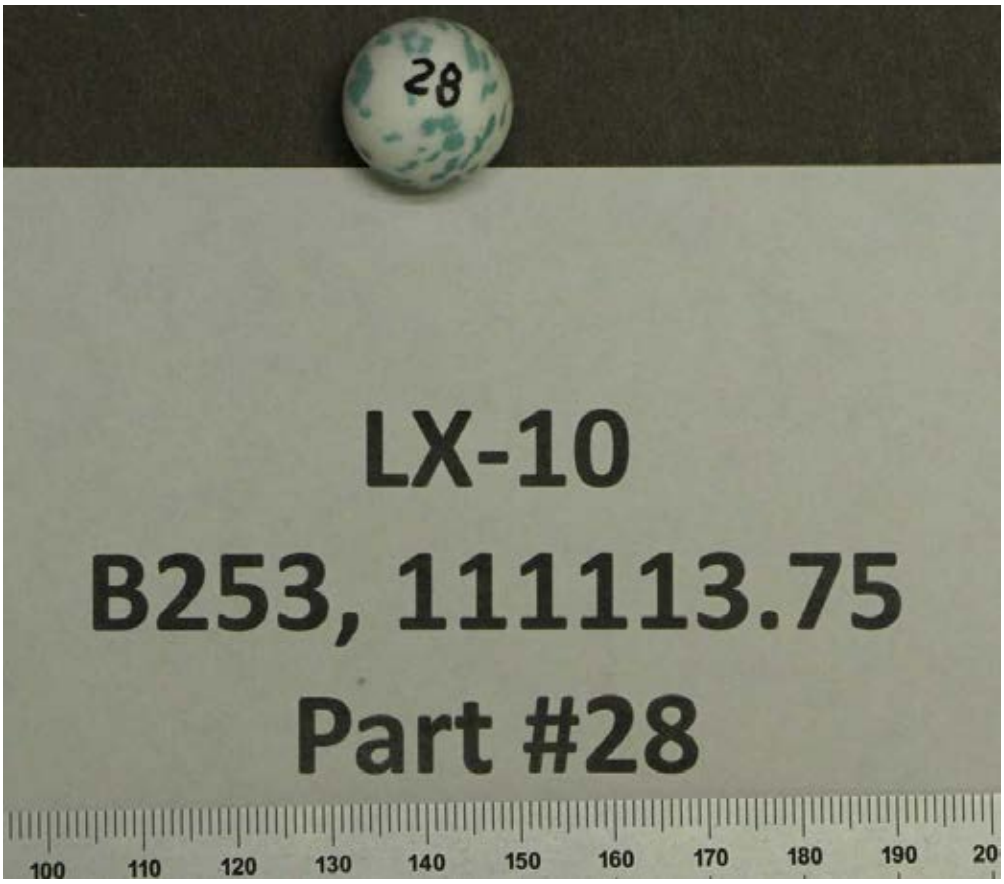
28
LX-10
B253, 111113.75
Part #28
100 110 120 130 140 150 160 170 180 190 20

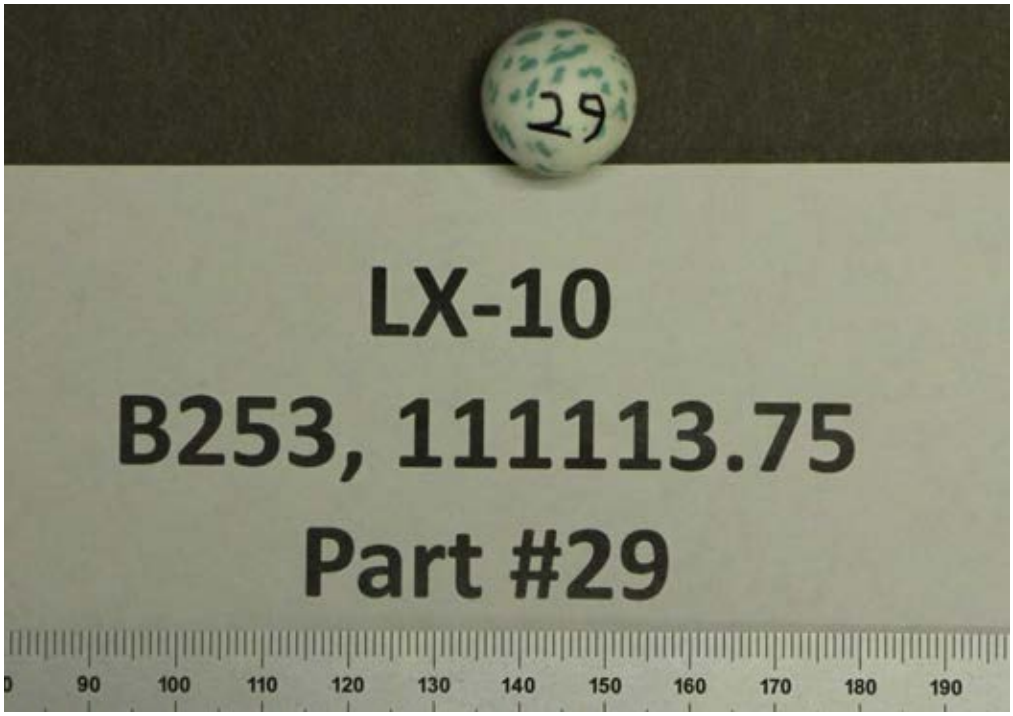
29
LX-10
B253, 111113.75
Part #29
90 100 110 120 130 140 150 160 170 180 190


30
LX-10
B253, 111113.75
Part #30
0 100 110 120 130 140 150 160 170 180 190 200

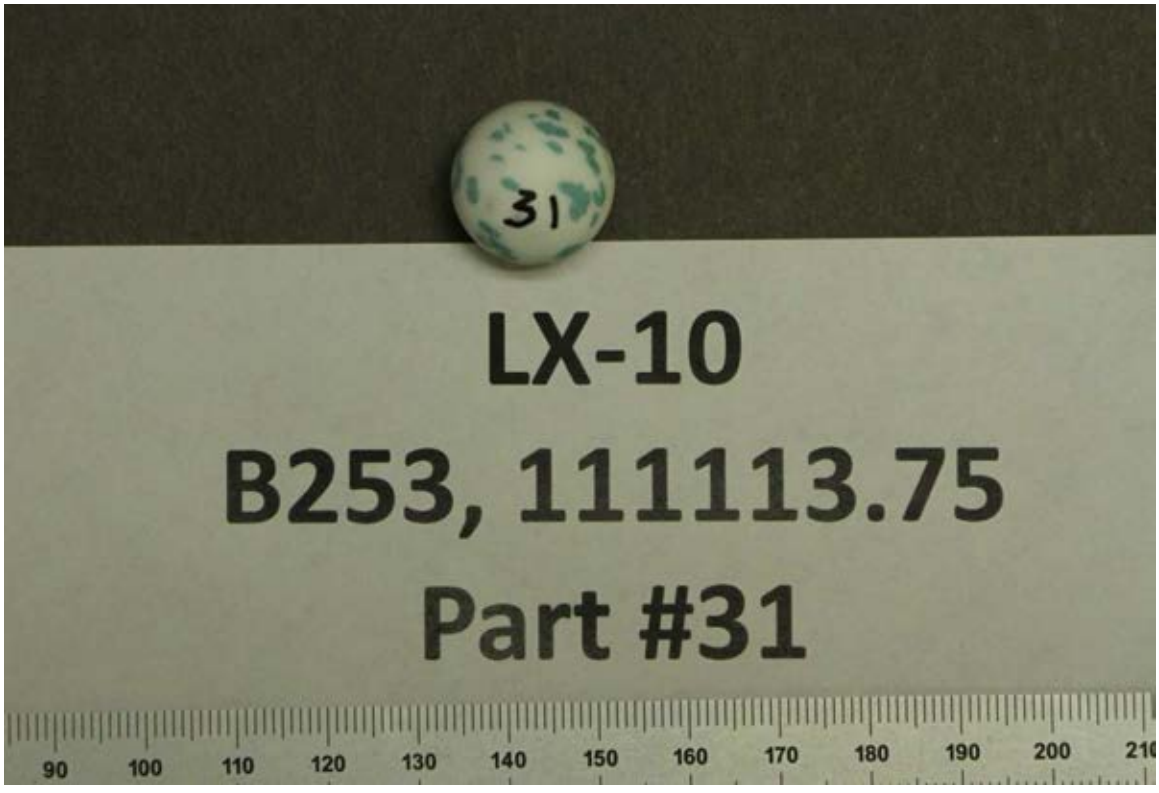
31
LX-10
B253, 111113.75
Part #31
90 100 110 120 130 140 150 160 170 180 190 200


32
LX-10
B253, 111113.75
Part #32

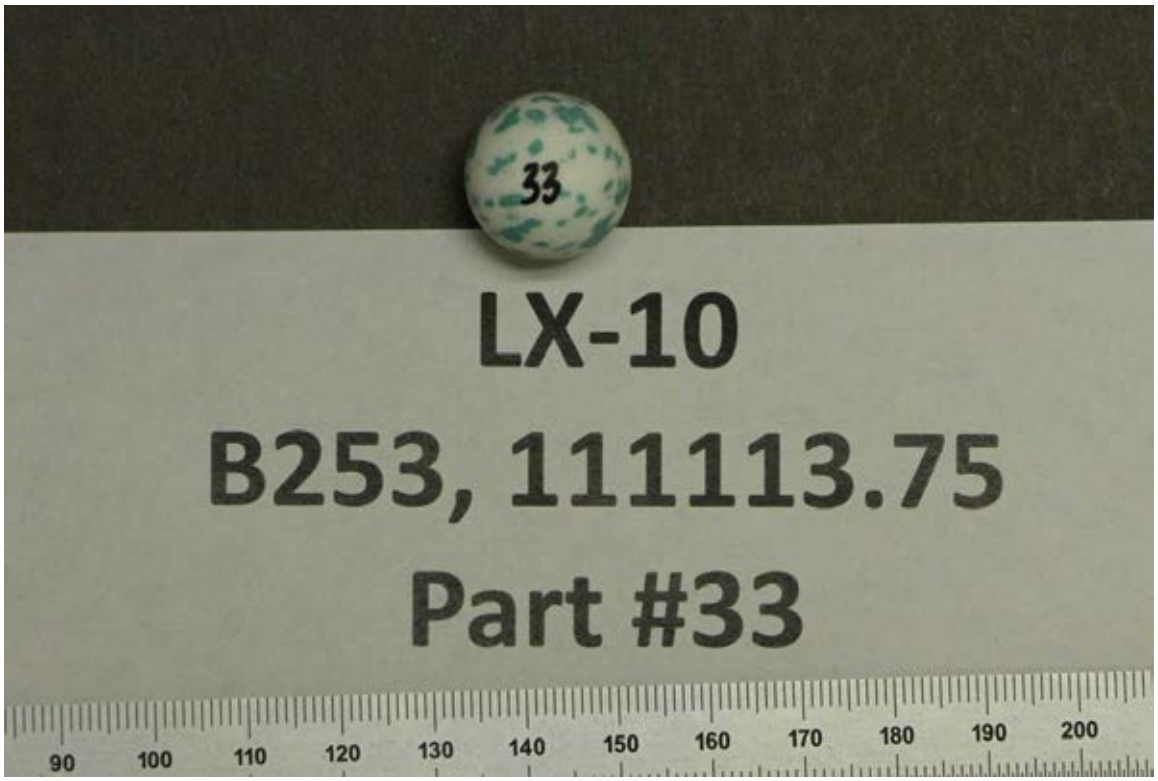
33
LX-10
B253, 111113.75
Part #33


34
LX-10
B253, 111113.75
Part #34
90 100 110 120 130 140 150 160 170 180 190


35
LX-10
B253, 111113.75
Part #35
120 130 140 150 160 170 180 190 200

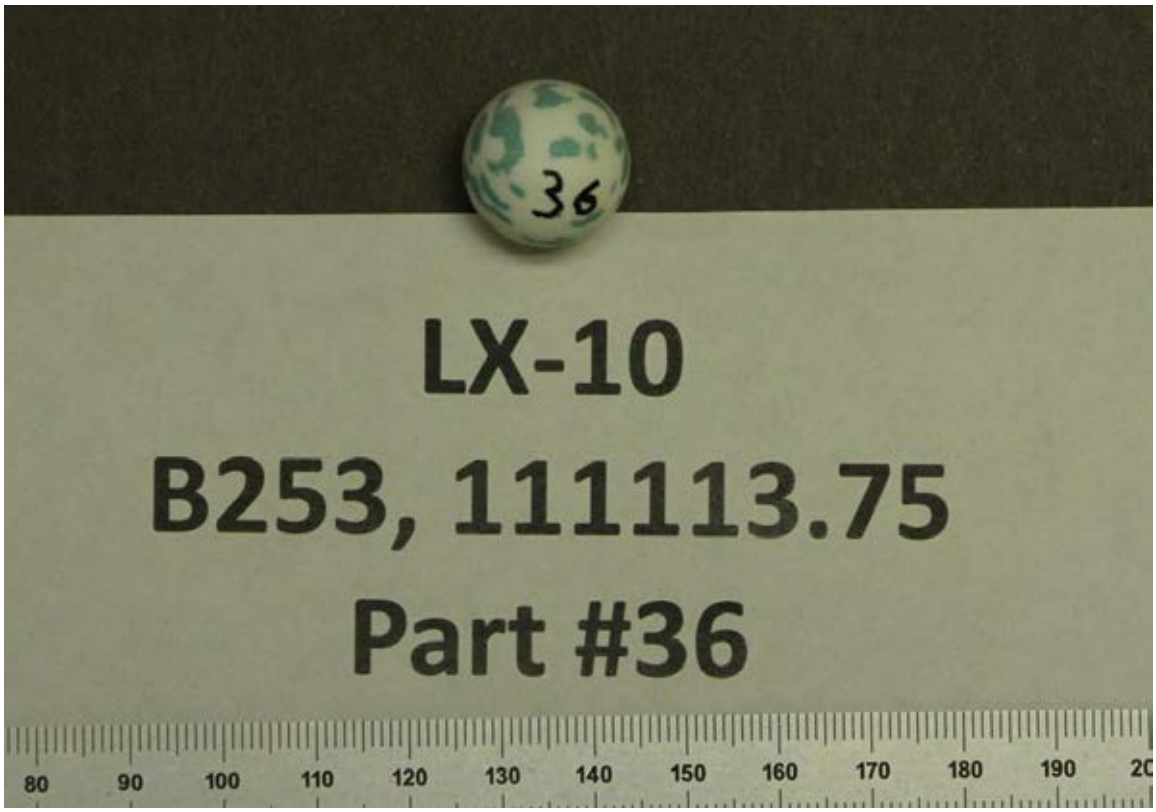
36
LX-10
B253, 111113.75
Part #36
80 90 100 110 120 130 140 150 160 170 180 190

Appendix B

CYLINDRICAL AND SPHERICAL IMPACT DAMAGED LX-10 SAMPLES

This page intentionally left blank.

Damaged Cylinders


LX-10
B253, 122013.75
Part #5, 121 ft/s


LX-10
B253, 122013.75
Part #6, 500ft/s

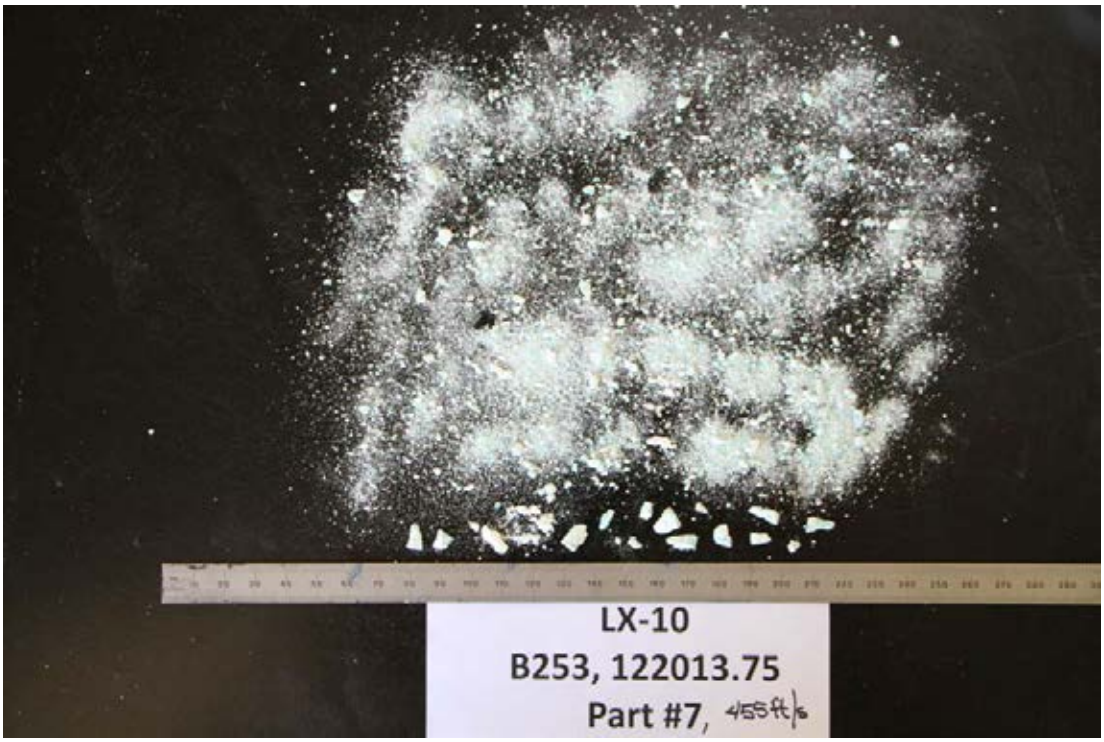
LX-10
B253, 122013.75
Part #7, 455 ft/s

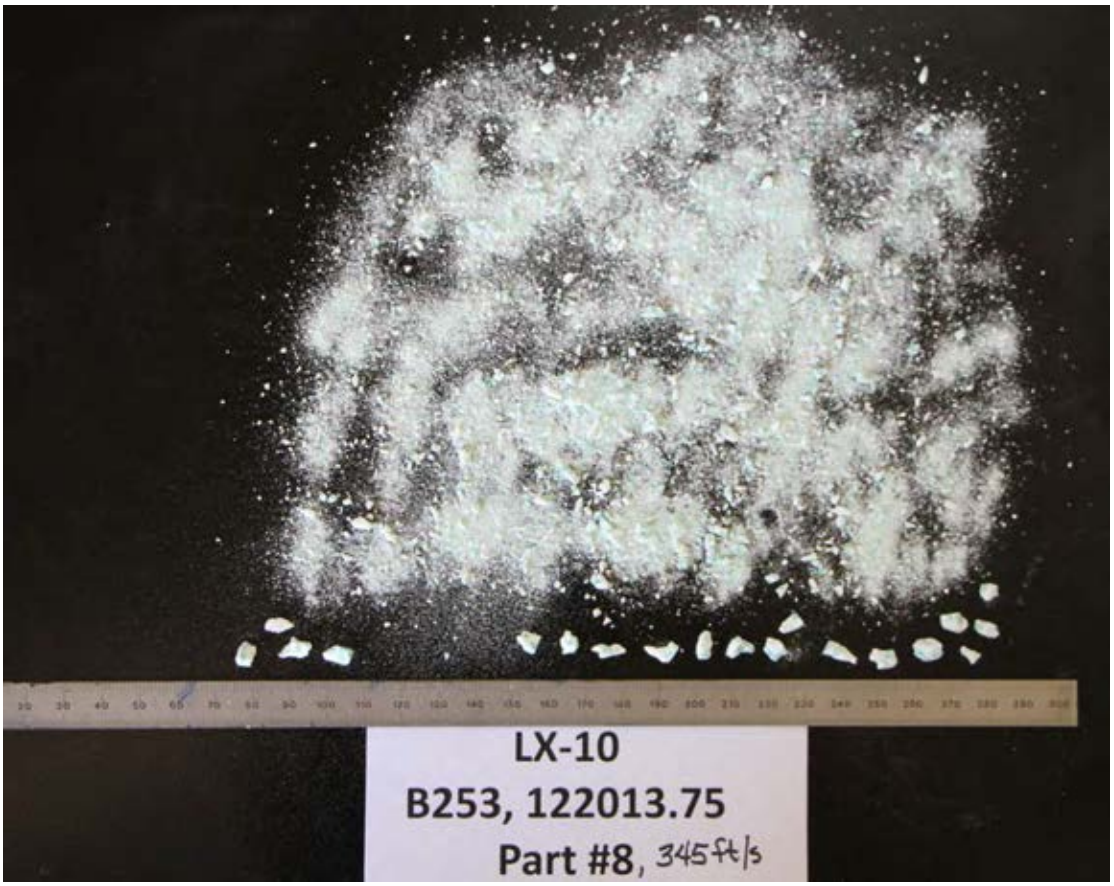
LX-10
B253, 122013.75
Part #8, 345 ft/s

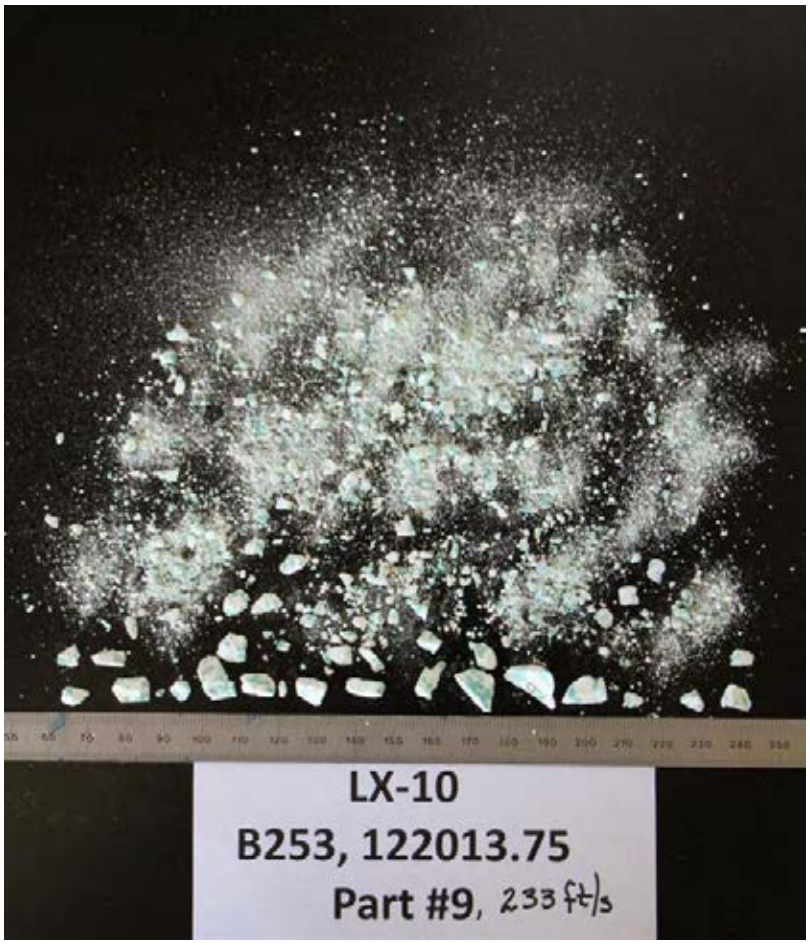
LX-10
B253, 122013.75
Part #9, 233 ft/s


LX-10
B253, 122013.75
Part #10, 208 ft/s

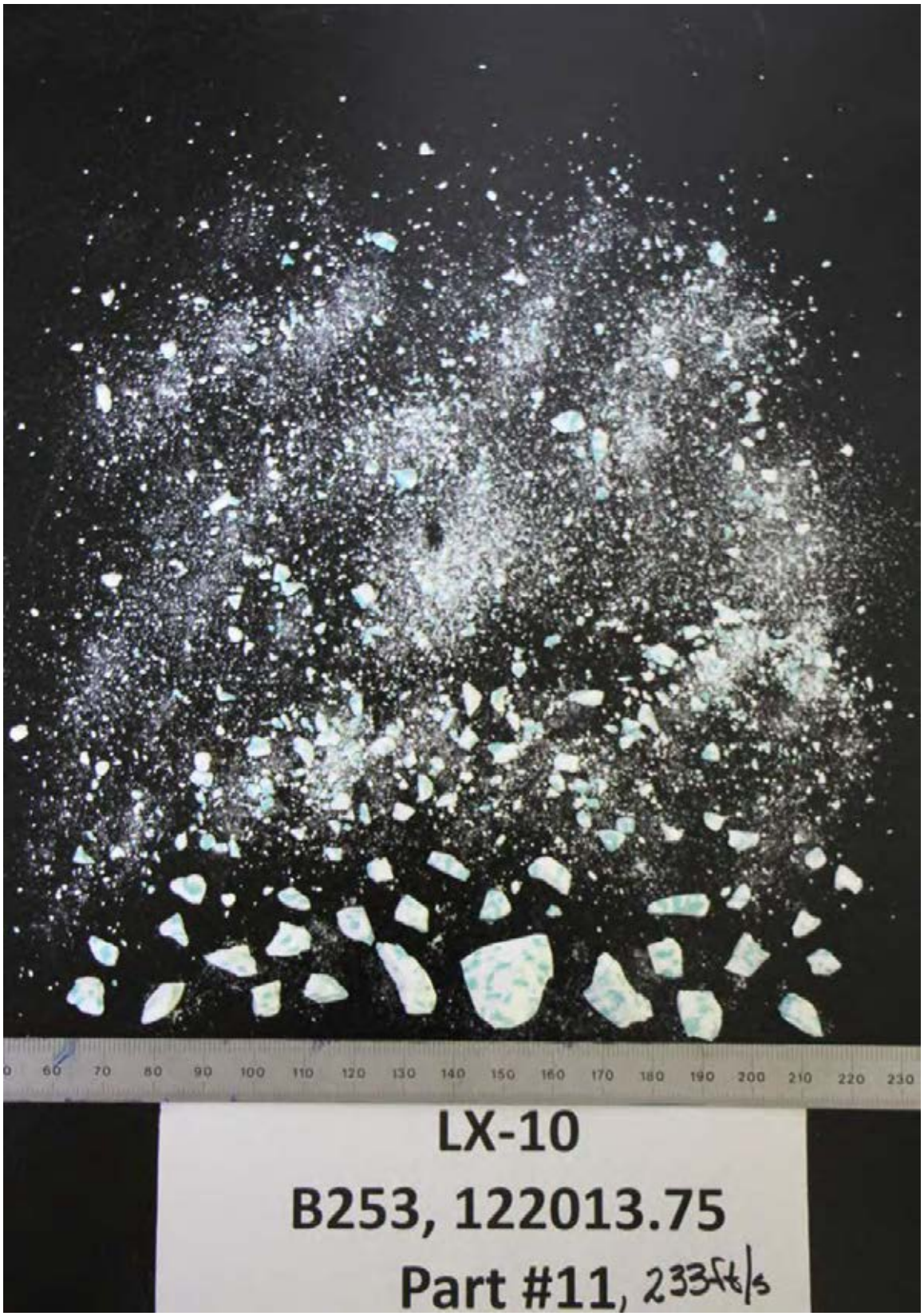
60 70 80 90 100 110 120 130 140 150 160 170 180 190 200 210 220 230
LX-10
B253, 122013.75
Part #11, 2335ft/s


60 70 80 90 100 110 120 130 140 150 160 170 180 190 200 210 220 230 240 250
LX-10
B253, 122013.75
Part #12, 200 ft/s

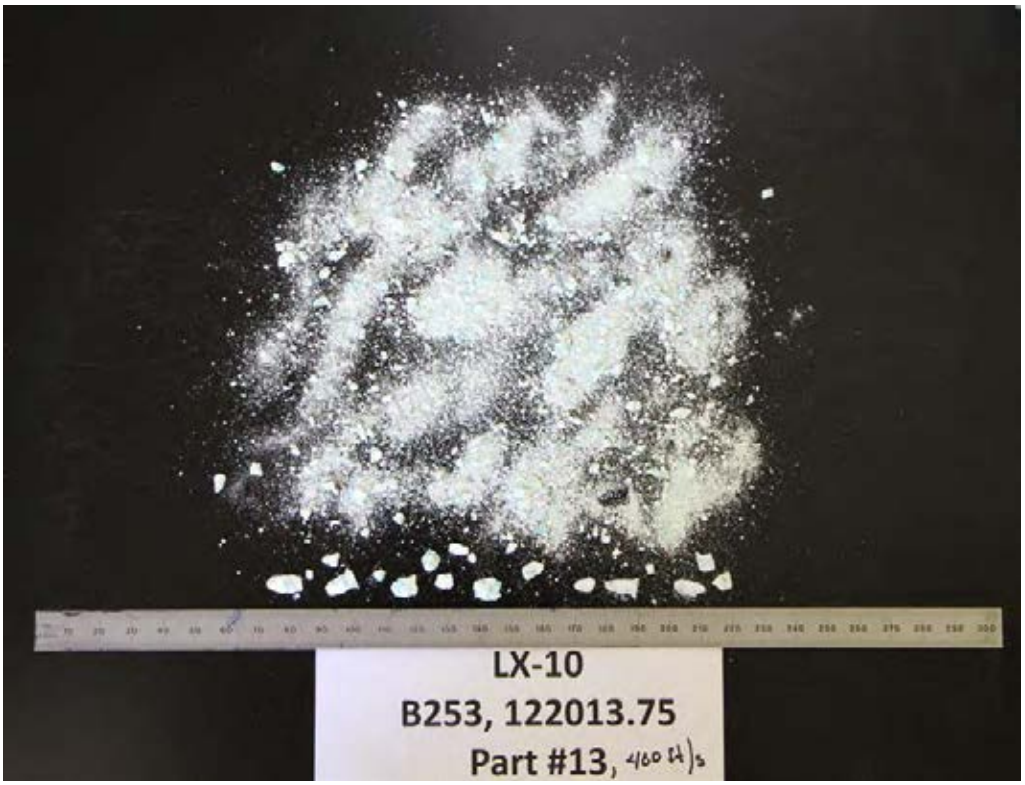
LX-10
B253, 122013.75
Part #13, 400 ft/s

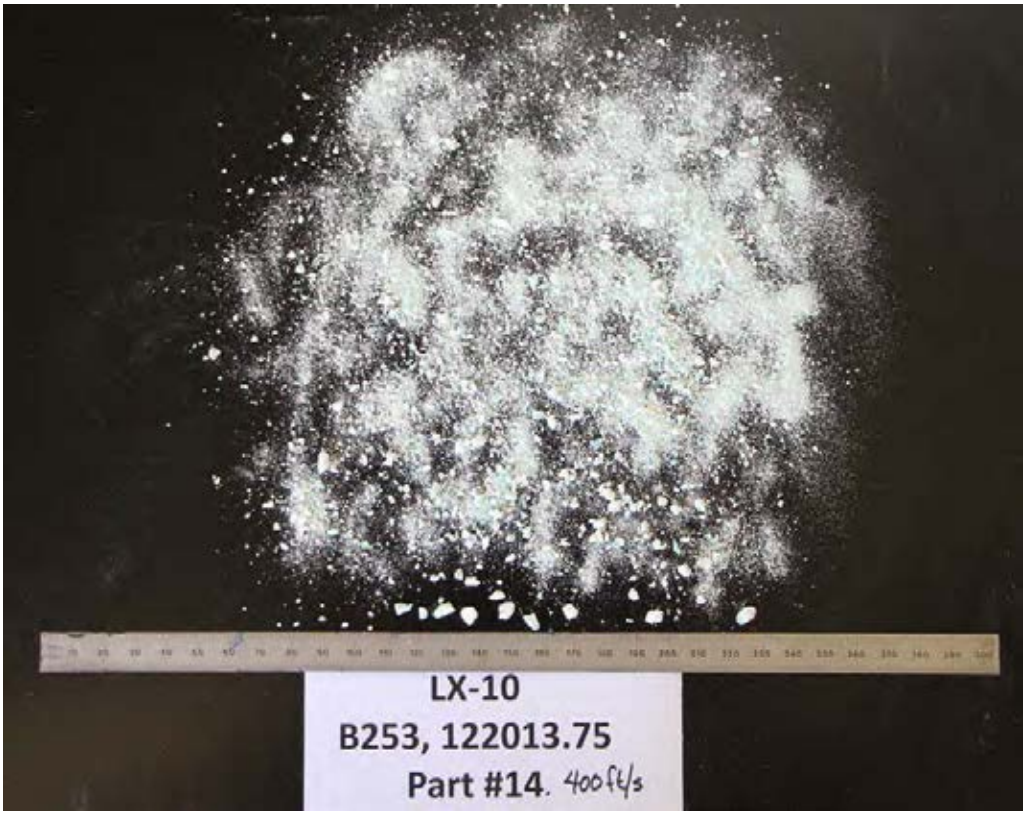
LX-10
B253, 122013.75
Part #14. 400 ft/s

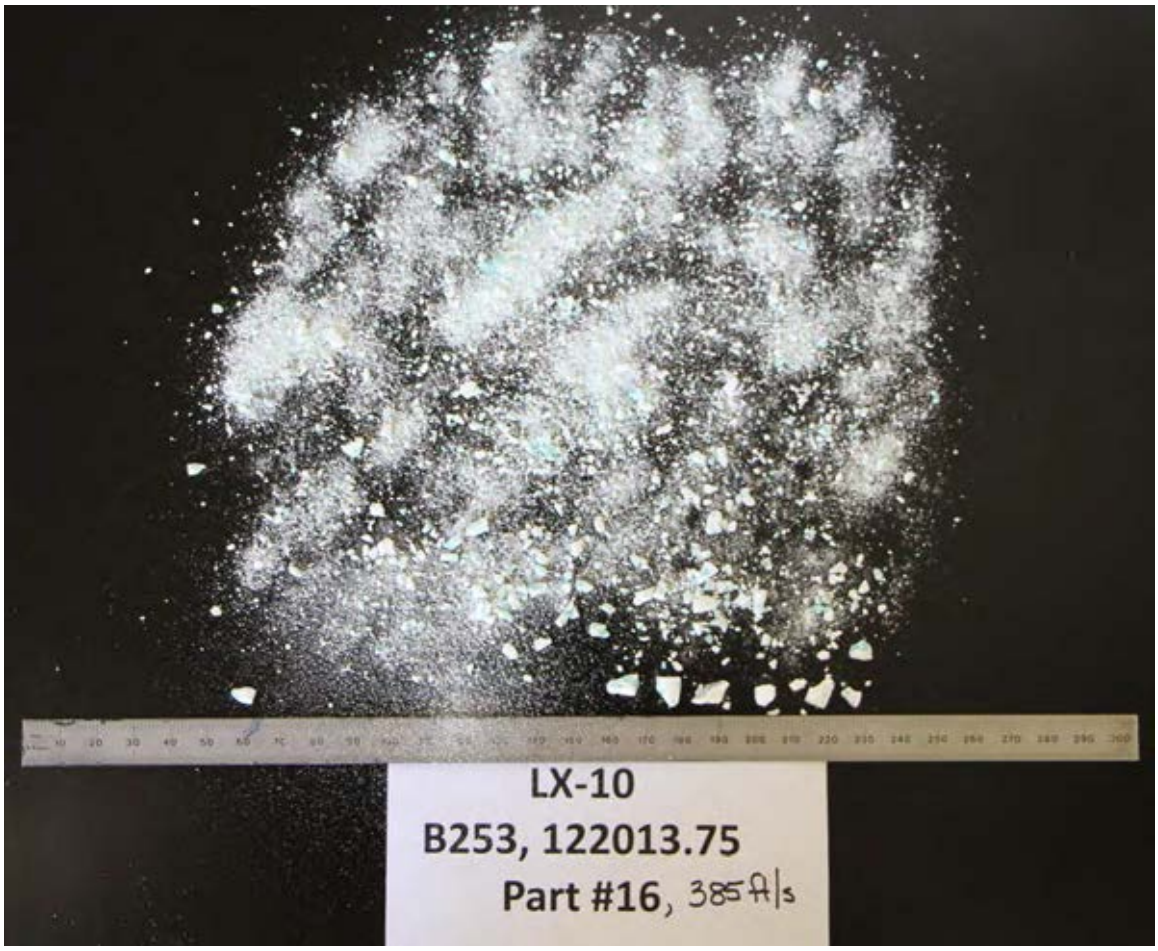
LX-10
B253, 122013.75
Part #16, 385 ft/s

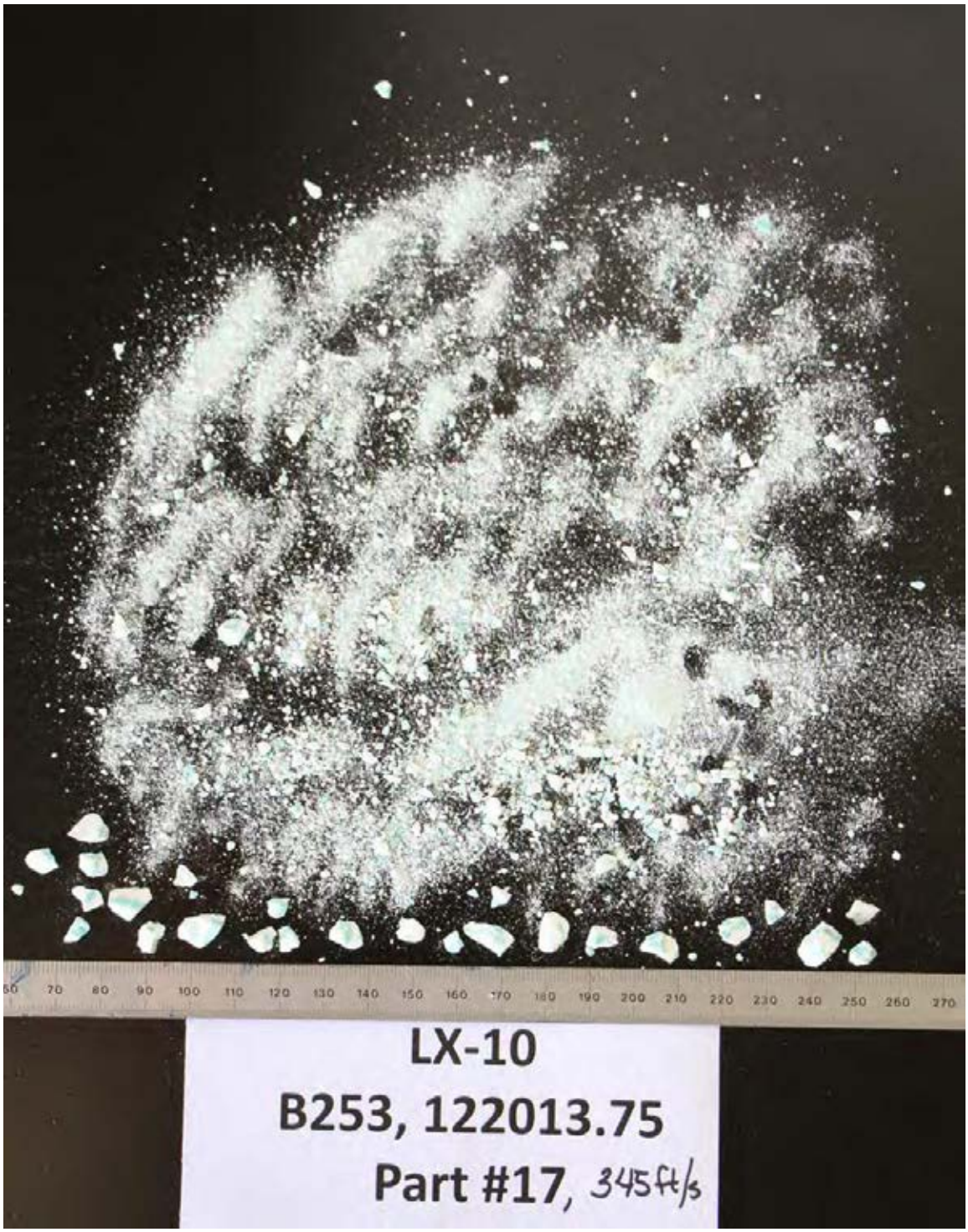
LX-10
B253, 122013.75
Part #17, 345ft/s

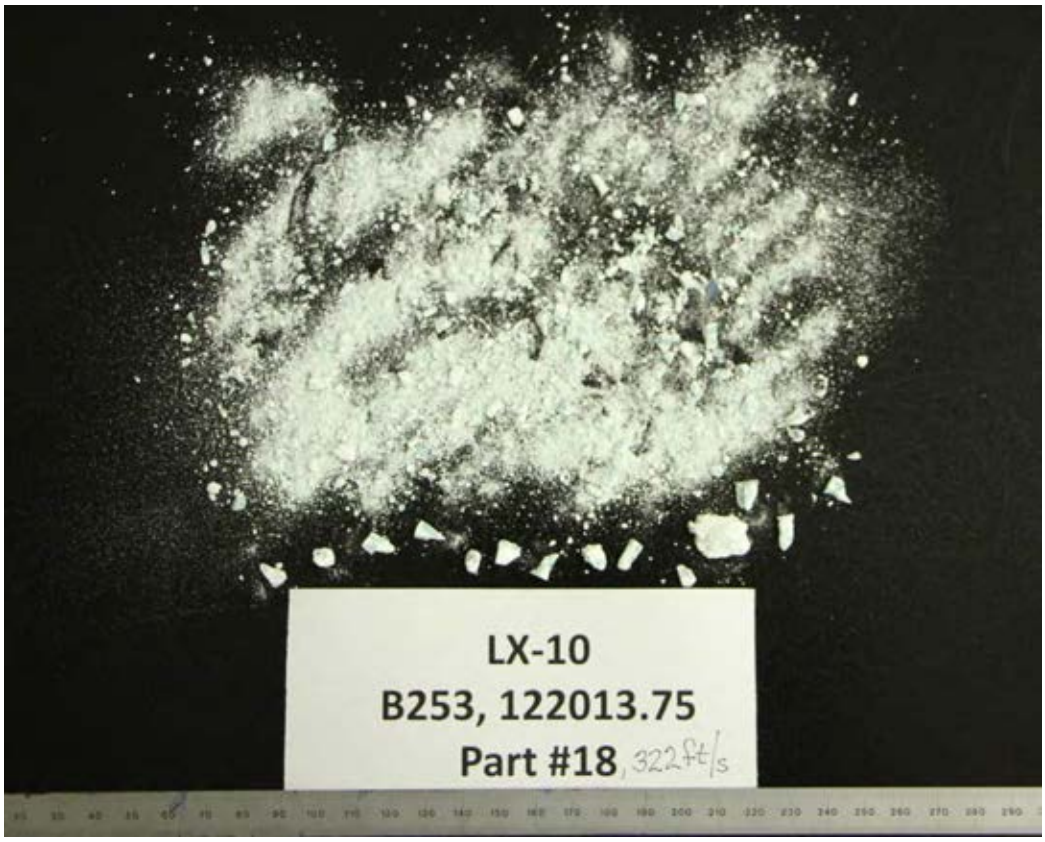
LX-10
B253, 122013.75
Part #18, 322ft/s

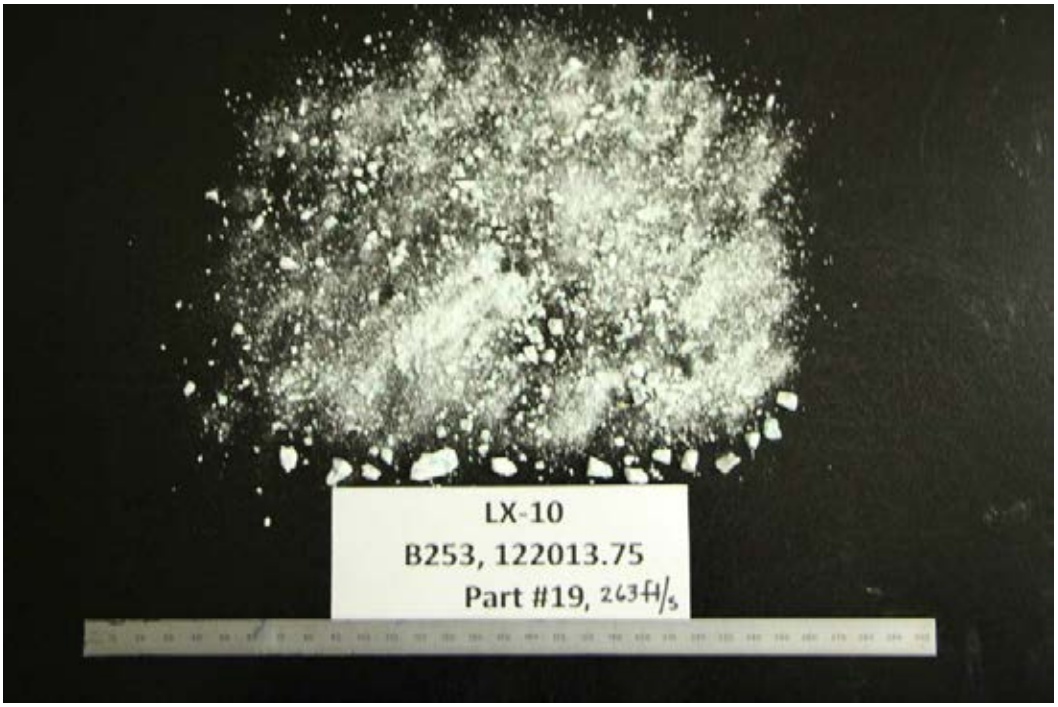
LX-10
B253, 122013.75
Part #19, 263ft/s

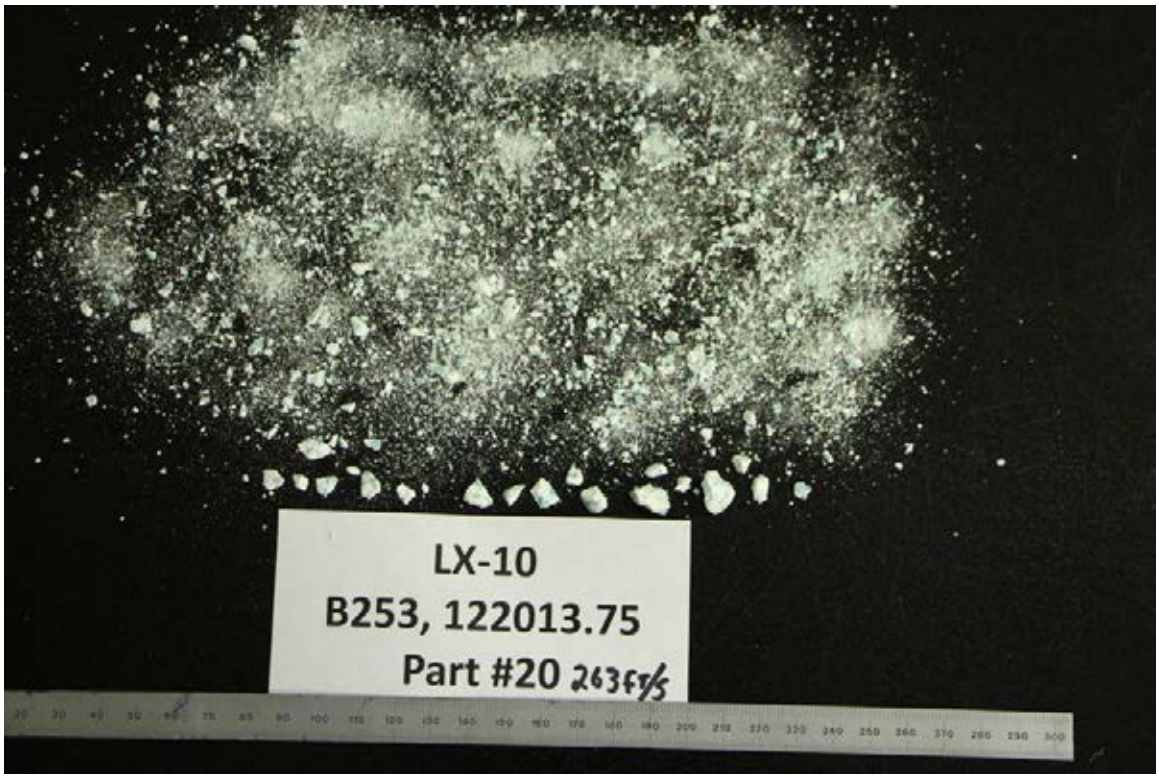
LX-10
B253, 122013.75
Part #20 2636 ft/s

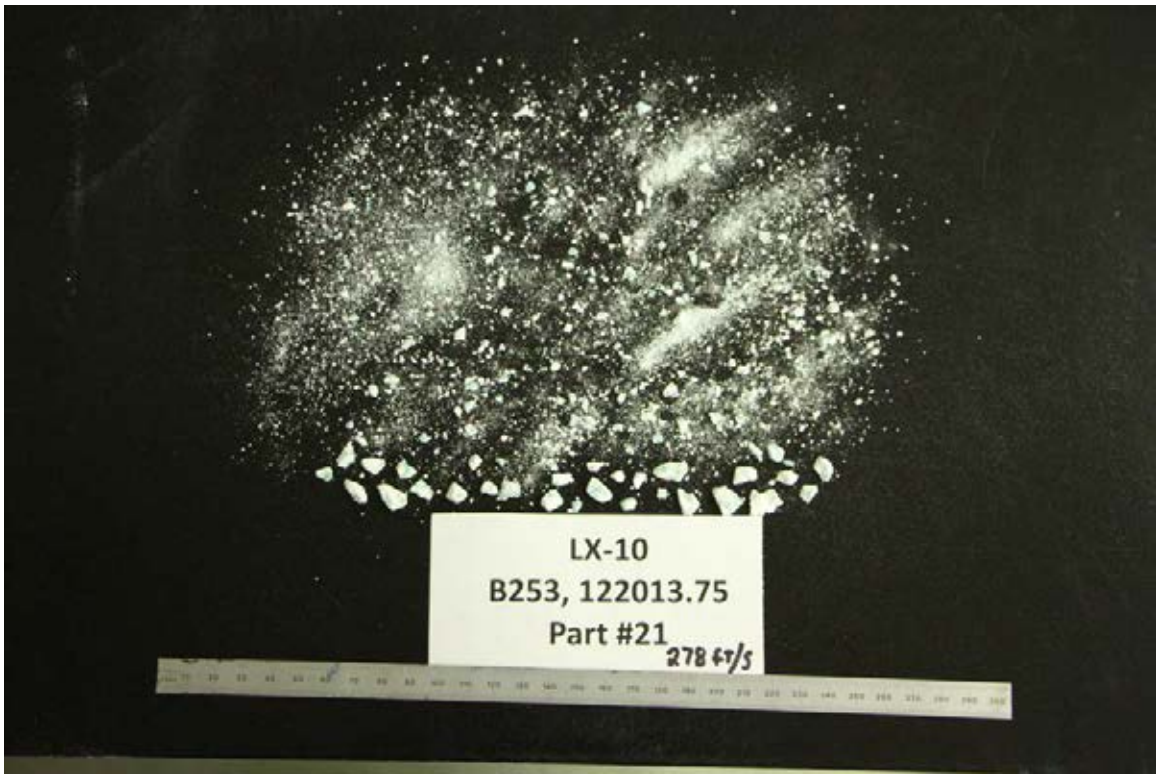
LX-10
B253, 122013.75
Part #21
2786 ft/s

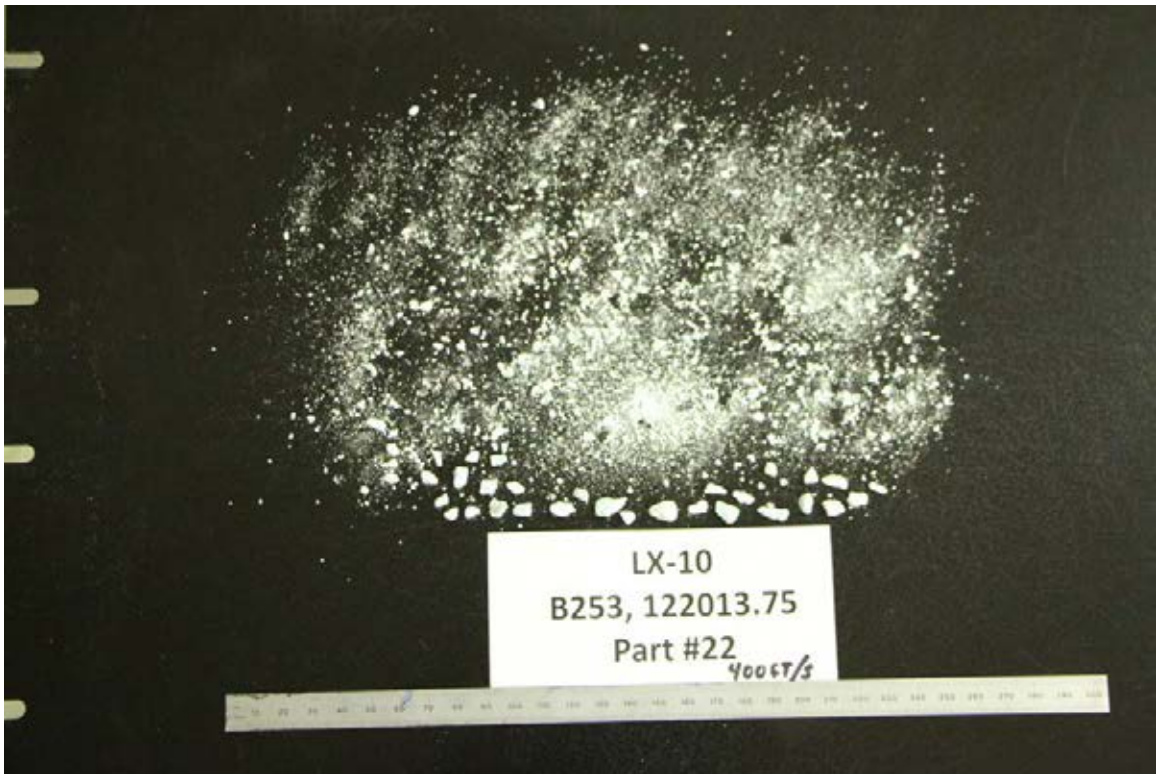
LX-10
B253, 122013.75
Part #22
4006T/S

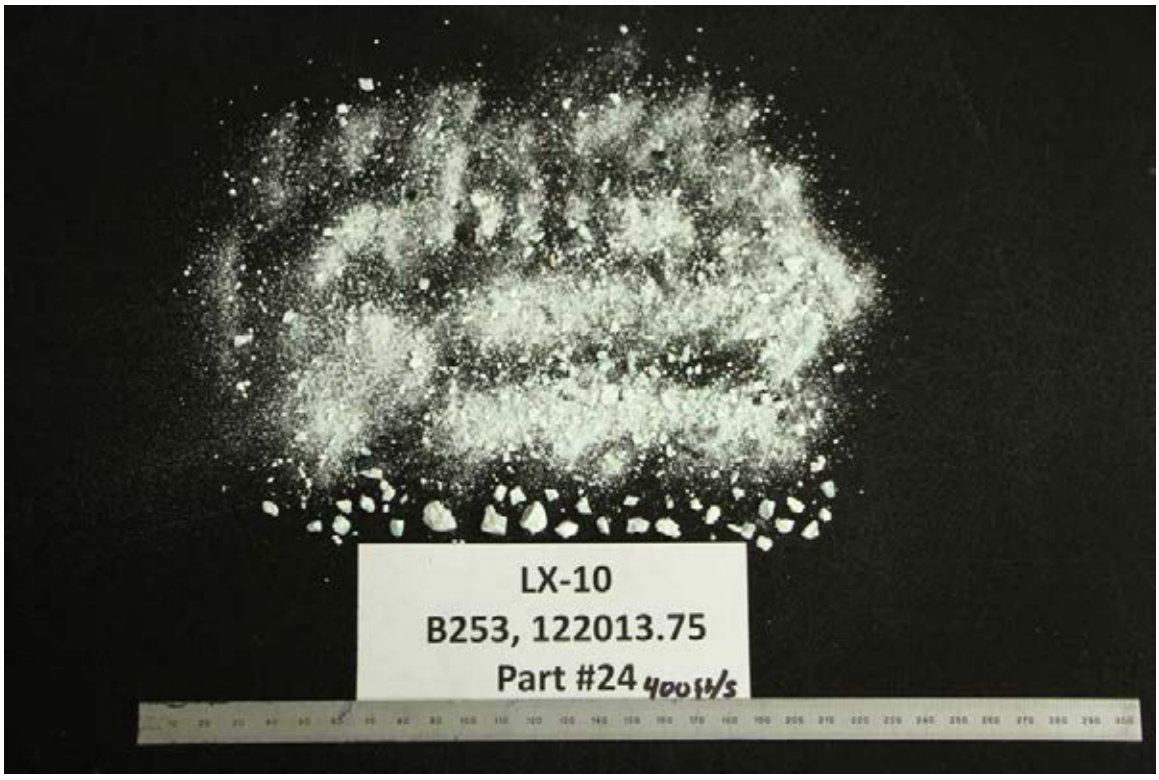
LX-10
B253, 122013.75
Part #24 4005T/S


LX-10
B253, 122013.75
192 g/s Part #25

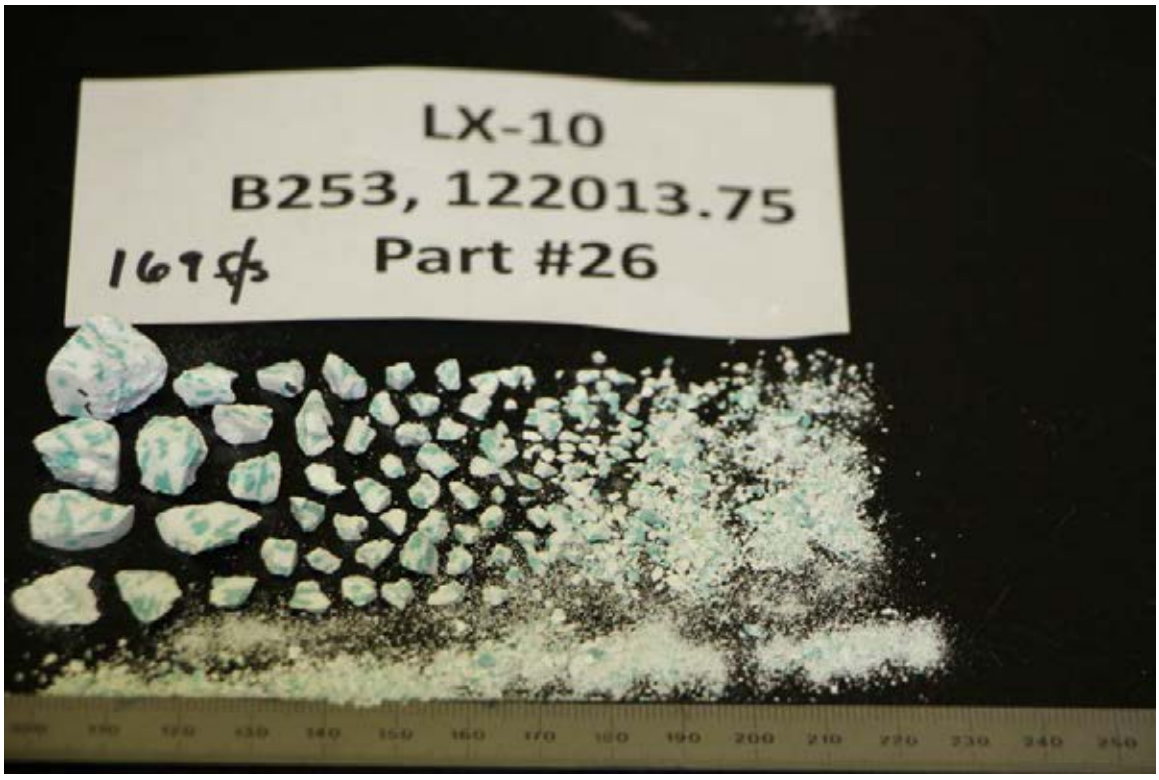
LX-10
B253, 122013.75
169 g/s Part #26


LX-10
B253, 122013.75
Part #27
151 ft/s

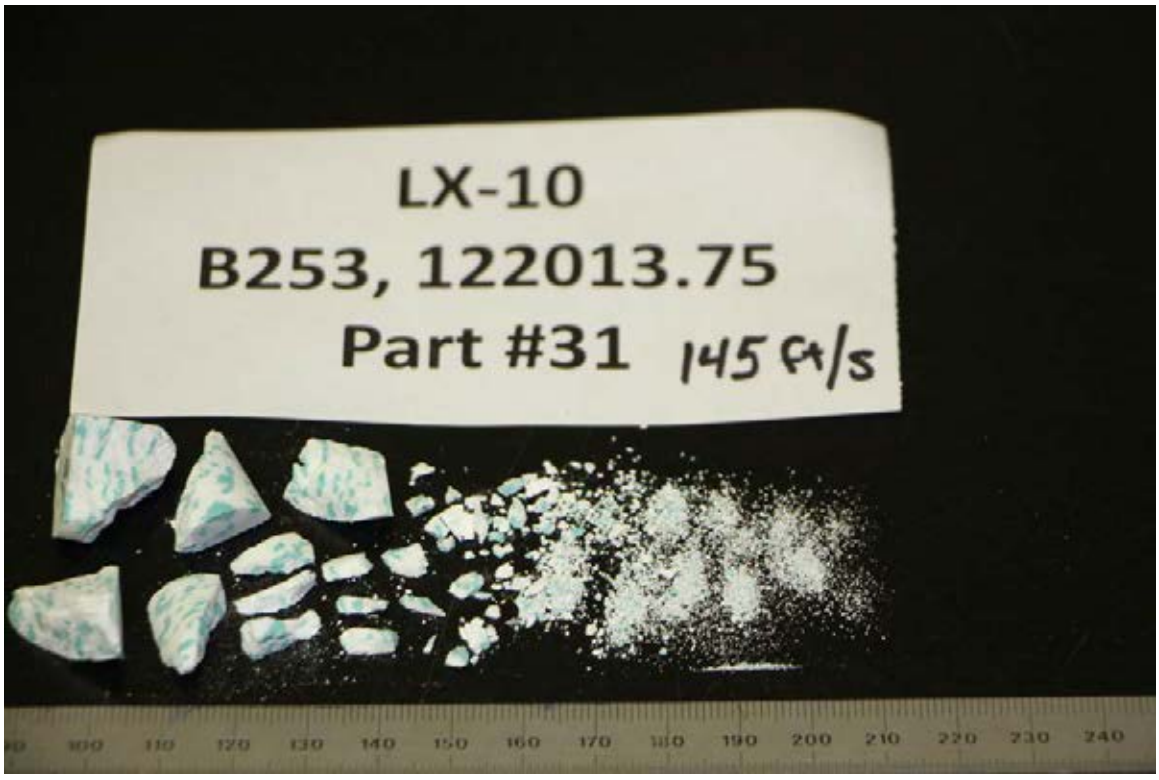
LX-10
B253, 122013.75
Part #31
145 ft/s


LX-10
B253, 122013.75
Part #32
333 ft/s


LX-10
B253, 122013.75
Part #33
322 ft/s


LX-10
B253, 122013.75
303 ft/s Part #34

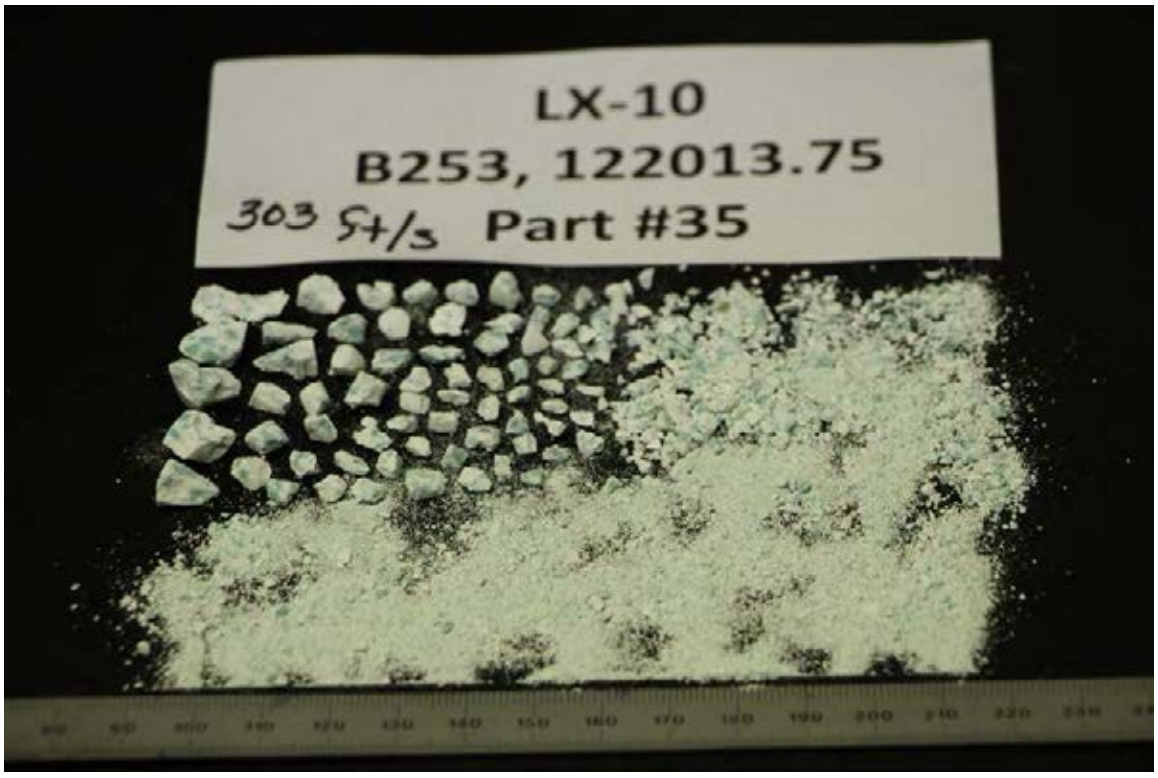
LX-10
B253, 122013.75
303 ft/s Part #35

Damaged Spheres

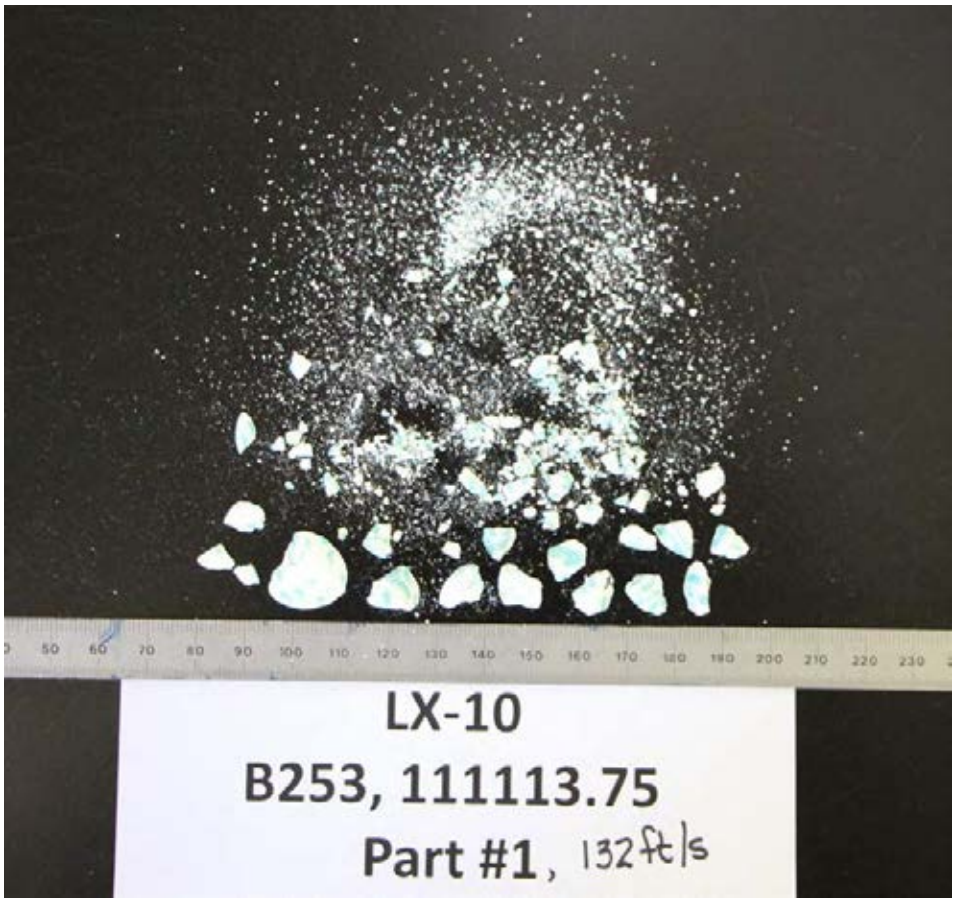

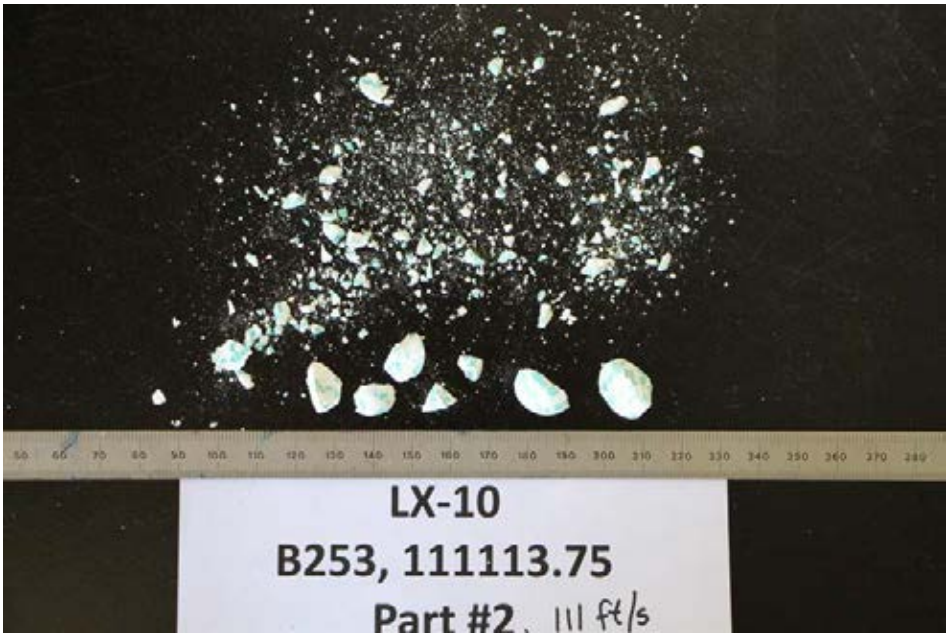

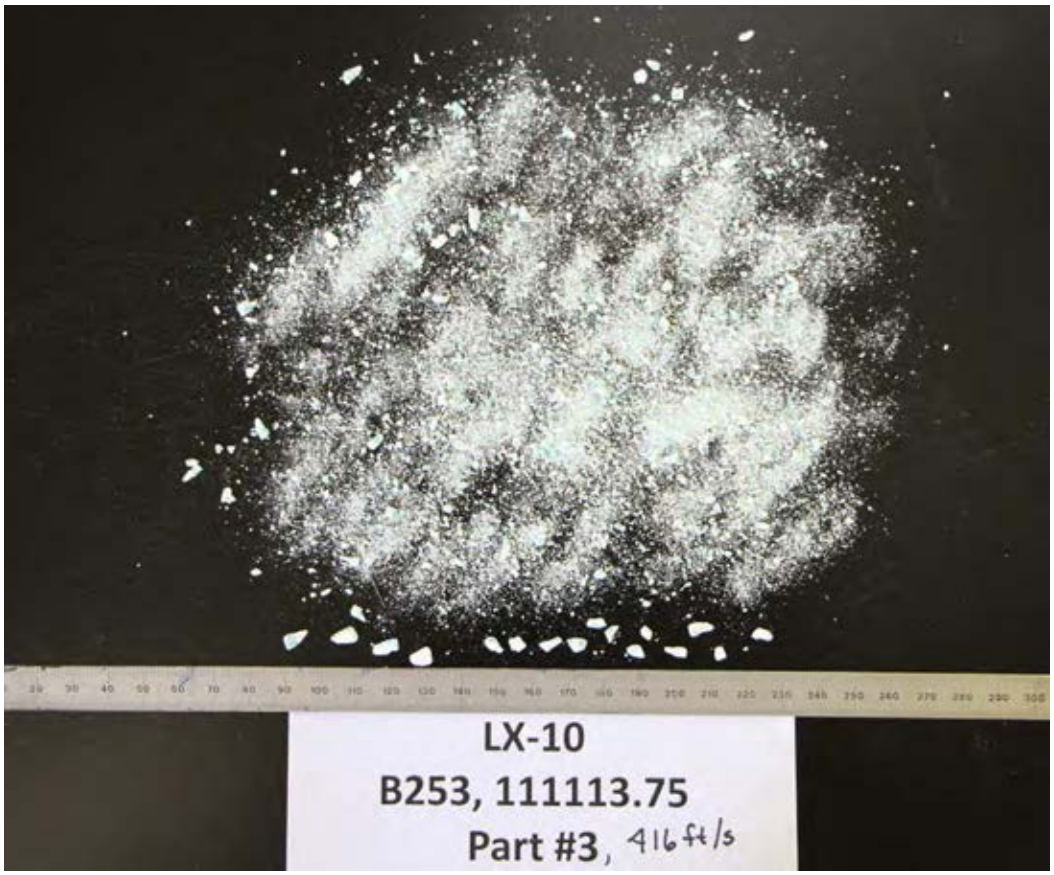
LX-10
B253, 111113.75
Part #3, 416 ft/s


LX-10
B253, 111113.75
Part #4, 416 ft/s

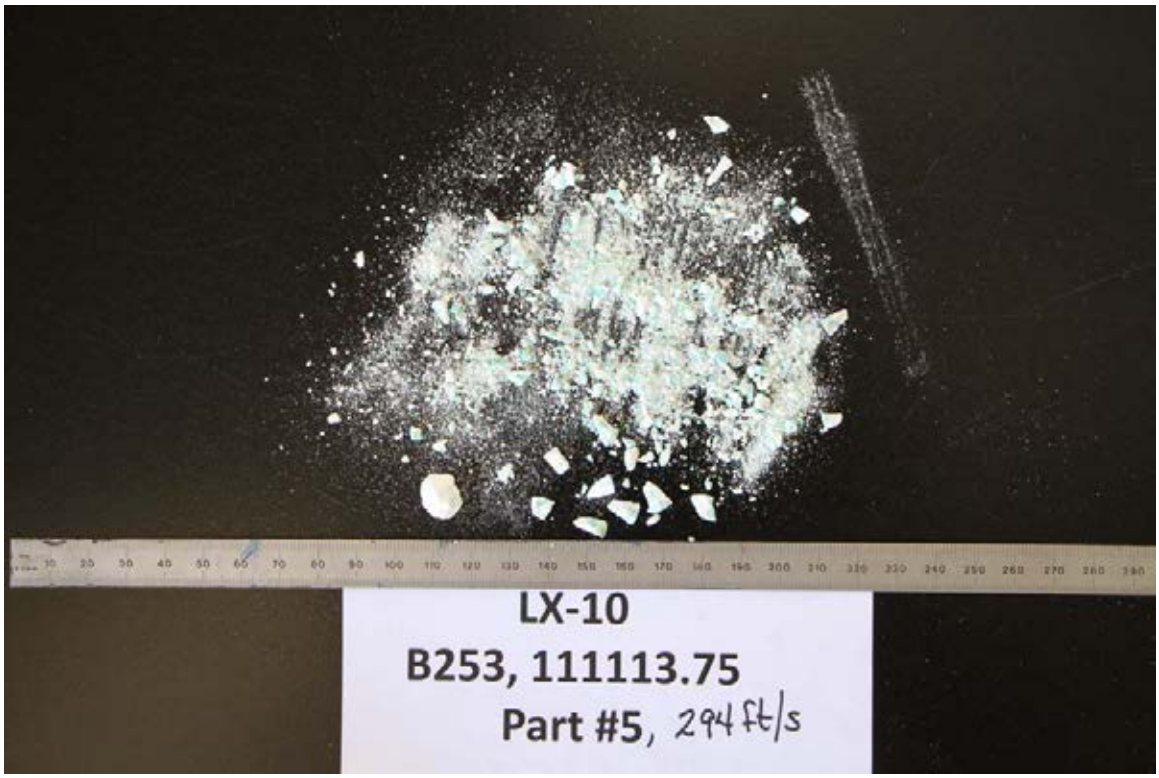
LX-10
B253, 111113.75
Part #5, 294 ft/s


LX-10
B253, 111113.75
Part #6, 294 ft/s

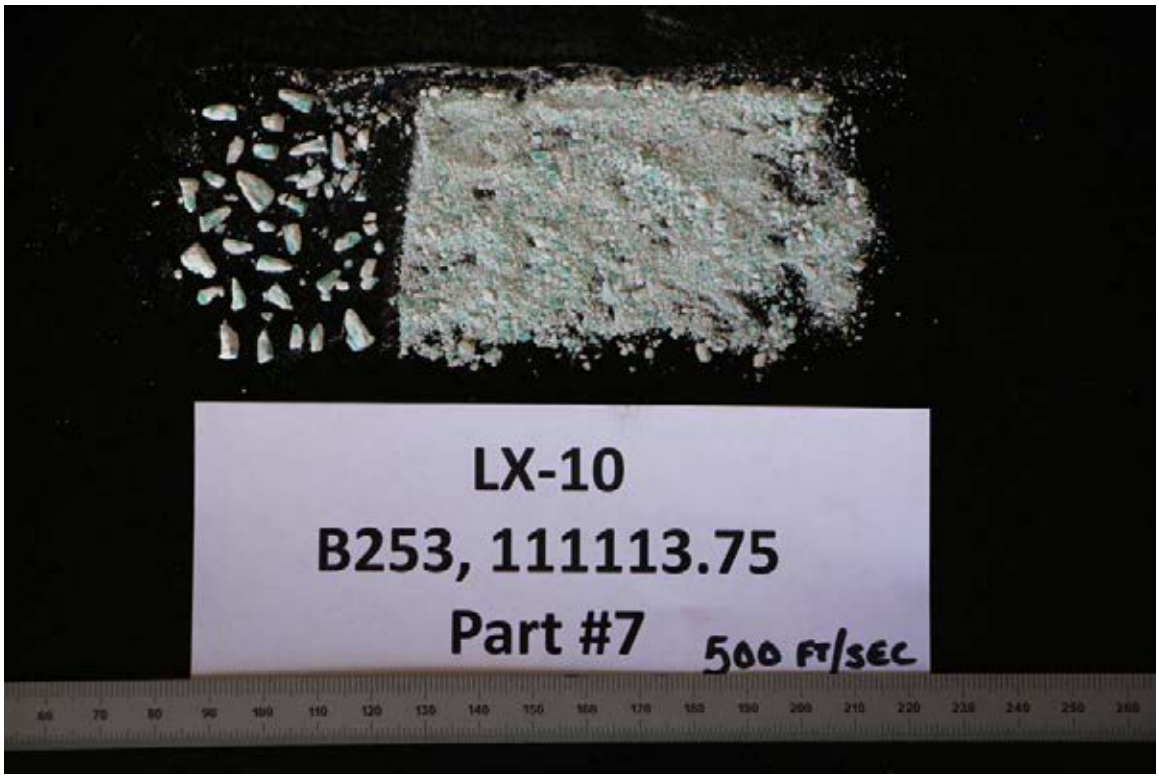
LX-10
B253, 111113.75
Part #7
500 FT/SEC

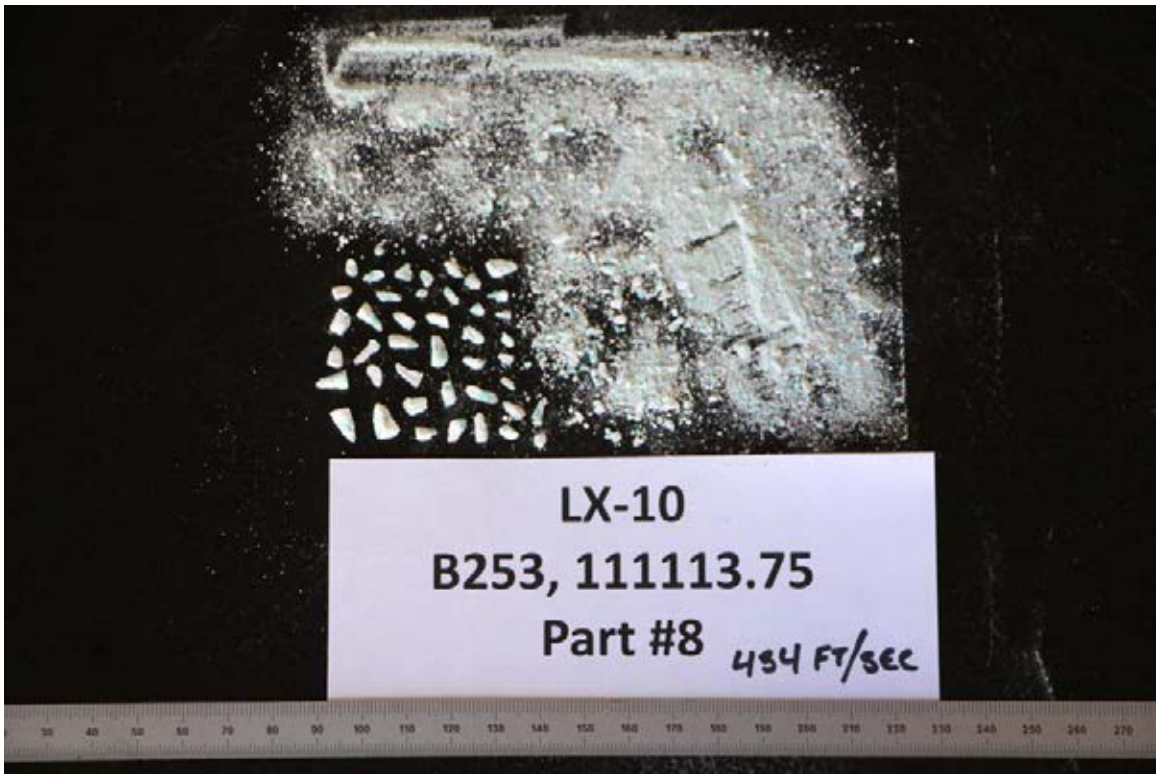
LX-10
B253, 111113.75
Part #8
454 FT/SEC


LX-10
B253, 111113.75
Part #9 400 FT/SEC

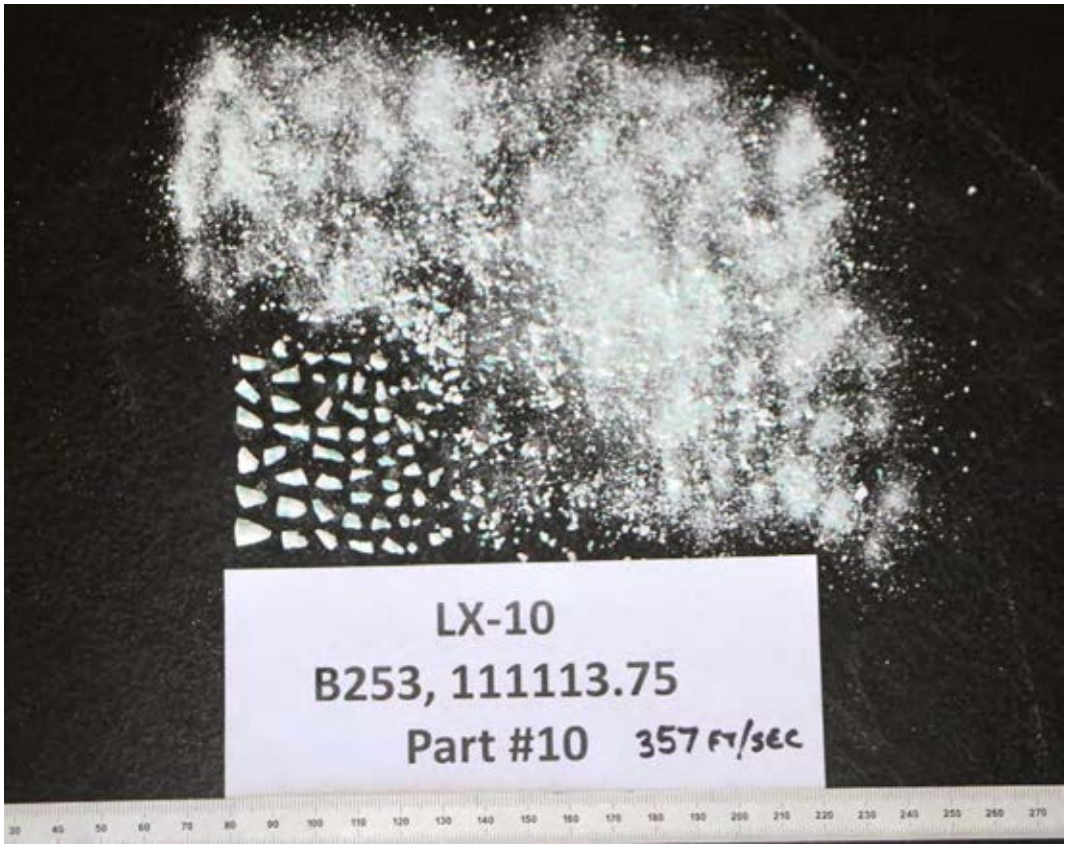
LX-10
B253, 111113.75
Part #10 357 FT/SEC

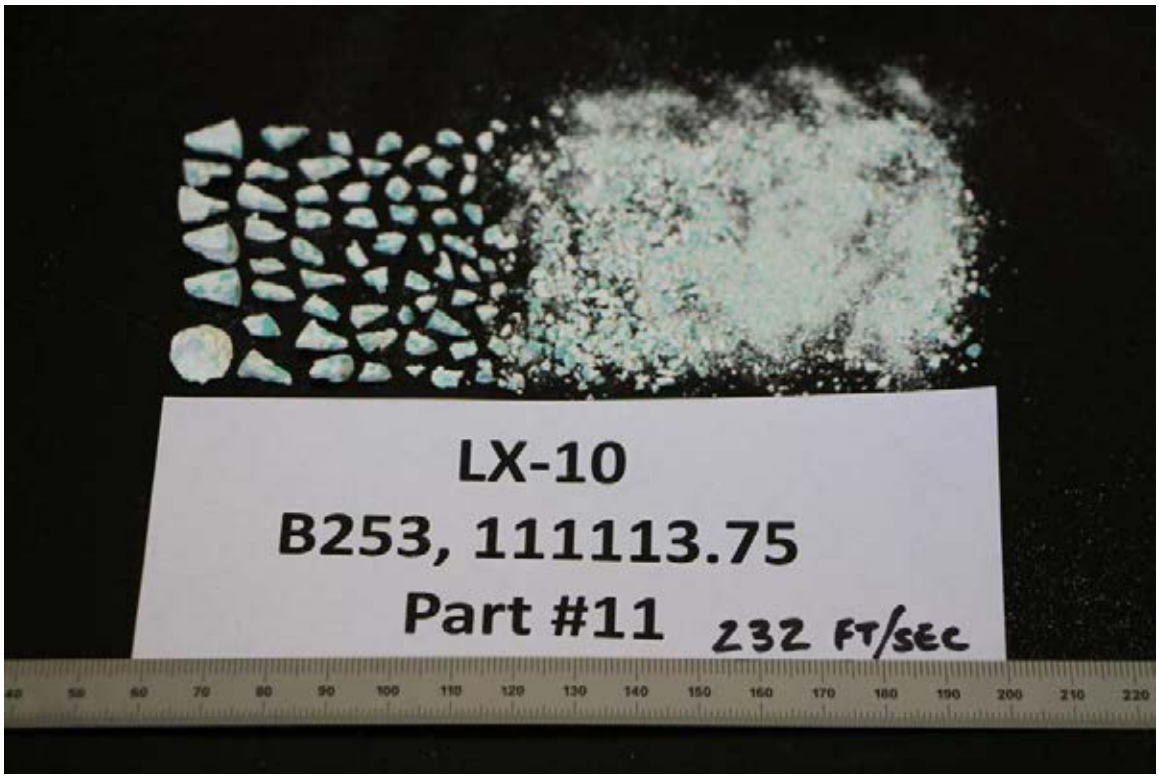
LX-10
B253, 111113.75
Part #11 232 FT/SEC

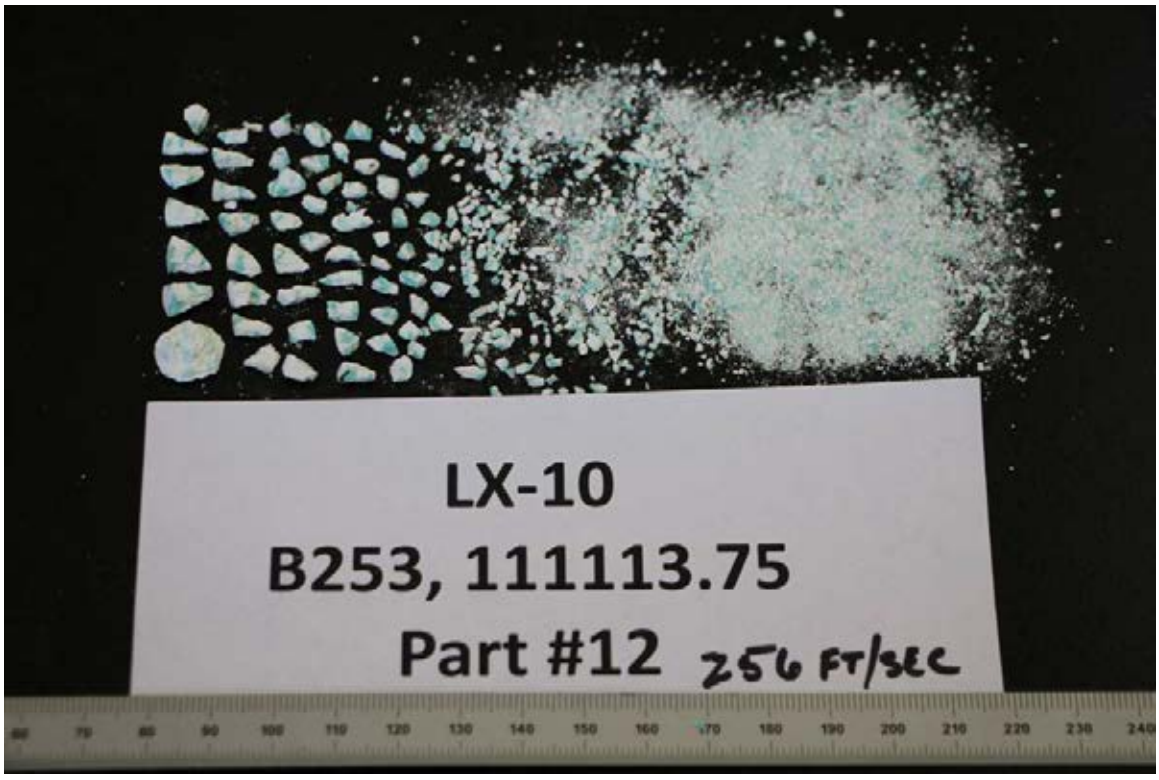
LX-10
B253, 111113.75
Part #12 256 FT/SEC


LX-10
B253, 111113.75
Part #13 222 FT/SEC

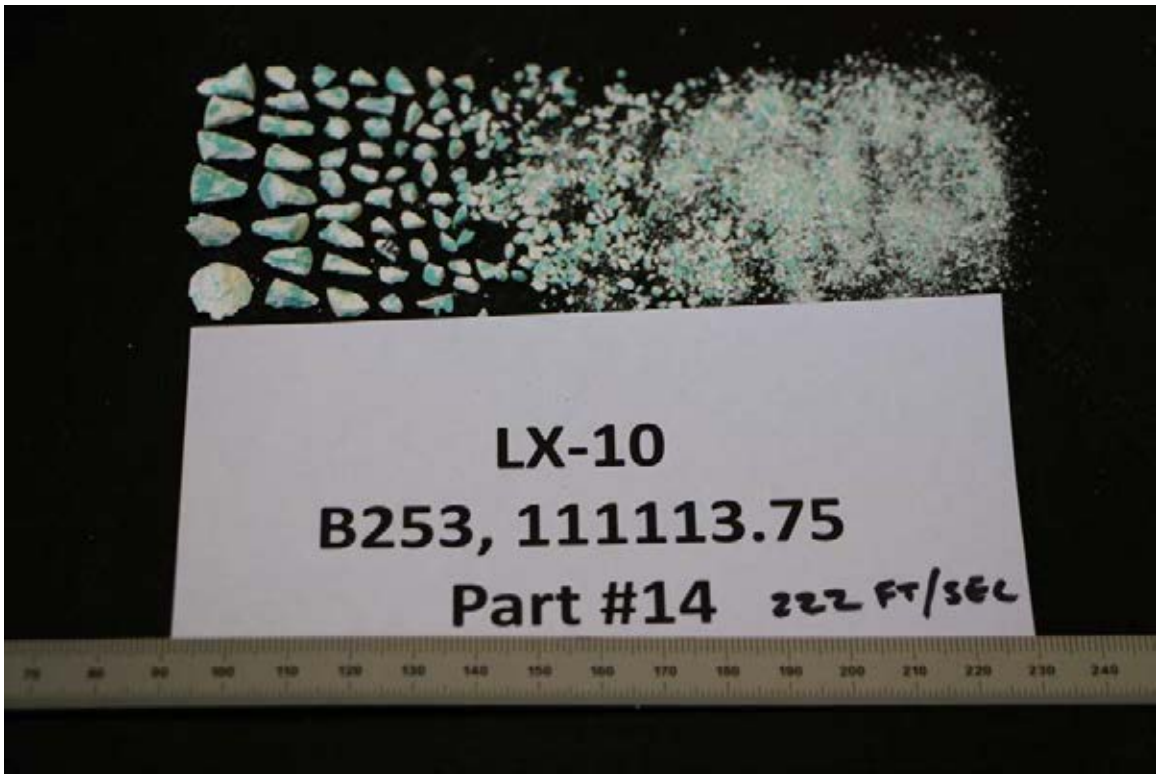
LX-10
B253, 111113.75
Part #14 222 FT/SEC

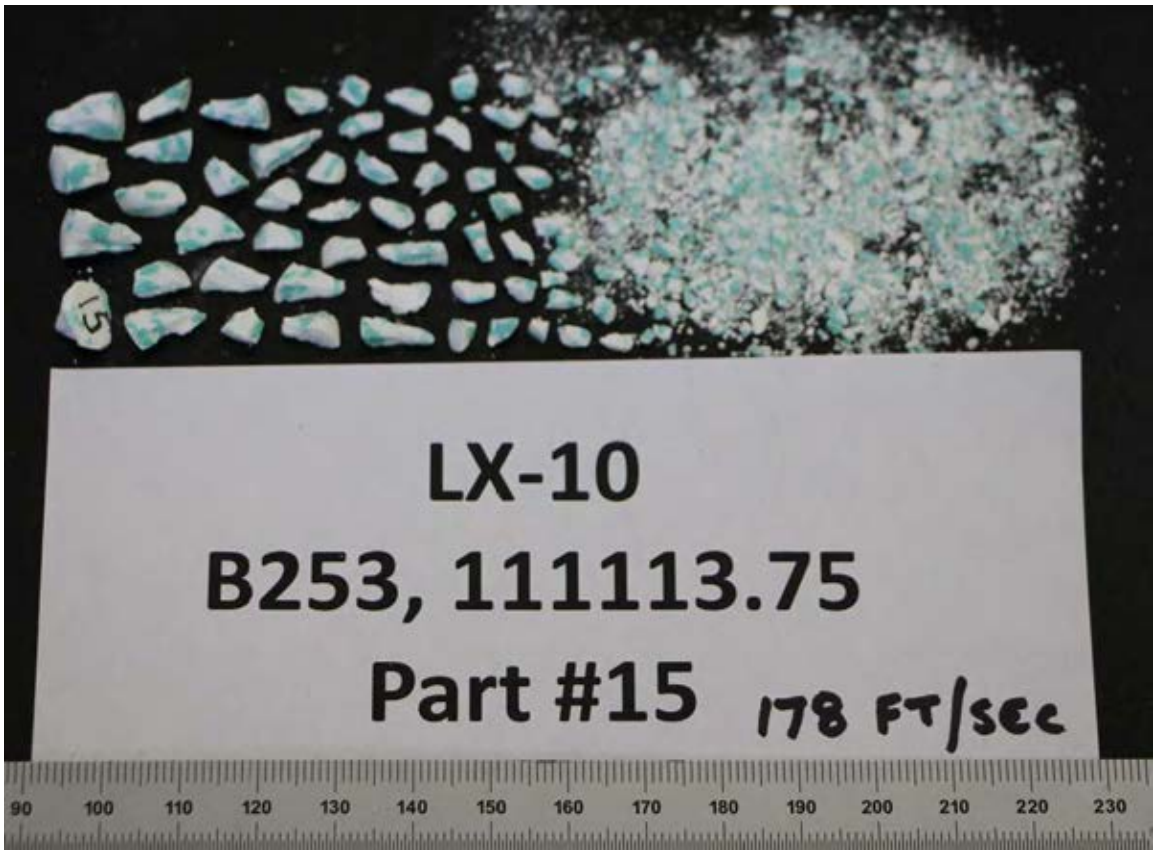
15
LX-10
B253, 111113.75
Part #15
178 FT/SEC
90 100 110 120 130 140 150 160 170 180 190 200 210 220 230


LX-10
B253, 111113.75
Part #16
178 FT/SEC
90 100 110 120 130 140 150 160 170 180 190 200 210 220 230

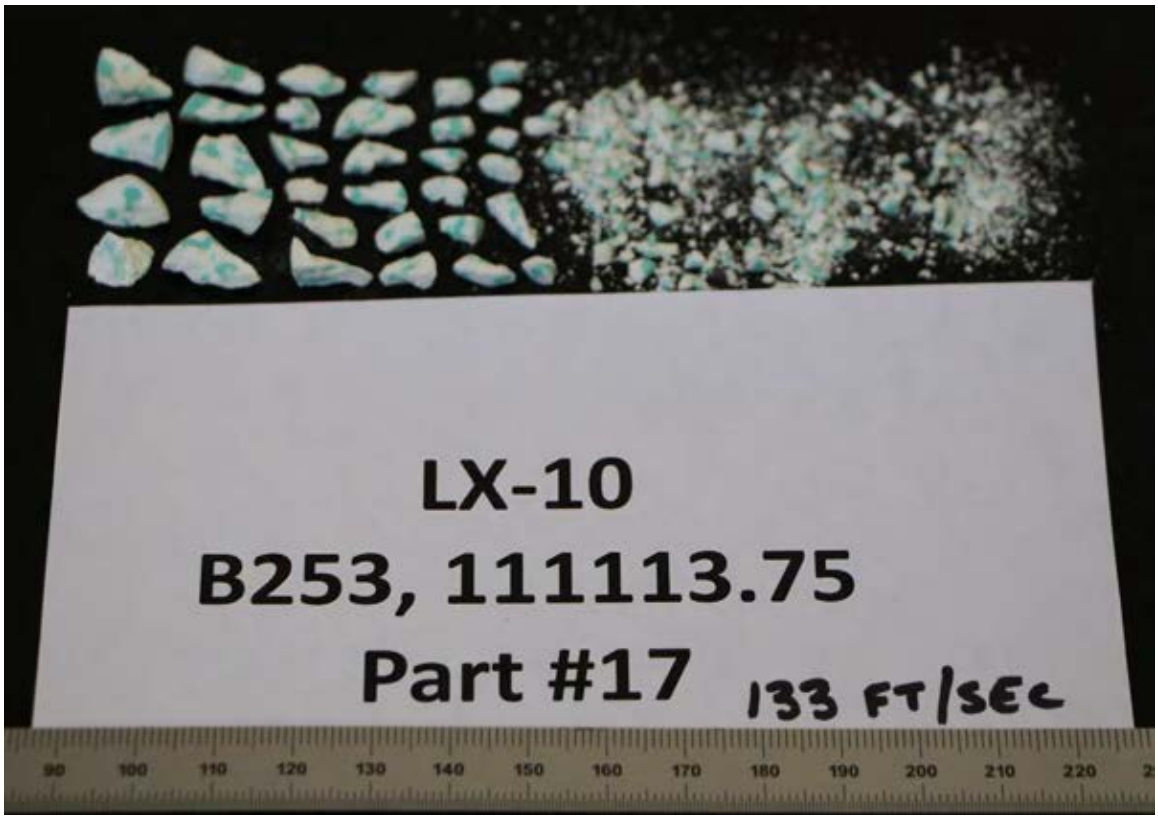
LX-10
B253, 111113.75
Part #17
133 FT/SEC

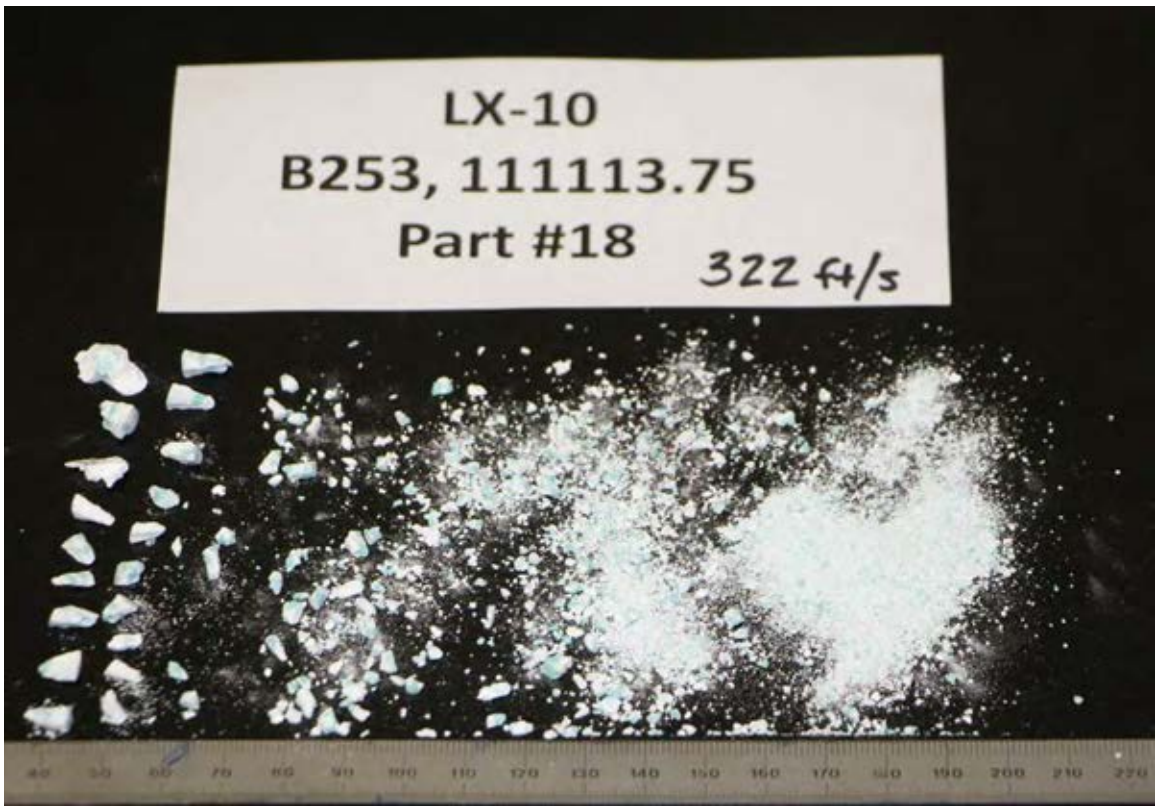
LX-10
B253, 111113.75
Part #18
322 ft/s

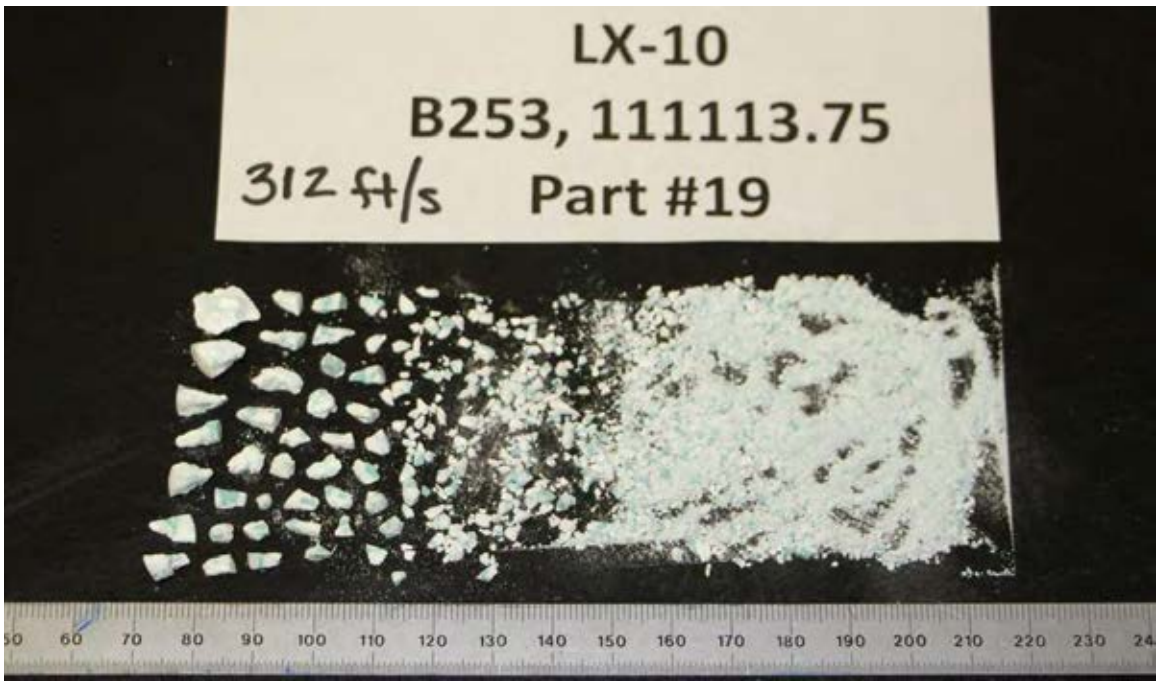
LX-10
B253, 111113.75
312 ft/s Part #19

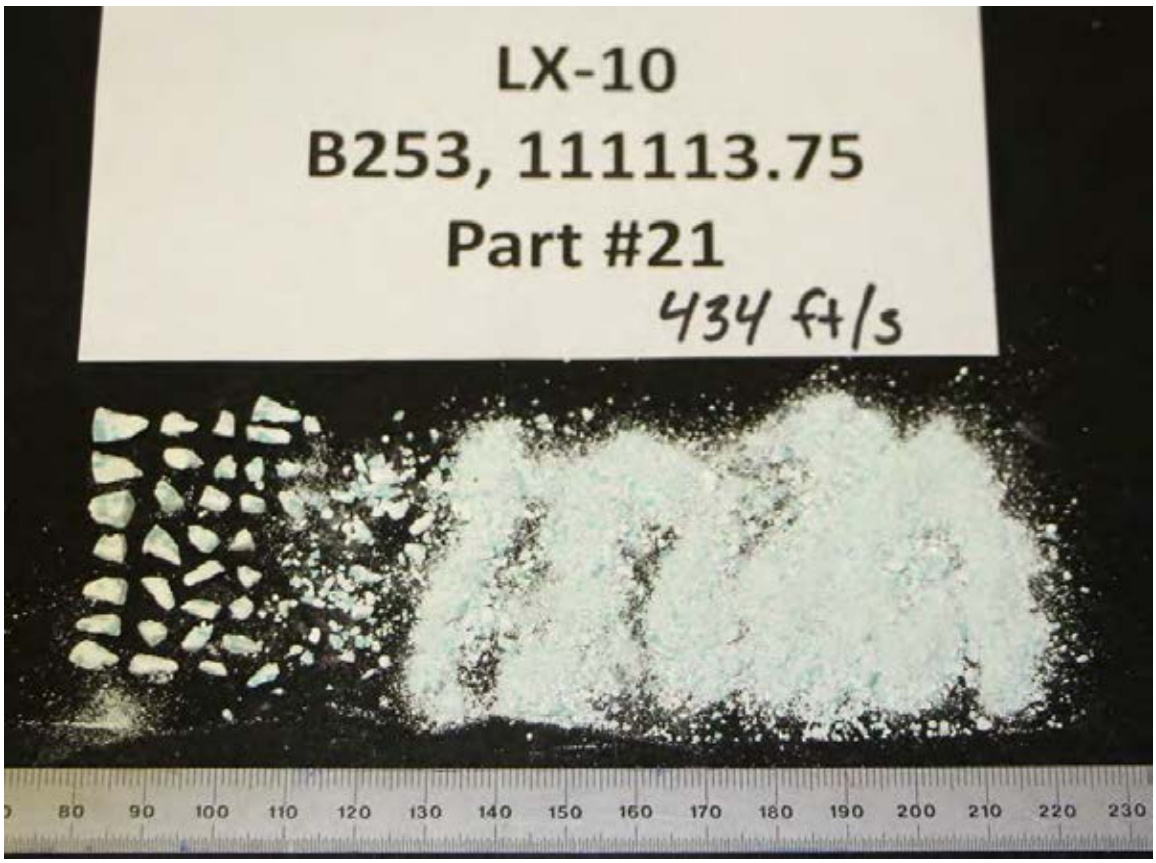
LX-10
B253, 111113.75
Part #21
434 ft/s

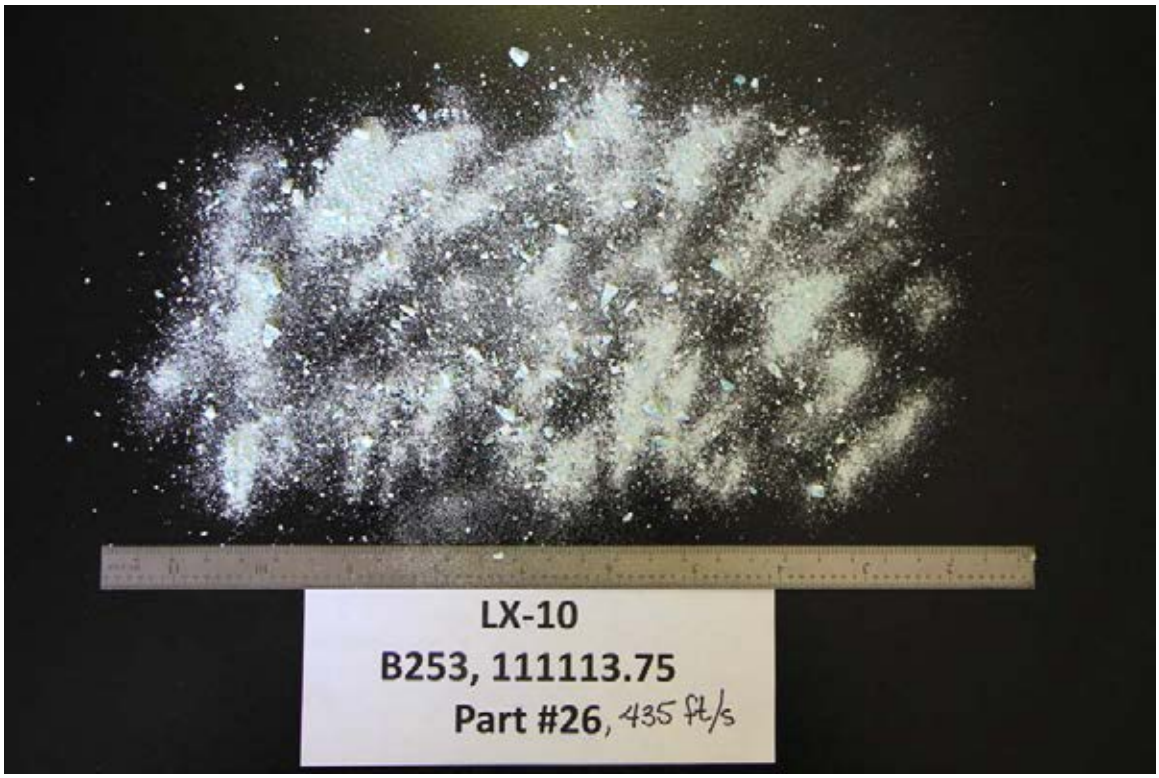
LX-10
B253, 111113.75
Part #26, 435 ft/s


LX-10
B253, 111113.75
Part #27 435 ft/s

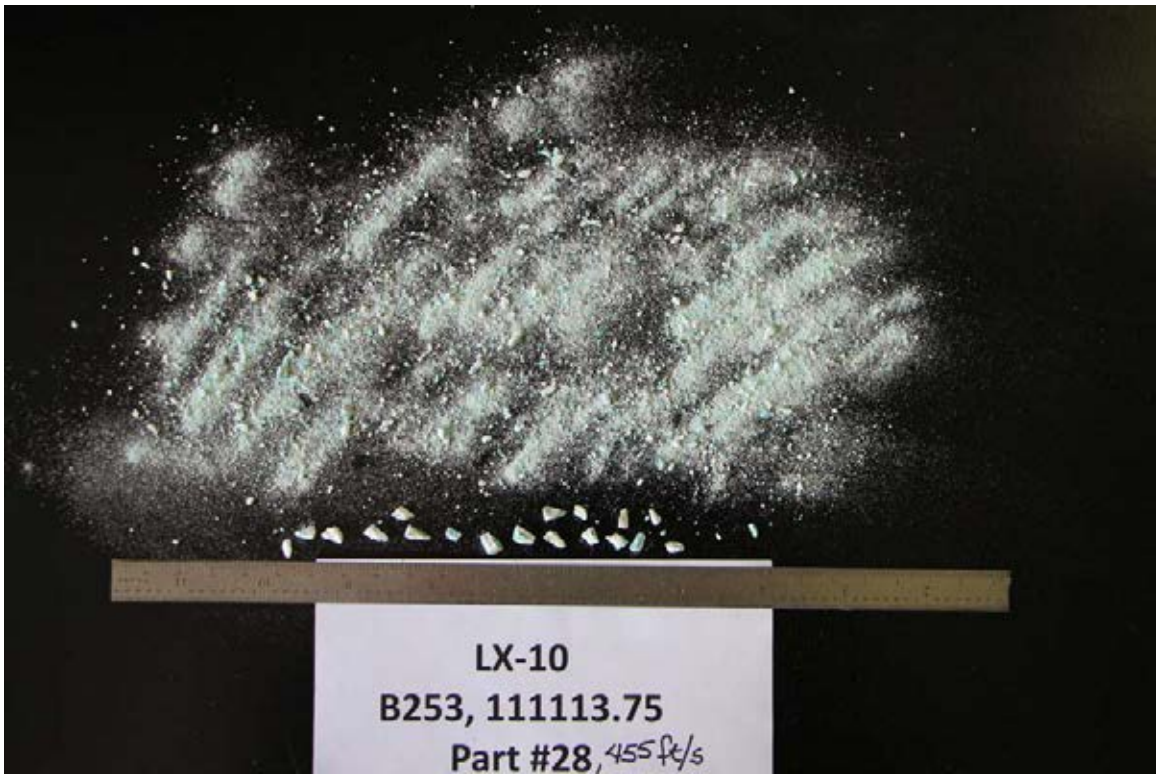
LX-10
B253, 111113.75
Part #28, 455 ft/s


LX-10
B253, 111113.75
Part #29, 476 ft/s

Appendix C

CHARACTERIZATION OF EXPLOSIVE BRITTLE FRACTURE/ COMPOSITION B BURNING RATE STUDIES

This page intentionally left blank.

CHARACTERIZATION OF EXPLOSIVE BRITTLE FRACTURE

A. I. Atwood, I. Purifoy, C.J. Wheeler, E. Woods, K. P. Ford
Naval Air Warfare Center Weapons Division, China Lake, CA 93555-6100
and
H. K. Springer
Lawrence Livermore National Laboratory, Livermore, CA

ABSTRACT

A progress report on the experimental evaluation brittle fracture in Compositions B (CompB) and LX-10 by impact is made in this paper. Cylindrical and spherical samples were impact damaged at impact velocities from 89 to 500 ft/sec. A closed bomb analysis was performed on the damaged cylindrical samples, and a particle size analysis was performed on the damaged spherical samples. Maximum dp/dt in excess of 2.5 Mpsi/s was observed in both explosives at impact velocities greater than about 100 ft/s for CompB and 200 ft/s for LX-10. A higher level of damage was observed in the CompB samples as indicated by higher maximum dp/dt and a larger mass fraction of fine particles generated under similar impact conditions.

BACKGROUND

Shotgun/friability testing is used to examine the damage vulnerability of an energetic material to mechanical insult. The test is used in the evaluation of deflagration-to-detonation transition (DDT) potential and in hazard classification testing (References C-1 and C-2).

Shotgun testing in the United States was originally designed to evaluate the damage thresholds of viscoelastic propellants and their potential to DDT. It has been used to determine the surface area increase as a function of impact velocity in these materials. The test has been extended to the evaluation of explosive formulations more recently (Reference C-3).

The modeling of mechanically induced brittle fracture is currently under investigation at Lawrence Livermore National Laboratory (LLNL), and this effort will provide data to support the ongoing studies to understand impact fracture and fragmentation.

OBJECTIVE

The objective of this study is to generate and examine the effect of mechanical insult on explosives whose primary damage mechanism is brittle fracture. This paper presents a progress report on two formulation types: melt cast and pressed, in two geometric configurations. The effort is designed to not only gain insight into the mechanisms of brittle fracture but to provide validation data for fracture models under development.

APPROACH

This study includes a two-part approach.

Part I of the study includes traditional shotgun/friability testing with 18-mm-diameter cylindrical explosive samples. The samples are fired from a smooth-bore, 18-mm gun against a steel target at various velocities. The resulting debris is collected and fired in a manometric closed vessel. The pressure-time history is recorded, and an analysis of the data performed to evaluate both the maximum dp/dt and burn area increase as a function of impact velocity.

Part II of the study is performed with 18-mm-diameter spherical explosive samples that are fired from the 18-mm gun at various velocities. The resulting debris is dry screened into size fractions from 3,360 to 106 μm. These samples are then returned to LLNL for further study at that facility.

EXPERIMENT

SHOTGUN

A schematic of the Naval Air Warfare Center Weapons Division (NAWCWD) 18-mm high-velocity impact device is shown in Figure C-1. The device was designed and built by Safety Management Services. The breach of the gun barrel was designed to operate with either powder or gas-driven actuation. The 18-mm barrel was fired using nitrogen in this study. The device incorporates a 2.3-liter accumulator tank with an air-actuated ball valve. This enables the operator to vary the propulsion gas pressure and thus the velocity of the explosive sample. Impact velocities of 89 to 435 ft/s (27.13 to 132.59 m/s) were achieved in this study.

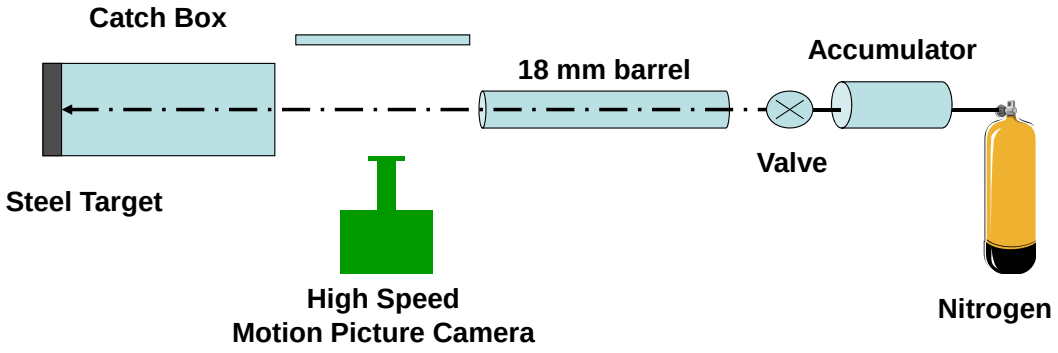

FIGURE C-1. Schematic of the 18-mm Impact Device Used for the Friability Study.

CLOSED BOMB

A 200 cm^3 Harwood Engineering powder bomb was sleeved to a volume of 108-cm^3 for this study. Ignition of the sample was by means of a Reynolds air bag squib firing into approximately 1.0 gram of DuPont PB smokeless powder acting as ignition aid. The squib and aid were packaged in a silk bag, and the entire ignition unit was similarly bagged with the samples.

A schematic of the closed bomb data acquisition system is shown in Figure C-2. Pressure-time data are acquired using a Kistler Model 607C4 pressure transducer. The amplified pressure signal is digitized and recorded on a Nicolet MultiPro digital data acquisition system. The pressure-time records obtained from the digital oscilloscope are processed to remove wild points, smoothed using a parametric spline, and differentiated.

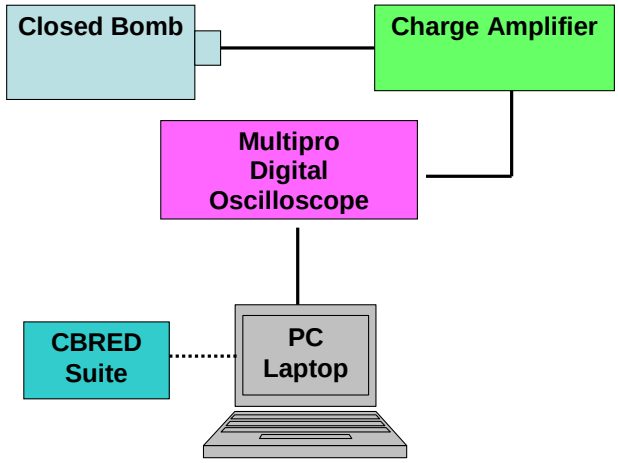

FIGURE C-2. Schematic of the Closed Bomb Data Acquisition System.

The closed bomb reduction program, CBRED II was used to reduce the closed bomb data obtained in this study (References C-4 through C-6).

The measured pressure-time history from a closed bomb firing is converted to a mass regression rate based on thermochemistry, as determined from a thermochemical equilibrium code (BLAKE in this study) (Reference C-7). In equation C-1, the mass burning rate ($\dot{m}$) of an energetic is the product of the surface area (A_b), the sample density (ρ), and the linear burning rate (r).

$$\dot{m} = \rho r A_b \qquad \text{(C-1)}$$

For the undamaged sample, the density and initial burn area are known or calculated, and the linear burning rate as a function of pressure can be determined. Once the linear burning rate has been determined for a formulation, it can then be used as input into the CBRED II program for the damaged sample evaluation. The pressure-time history for the closed bomb firing of the damaged sample is again converted to mass burning

rate-time in the program. Referring again to the above equation for the damaged sample, the density (assumed to be unchanged) and linear burning rate are known, and the burn area as a function of time and distance burned can be determined.

It can be seen from the discussion above, that the closed bomb analysis relies on a sample with good combustion properties. The linear burning rate must be known or measured. Equilibrium thermochemistry is employed and gaseous combustion products are assumed for the optimal application of the analysis. Good sample integrity (no flaws from manufacturing or deconsolidation during combustion) and uniformity are key to optimal data reduction. Instantaneous ignition on all sample surfaces is also assumed, and the heat loss to the vessel minimized and addressed in the analysis.

PARTICLE SIZE ANALYSIS

The recovered damaged spherical samples were dry screened to obtain an understanding of the particle size distribution of the fragments as a function of impact velocity. The damaged samples were dry screened from 3,360 to 106 μm using a set of 14 screens.

The final screening technique developed includes sending the entire damaged sample first through the 355 μm mesh screen. The sample remaining on the top of the 355 μm screen is then sent through the 3,360, 1,000, 840, 590, 500, and 420 μm mesh screens. The sample smaller than 355 μm is sent through the 250, 212, and 180 μm screens and the less than 180 μm fraction sent through the 150, 125, and 106 μm mesh screens. It was found that the size fractions below 200 μm required a large amount of agitation in order to achieve particle separation. An alternate method for particle size analysis should be employed to obtain the size fractions below 106 μm.

A shortfall of most size analysis methods, including screening, is that they are based on a spherical particle. The size analysis error will increase as the length to diameter ratio increases in the fragments generated upon impact. It is assumed that microscopy will be applied to the size fractions at LLNL in order to evaluate the particle morphology.

SAMPLES

Explosives generated with two processing techniques have been investigated in this study; the melt cast Composition B (CompB) and the pressed LX-10. Two geometries, cylindrical and spherical, of each explosive were manufactured. The cylindrical samples were used for the traditional shotgun/ friability work, and the spherical samples were used for the screening. Spherical samples were selected to reduce the tumbling effects often observed at low velocities, but the low mass of the 18-mm-diameter sample prevented its use in the closed bomb work.

COMPOSITION B

Trinitrotoluene (TNT) and cyclotrimethylenetrinitramine (RDX) are the principal ingredients of CompB explosive. CompB has been widely used in as the explosive fill in all types of ordnance. The general composition consists of 59.5 weight percent RDX in 39.4 weight percent TNT with about 1 weight percent desensitizing wax. Melt cast shotgun samples of CompB were formulated by BAE Systems, Batch CBIA-433807, lot BAE10E234-007, type 1, Grade A, for the closed bomb testing described in this paper. The RDX content was 61.0 weight percent with 38.0 weight percent TNT.

The CompB friability cylinders were 17.9754 ± 0.0051 mm in diameter and 22.7251 ± 0271 mm in length. They weighed 9.8944 ± 0.0335 grams. A typical sample is shown in Figure C-3.

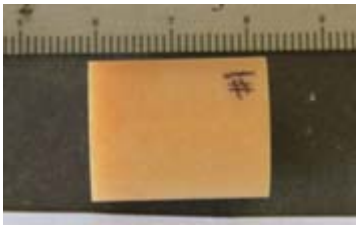

FIGURE C-3. Typical CompB Friability Sample (mm Scale Divisions).

The friability spheres were 18.00 ± 0.01 mm in diameter and they weighed 5.2630 ± 0.0066 grams. A typical sample is shown in Figure C-4.

FIGURE C-4. Spherical CompB Sample (mm Scale).

LX-10

LX-10 is a pressed explosive composed of 95 weight percent cyclotetramethylenetetranitramine (HMX) and 5 weight percent Viton. The LX-10 used in this study contained HMX with a mean particle size of 138.1 μm.

The LX-10 cylinder diameter was 18.0163 ±0.0062 mm and 21.0475 ± 0.0429 mm in length at a weight of 9.908 ± 0.0156 grams. A typical LX-10 sample is shown in Figure C-5. The bi-color of the sample is for identification purposes and both components contain the same ingredients.

FIGURE C-5. Typical Cylindrical CompB Friability Sample (mm Scale Divisions).

The LX-10 sphere diameter was 18.0129 ± 0.0067 mm and at a weight of 5.678 ± 0.0063 grams. A typical LX-10 spherical sample is shown in Figure C-6.

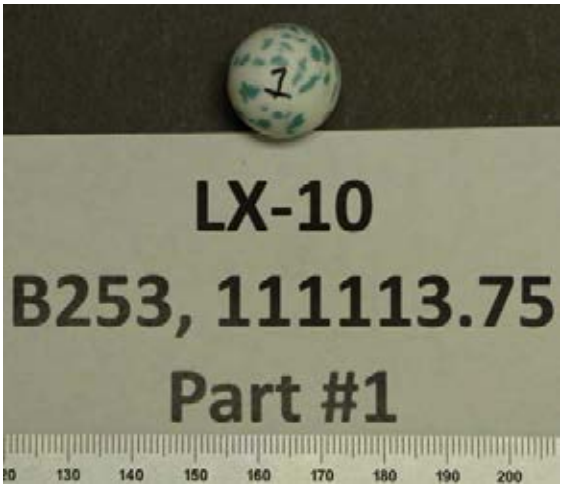

FIGURE C-6. Spherical LX-10 Sample (mm Scale).

RESULTS

Undamaged cylindrical explosive samples were burned in the closed bomb to obtain the necessary burning rates for the CBRED analysis. A plot of burning rate versus pressure is given for the CompB and LX-10 in Figure C-7. The LX-10 burning rates were reproducible for the range of pressures tested; however, the CompB burning rates were not reproducible. The possible causes of the CompB burning rate differences are the subject of a companion paper (Reference C-8). The contribution of burning rate on the determination of changes in the burn area will be illustrated with the CompB data but, the values must be viewed with caution due to such a large discrepancy in the burning rate data. The LX-10 explosive has a burning rate at more than two times lower than the lowest burning rate measured for CompB.

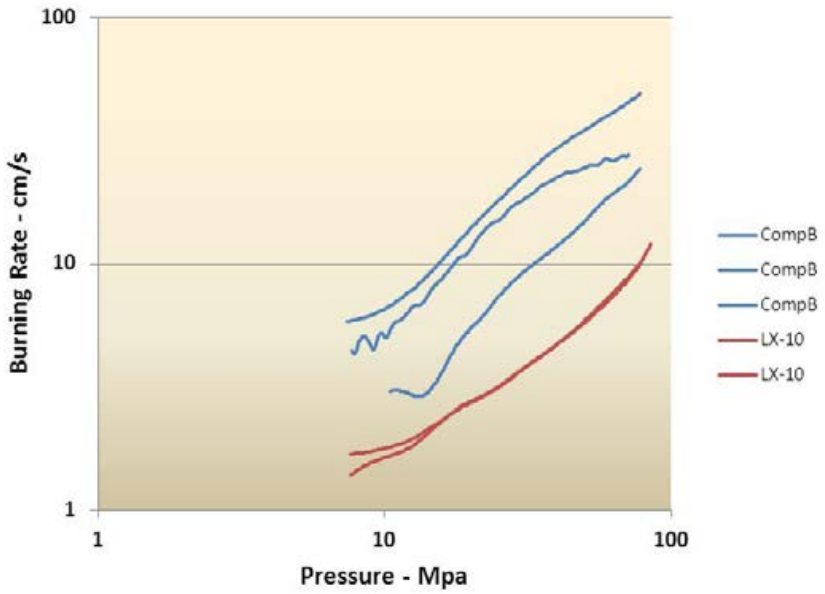

FIGURE C-7. Explosive Burning Rate Versus Pressure Data.

The percent of the damaged sample recovered decreased as the impact velocity increased. This is illustrated for the plot of percent recovered versus impact velocity of the cylindrical samples of both explosive formulations in Figure C-8. A similar observation was made for the damaged spherical samples. Aerosolization of the samples was observed at the highest impact velocities in both formulations. A power law relationship was developed for the normalized cumulative fragment number as a function of normalized fragment mass to account for the mass loss in the experiment (Reference C-9).

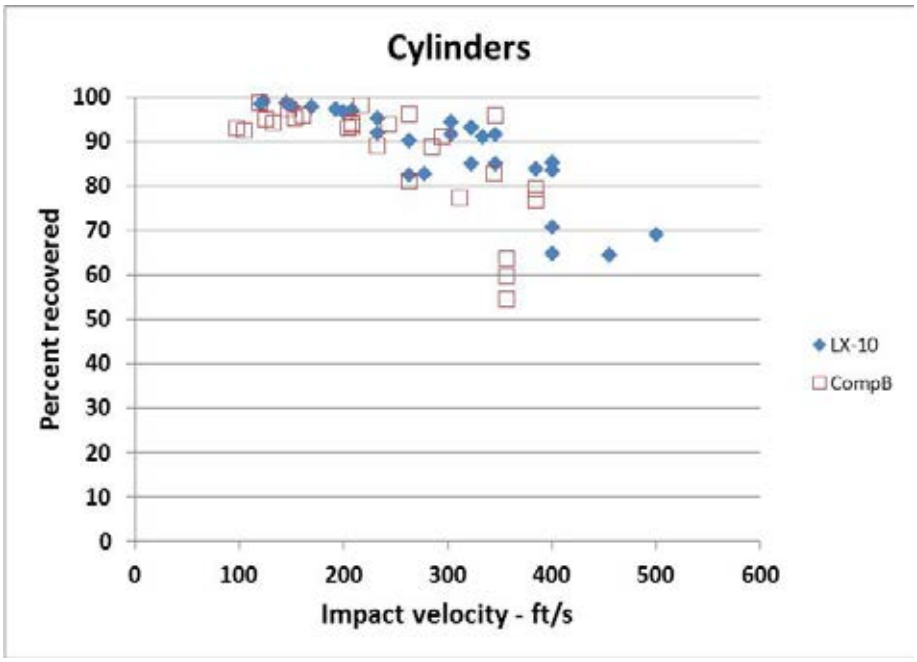

FIGURE C-8. Percent Recovered Versus Impact Velocity for CompB and LX-10.

Cylindrical CompB samples impact damaged at 105 and 385 ft/s can be seen in Figures C-9 and C-10, respectively. The increased damage with increasing velocity is visible with the decreased number of large fragments and increased amounts of fine powder.

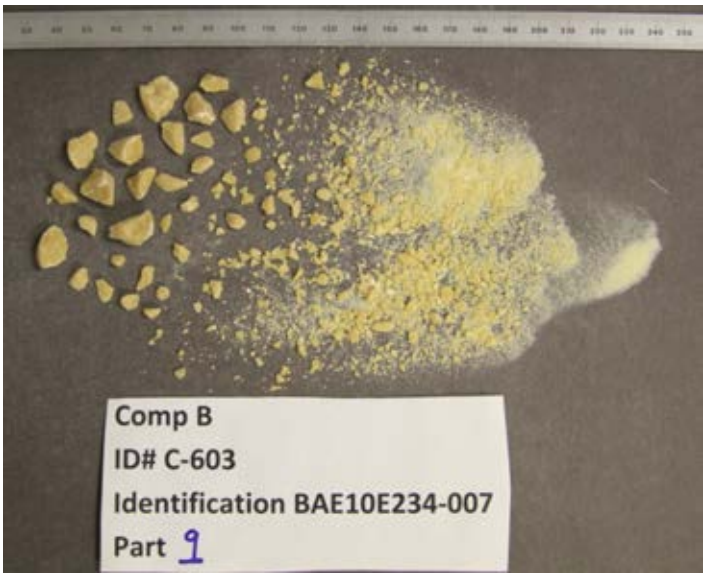

FIGURE C-9. Cylindrical CompB Sample Impact Damaged at 105 ft/s.

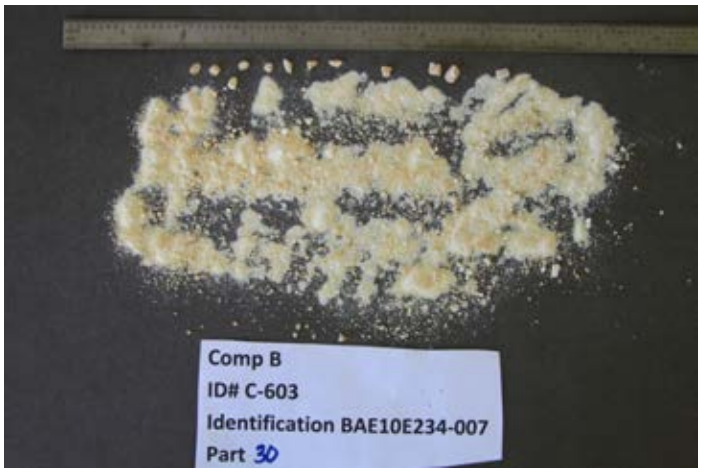

FIGURE C-10. Cylindrical CompB Sample
Impact Damaged at 385 ft/s.

Cylindrical LX-10 samples impact damaged at 121 and 385 ft/s can be seen in Figures C-11 and C-12, respectively. The increased damage with increasing velocity is again visible.

FIGURE C-11. Cylindrical LX-10 Sample Impact Damaged at 121 ft/s.

FIGURE C-12. Cylindrical LX-10 Sample Impact Damaged at 385 ft/s.

A plot of the maximum dp/dt versus impact velocity is given in Figure C-13. Despite the scatter observed in both samples, it appears that the Composition B (with the lower burning rate) is more friable than LX-10 under the conditions of the test. Both explosives generate a maximum dp/dt greater than 2.5 Mpsi/s at impact velocities greater than 100 for CompB and 200 ft/s for LX-10, an indication of a propensity for DDT (Reference C-10) in both explosives.

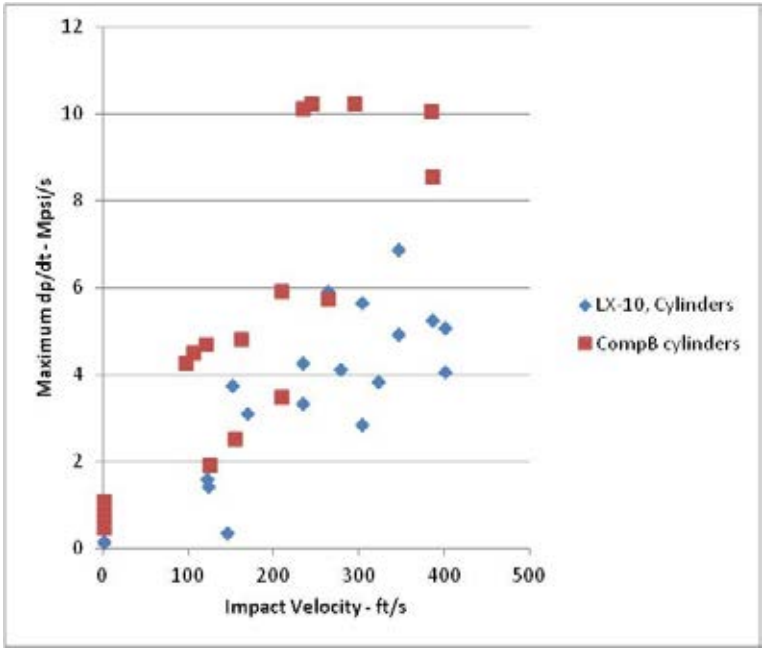

FIGURE C-13. Maximum dp/dt Versus Impact Velocity for CompB and LX-10.

A closed bomb analysis of the differentiated CompB data was made with the highest and lowest burning rate, and the effect can be seen in the plot of maximum burn area ratio versus impact velocity in Figure C-14. A difference of about two times reflects the difference in the measured burning rate. If the high burning rate is to be believed, then the maximum dp/dt levels observed in Figure C-13 can be attributed primarily to the burning rate; and, if the low burning rates are assumed, then the damage is primarily responsible.

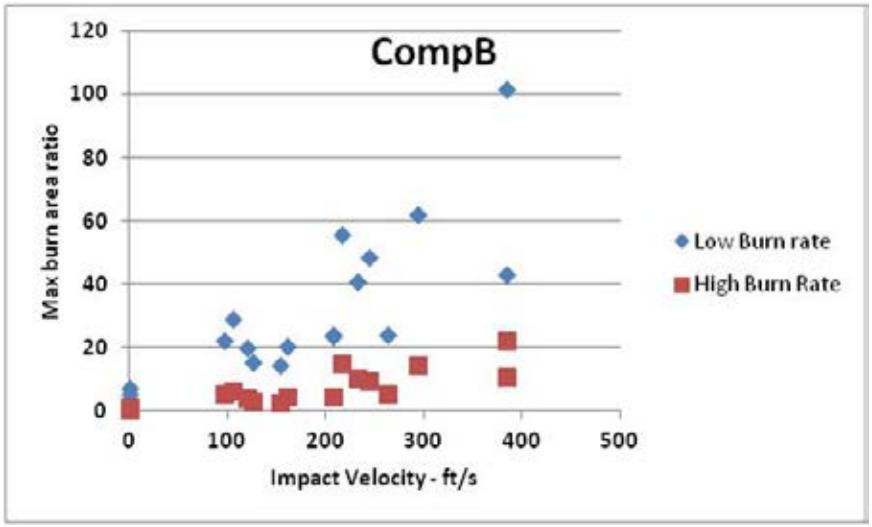

FIGURE C-14. Burning Rate Effects on CompB Maximum Burn Area Ratio.

A closed bomb analysis of the differentiated LX-10 data was made, and the maximum burn area ratio versus impact velocity is plotted in Figure C-15.

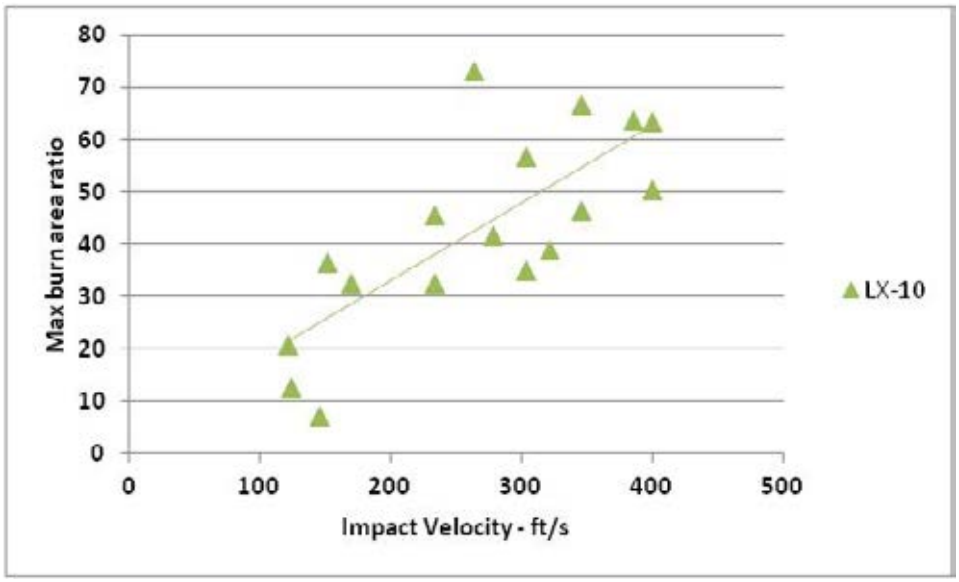

FIGURE C-15. LX-10 Maximum Burn Area Ratio Versus Impact Velocity.

Particle size analysis by dry screening of the CompB spherical samples impact damaged at velocities less than 200 ft/s is given in Figure C-16 and Figure C-17 for LX-10. The majority of the total mass fraction remains in the two coarsest fractions for both explosives.

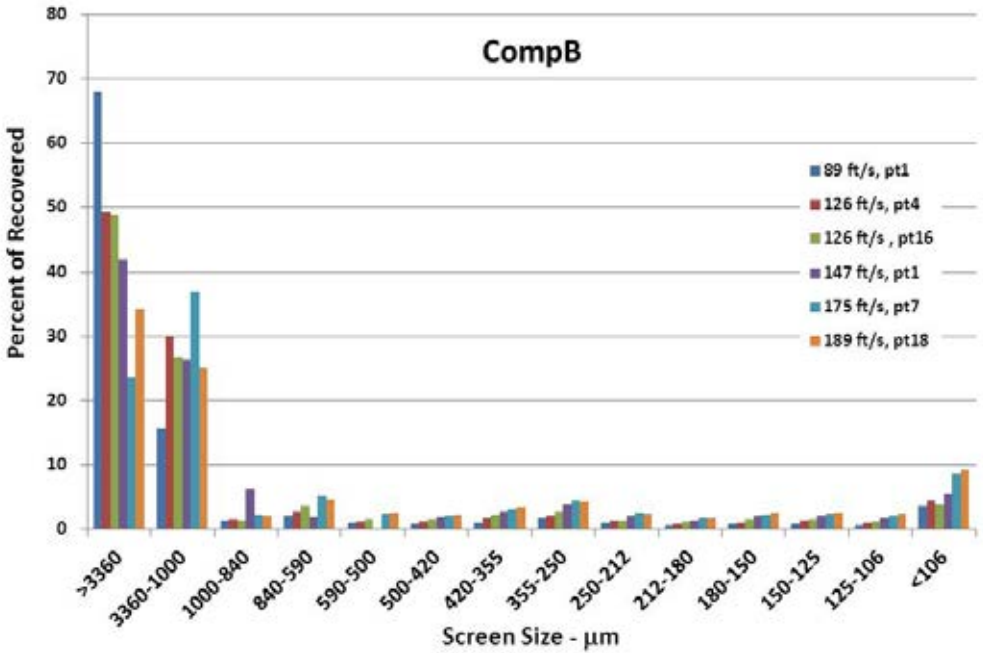

FIGURE C-16. CompB Size Analysis for Impact Velocities Less Than 200 ft/s.

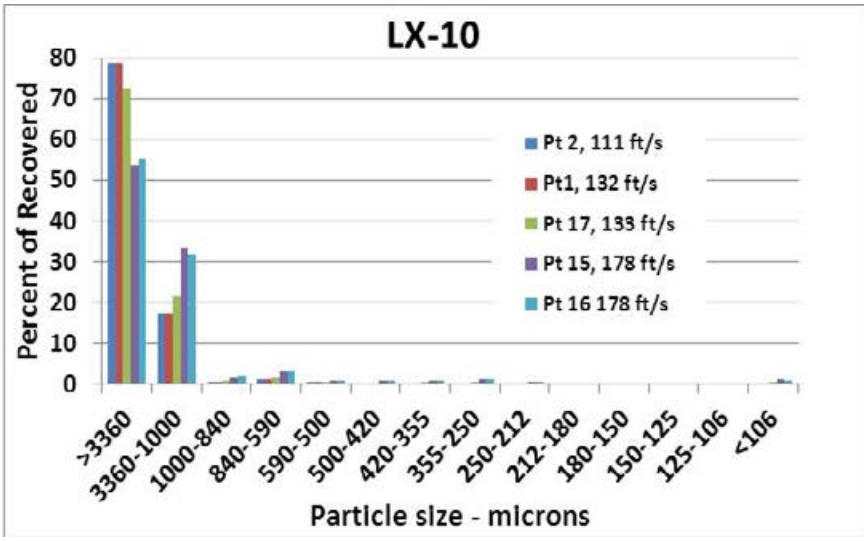

FIGURE C-17. LX-10 Size Analysis for Impact Velocities Less Than 200 ft/s.

The decrease in large fragments with increasing velocity can be seen in the plot of the fraction greater than 3,360 μm versus impact velocity for both explosives (Figure C-18). The CompB fraction is less than the LX-10 fraction in all cases, indicating the generation of a larger fraction of fine material under equivalent conditions.

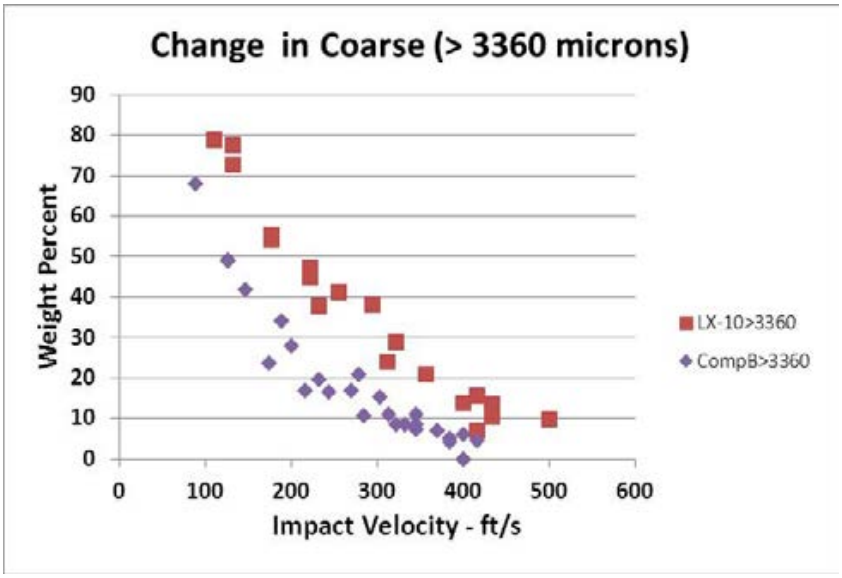

FIGURE C-18. Change in Diameter Greater Than 3,360 μm Size Fraction.

Particle size analysis by dry screening of the CompB spherical samples impact damaged at velocities between 370 and 417 ft/s is given in Figure C-19 for CompB and between 357 and 500 ft/s in Figure C-20 for LX-10. The majority of the total mass fraction remains in the two coarsest fractions for both explosives. A bimodal distribution is seen in the CompB samples with about 50% of the recovered fraction falling into either the fraction 3,360 to 1,000 or less than 106 μm. The distribution of LX-10 particulates remains mostly in the two coarsest fractions under similar damage conditions.

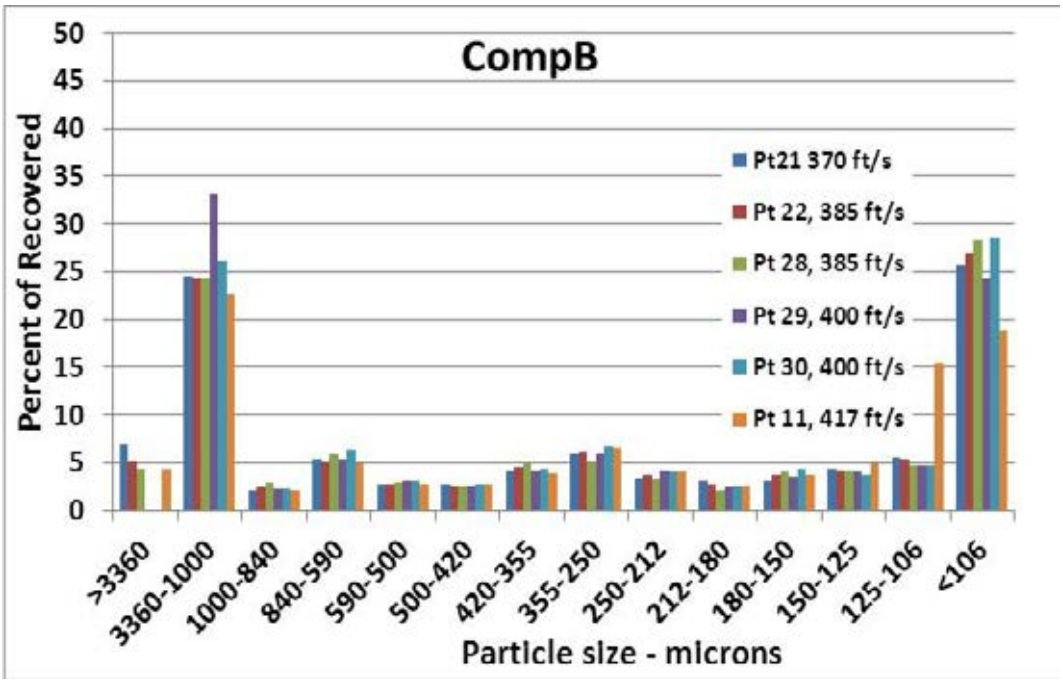

FIGURE C-19. CompB Size Analysis for
Impact Velocities 370 to 417 ft/s.

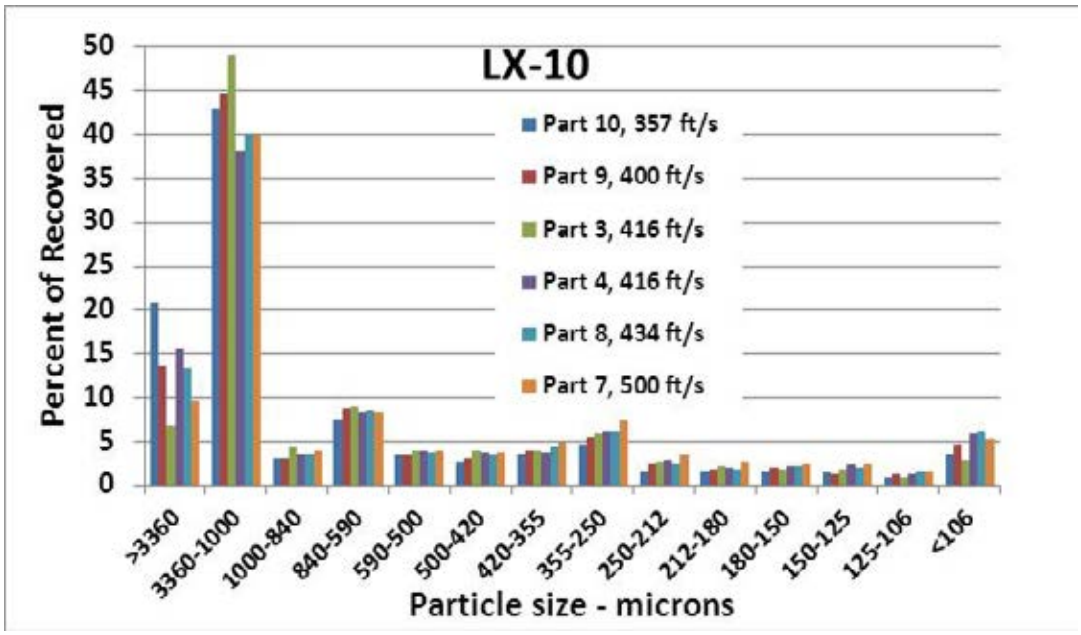

FIGURE C-20. LX-10 Size Analysis for
Impact Velocities 357 to 500 ft/s.

The increase in fine particles with increasing velocity can be seen in the plot of the fraction less than 106 μm versus impact velocity for both explosives (Figure C-21). The

CompB fraction is greater than the LX-10 fraction in all cases, indicative of a higher level of damage at similar conditions.

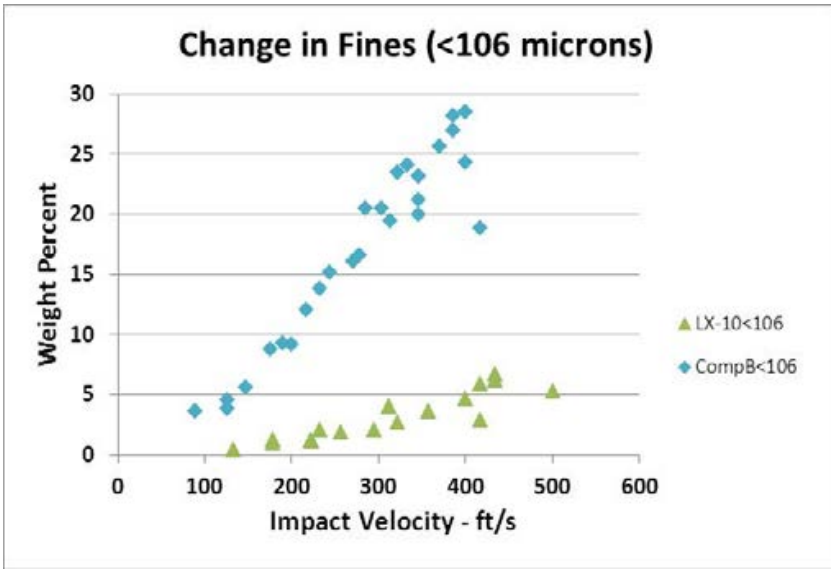

FIGURE C-21. Change in Fine Particles <106 μm Size Fraction.

Particle size analysis of impact damaged cylindrical samples is currently being performed, and the preliminary data suggest similar distribution trends as those observed for the spherical samples.

SUMMARY AND CONCLUSIONS

The fracture behaviors of CompB and LX-10 have been examined as a function of impact velocity. Impact damage increases with impact velocity. The level of fine particles generated impacted the collection efficiency for both explosives for both geometries tested.

LX-10 explosive demonstrated a reproducible closed bomb burning rate for the pressures tested as compared to a highly variable burning rate for the CompB explosive. Evaluation of damage based on closed bomb analysis is dependent on a consistent burning rate. Dry screening is being pursued as an alternate method to evaluate the level of damage.

The CompB explosive demonstrated a higher level of damage as indicated by the maximum dp/dt than that of LX-10 despite demonstrating a lower, albeit, variable burning rate. Both explosives were highly friable with a maximum dp/dt level greater than 2.5 Mpsi/s generated at velocities above 100 ft/s for CompB and 200 ft/s for LX-10.

Particle size analysis of the damaged CompB produced a bimodal distribution with the majority of recovered sample falling into two size fractions 3,360 to 1,000 μm and

less than 106 μm. Particle size analysis of the damaged LX-10 resulted in the majority of the recovered sample remaining is the two coarsest fractions with minimal fines produces. These data also support the conclusion that, under the damage conditions of the test, CompB is more friable.

FUTURE WORK

Future work calls for the performance of particle size analysis of the cylindrical geometry of the CompB and LX-10 samples. Select LX-10 samples will then be recombined and fired in the closed bomb and evaluated for maximum dp/dt and burn area. These data will be used to understand possible geometric effects on the fracture behavior and to begin to relate the particle size data with the closed bomb results.

The particle size data will be used to determine a maximum surface area of the sample and compared to that determined by closed bomb. A geometric form will have to be determined by microscopic examination of the sample.

A comparison of the brittle fracture explosives will be made to a viscoelastic sample.

REFERENCES

C-1. J. Isler. "Contribution du Mode de Combustion des Explosifs Compacts au Processus de la Transition Combustion-Deflagration-Detonation," *Proceedings of 19th International Annual Conference of ICT*, 1988, translation by T. S. Laker, Energetics Research Division, NAWCWD. Publication UNCLASSIFIED.

C-2. ST/SG/AC.10/11/REV.4/Amend.2. "Recommendations on the Transport of Dangerous Goods," Manual of Tests and Criteria, United Nations, New York, 2007.

C-3. A. I. Atwood, K. P. Ford, D. T. Bui, P. O. Curran, and T. M. Lyle. "Assessment of Mechanically Induced Damage in Solid Energetic Materials," *Seventh International Symposium on Special Topics in Chemical Propulsion (7-ISICP) Advancements in Energetic Materials & Chemical Propulsion*, Kyoto, Japan, September 2007. (Also published in *International Journal of Energetic Materials and Chemical Propulsion*, Begell House, Redding, Connecticut, Vol. 8, No. 5, pp. 391-410, December 2009.) Publication UNCLASSIFIED.

C-4. Army Ballistic Research Laboratory. *A Versatile User-Oriented Closed Bomb Data Reduction Program (CBRED)*, by C. F. Price and A. Juhasz. Aberdeen Proving Ground, Maryland, BRL, September 1977. (BRL R2018, publication UNCLASSIFIED.)

C-5. C. F. Price and A. I. Atwood. "CBRED II: A Versatile Tool for the Characterization of Damaged Propellants," *Proceedings of the 1991 JANNAF*

Propulsion Systems Hazards Subcommittee Meeting, Columbia, Maryland, Chemical Propulsion Information Agency, CPIA Publication No. 562, pp. 425-432, March 1991. Paper UNCLASSIFIED; publication UNCLASSIFIED.

C-6. A. I. Atwood et al. "Assessment of Mechanically Induced Damage in Solid Energetic Materials." *In: Seventh International Symposium on Special Topics in Chemical Propulsion (7-ISICP) Advancements in Energetic Materials and Chemical Propulsion*. Kyoto, Japan, 2007. Paper UNCLASSIFIED.

C-7. Army Ballistic Research Laboratory. *BLAKE – A Thermodynamics Code Based on TIGER: User's Guide and Manual*, by E. Freedman. Aberdeen Proving Ground, Maryland, BRL, July 1982. (BRL-TR-02411, publication UNCLASSIFIED.)

C-8. A. I. Atwood, A. D. Farmer, C. J. Wheeler, E. Woods, E. A. Glascoe, J. M. Kayman, K.P . Ford, and H. K. Springer. *Composition B Burning Rate Studies*, to be *presented at the 2014 JANNAF Propulsion Systems Hazards Subcommittee Meeting, Albuquerque, New Mexico*, December 2014, Columbia, Maryland, Chemical Propulsion Information Agency, 2014. Paper UNCLASSIFIED, publication UNCLASSIFIED.

C-9. Lawrence Livermore National Laboratory. *Analysis of Composition B Sphere Impact Fragmentation Experiments*, by H. K. Springer, A. I. Atwood, and K. P. Ford. Livermore, California, LLNL, June 2014. (LLNL-TR-650866, publication UNCLASSIFIED.)

C-10. A. G. Butcher, R. L. Keefe, N. J. Robinson, and M. W. Beckstead. Effects of Igniter and Compaction on DDT Run-Up in Plastic Pipes, *Seventh Symposium (International) on Detonation*, Naval Surface Weapons Center, Annapolis, Maryland, NSWC, June 1981. (NSWC MP 84-334, publication UNCLASSIFIED.)

This page intentionally left blank.

COMPOSITION B BURNING RATE STUDIES

A. I. Atwood, A. D. Farmer, C. J. Wheeler, E. Woods, J. M. Kalman, and K. P. Ford
Naval Air Warfare Center Weapons Division, China Lake, CA
and
E. A. Glascoe and H. K. Springer
Lawrence Livermore National Laboratory, Livermore, CA

ABSTRACT

An investigation of the burning rate properties of Trinitrotoluene (TNT) and variants of Composition B (CompB) explosive was made as a result of the large variation in burning rate observed in closed bomb firings of CompB explosive samples being used for a friability investigation. Neat TNT and CompB with 30, 59.5, and 70 weight percent (RDX) were formulated. Neat TNT would not self-deflagrate at pressures below 5.52 MPa (800 psia). The addition of RDX to TNT appeared to increase the burning rate slightly, but not linearly with RDX addition.

INTRODUCTION

The investigation of the burning characteristics of Composition B (CompB) is part of a larger, ongoing study to analyze the behavior of explosive fracture due to mechanical insult (Reference C-11). The burning rate of a damaged energetic material is directly linked to its mass regression rate. The burning rate contribution to the mass regression rate must be addressed in order to examine the contribution of damage alone. This is particularly true if the damage levels of two materials with different burning rates are to be compared.

BACKGROUND

The linear burning rate, in its simplest form, is the rate of conversion of energetic solid to gas in a direction normal to a planar surface. The Saint Robert-Vieille law is often used to describe the burning rate over limited ranges of pressure.

$$r=bp^n \qquad \text{(C-2)}$$

In equation C-2, r is the linear burning rate, p is the pressure, n is the burning rate pressure exponent, and b is a constant of proportionality. The sensitivity of the burning rate to changes in pressure increases as n approaches unity and, for solid rocket propellants, can cause rocket motor performance to suffer. Burning rate pressure exponents greater than unity are often indicative of grain deconsolidation during the combustion process (Reference C-12).

Typically, the Saint Robert-Vieille law does not hold over a broad pressure range, and solid rocket propellants will exhibit a “slope break,” or change in the burning rate

pressure exponent at a characteristic pressure, p*, where the burning rate changes from a lower to a higher value.

Burning rates are needed for damage evaluation in friability studies in order to separate the burning rate contribution to the pressurization rate (maximum dp/dt) from the change in surface area due to damage. Undamaged samples of known geometry are used to make these measurements. Typically closed bomb burning rates are within 3 percent or better of each other (Reference C-13). The closed bomb burning rates determined for undamaged CompB were much greater. Measurements of explosive burning rates are not common, and the combustion is not optimum as the formulations tend to be fuel rich. Solids settling at manufacture and deconsolidation during combustion were thought to be two potential causes of the observed differences.

The current study employed a photographic technique to directly observe the CompB burning behavior. A series of model CompB mixes were formulated with varying amounts of cyclotrimethylenetrinitramine (RDX) from 0 to 70 weight percent in order to gain an understanding of the contribution of the ingredients to the observed burning behavior.

SAMPLE

Trinitrotoluene (TNT) and RDX are the principal ingredients of CompB explosive. CompB has been widely used as the explosive fill in all types of ordnance. The general composition consists of 59.5 weight percent RDX in 39.4 weight percent TNT with about 1 weight percent desensitizing wax.

Melt cast shotgun samples of CompB were formulated by BAE Systems, Batch CBIA-433807, lot BAE10E234-007 for the closed bomb testing described in this paper.

Two samples of CompB were used in the high-pressure strand burning technique. Pellets of CompB were pressed at Lawrence Livermore National Laboratory (LLNL), while a second series was manufactured by the melt cast technique at the U.S. Army Aviation and Missile Research, Development, and Engineering Command (AMRDEC), Huntsville, AL.

CompB samples used for the photographic technique were manufactured at the Naval Air Warfare Center Weapons Division (NAWCWD), China Lake, CA. The melt cast samples were cast into thin sheets to reduce the potential for settling of the RDX particles. Four model CompB mixes with an RDX content of 0 (neat TNT), 30, 59.5, and 70 weight percent were formulated.

EXPERIMENT

Burning rates were obtained over a range of pressures from 1.38 MPa (200 psia) to about 78 MPa (11,300 psia). The burning rates illustrated in this paper were generated

using a technique that incorporates both low- and high-loading density combustion bombs. The technique involves the use of a combination of cinephotomicroscopy and closed bomb testing. The burning rates generated for the CompB friability study were also compared against the LLNL high-pressure strand burning technique.

Combustion bombs have been widely used to assess solid propellant combustion behavior for many years. Highly loaded closed bomb techniques are heavily used in the gun and explosives communities, with limited use by the solid rocket propellant community. The solid rocket propellant community has used the closed bomb for the evaluation of propellant friability and its propensity for deflagration-to-detonation transition (DDT) (Reference C-14). Strand or window burners have had more use in the solid propellant community. There are numerous types and styles of combustion vessels, but they can be divided into two categories based on their loading density or the weight of the sample divided by the total bomb volume. Low loading density bombs (<0.007 g/cm^3) experience little pressure rise during a test, and high loading density bombs (>0.02 g/cm^3) see pressure rises greater than 14 MPa during a test.

A window bomb technique (low loading density) was used in this study to generate burning rate data from about 1.38 to 55 MPa (200 to 8,000 psia). A schematic of the experimental system is shown in Figure C-22. Since little pressure is generated in these bombs during a test, they must be pressurized to the specific pressure of interest. The test sample is photographed using a high-speed digital camera at a framing rate of 500 pictures per second and 1X magnification. The burning rate is determined directly by measuring the sample regression of the spatially and temporally calibrated image. If needed, higher magnification and framing rates can be used to obtain an accurate description of the combustion process. The experimental error in measurement is due to the clarity of the image and the planarity of the burn front progression. Typical burning rate variations at each pressure range between 2 and 5%.

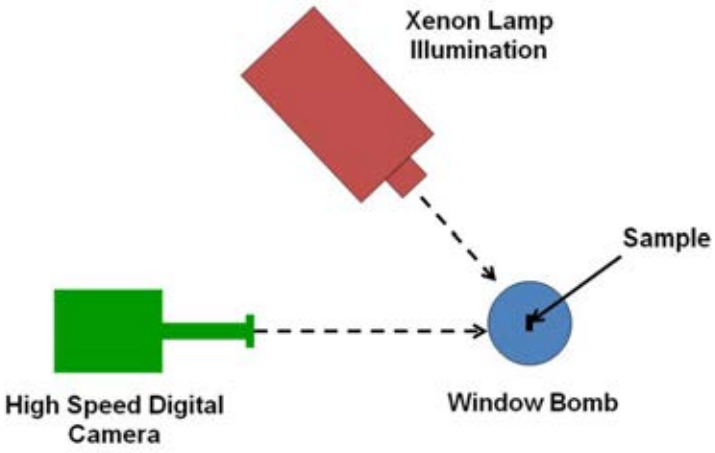

FIGURE C-22. A Schematic of the Window Bomb Burning Rate Apparatus.

The high loading density closed bomb operates at an increasing pressure due to the mass of propellant gasses added during the burning event. The pressure versus time history is collected over the event, and the reduction to burning rate relies on the following:

1. The burning surface is known and input as a geometric form function. All surfaces are simultaneously ignited and regress uniformly, and the regression rate depends only on pressure and propellant temperature.
2. Heat losses from the bomb are minimal.
3. The equation of state for the gases is known.

Burning rates at pressures from 13.8 to 78 MPa (2,000 to 11,300 psi) are generated using a Harwood manufactured powder bomb in this study. The vessel end closure is fitted with the igniter leads and pressure gage. Venting is through the opposite end of the vessel. The inside of the bomb is fitted with a stainless steel liner to protect the inner surface and to change the bomb volume if needed. Ignition is by a MK2 electric squib and a portion of DuPont smokeless powder acting as aid. A schematic of the closed bomb system is shown in Figure C-23. Pressure-time data are acquired using a Kistler model 607C4 pressure transducer. The amplified signal is digitized and recorded on a Multipro data acquisition system.

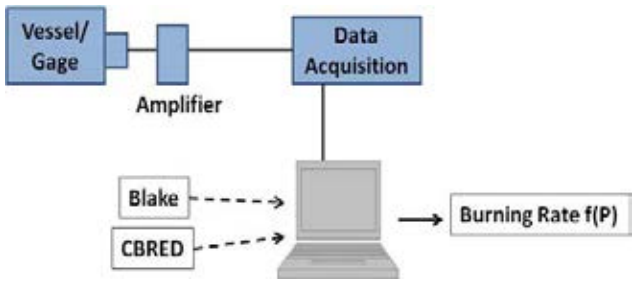

FIGURE C-23. Schematic of the Closed Bomb System.

The recorded pressure-time history is first subjected to smoothing and differentiation prior to its conversion to a mass regression rate, m. The Blake thermochemical code (Reference C-15) is used to obtain the thermochemical parameters of impetus, co-volume, temperature, and specific heat as a function of pressure for the propellants.

Closed bomb reduction transforms the measured pressure time history into a mass regression rate through the application of an equation of state. The Closed Bomb Reduction (CBRED) code is employed to reduce the pressure time data (Reference C-16). CBRED uses a Noble-Able co-volume equation of state (Equation C-3).

$$P(V_s - nw_e) = w_pF \qquad \text{(C-3)}$$

In equation 2, P is the system pressure; V_s is the system volume; n is the co-volume; w_e is the weight of explosive burned; F is the Impetus, f (temperature, molecular weight); and w_p is the initial weight of explosive.

One of the options to the CBRED analysis is the ability to introduce the equation of state parameters as a function of pressure. This option is particularly important at the lower pressure regions of the burning rate curve where the thermochemistry is most sensitive to pressure.

$$\dot{m} = \rho r A_b \qquad \text{(C-4)}$$

Equation C-4 is employed in the differentiated form, along with a differentiated energy balance (accounting for the heat losses) to derive the mass rate of gasification as a function of time. The mass regression rate ($\dot{m}$) is the product of the burning surface area (A_b), the sample density (ρ), and the linear burning rate (r).

Undamaged samples of a known geometry are used to determine the burning rate as a function of pressure. The measured pressure-time history from a closed bomb firing is converted to a mass regression rate based on thermochemistry as determined from the thermochemical equilibrium code (BLAKE in this study). The thermochemistry of TNT not included in the BLAKE library was taken from that of the Propellant Evaluation Program (PEP) (Reference C-17) for this study.

An accurate description of the surface area (A_b) described by form function, the simultaneous ignition of all surfaces, and the uniform regression of the surfaces are some of the normal assumptions made in the reduction of closed bomb data to burning rate. Once the linear burning rate is known for a particular energetic, the change in surface area can be evaluated (A_b) for a damage sample. Samples intentionally damaged as a function of impact velocity are used to evaluate the friability of the specific energetic. If damage characteristics of a particular formulation are to be assessed, then the burning rate of that material must be well defined.

The closed bomb burning rate measurement technique is illustrated in Figure C-24. The closed bomb burning rates obtained at two loading densities are plotted in Figure C-24a. The low pressure measurements are plotted from 0.09 to 55 MPa (13 to 8,000 psia) in Figure C-24b. The combined data can be seen in Figure C-24c. The combined data can be fitted to generate a composite burning rate curve.

The linear burning rate of the sample is directly measured in the LLNL high pressure strand burner. Burns are performed under constant volume in an atmosphere of argon. The pressure is measured in-situ throughout the burn and the progression is monitored via silver breakwires than are embedded within the sample. A typical sample consists of 9 individual pellets (0.25-inch-diameter by 0.25-inch-length) and 10 burnwires; the exterior surface is encapsulated with an organic-polymeric material to prevent flame spread down the sides. The sample is pre-pressurized to a desired pressure using argon;

the sample is ignited via an ignition train consisting of a wire, $BKNO_3$, and a thin Hexanitrostilbene (HNS) pellet. The burning sample results in a pressure rise on the order of 3 to 5 times the initial pressure. Many towers may be employed in order to investigate pressures ranging from 10 to 600 MPa (1,450 to 87,000 psi) (Reference C-18). The high pressure strand technique employs the use of breakwires, common to the low loading density strand burner, but sample deflagration pressurizes the vessel making it a high loading density technique.

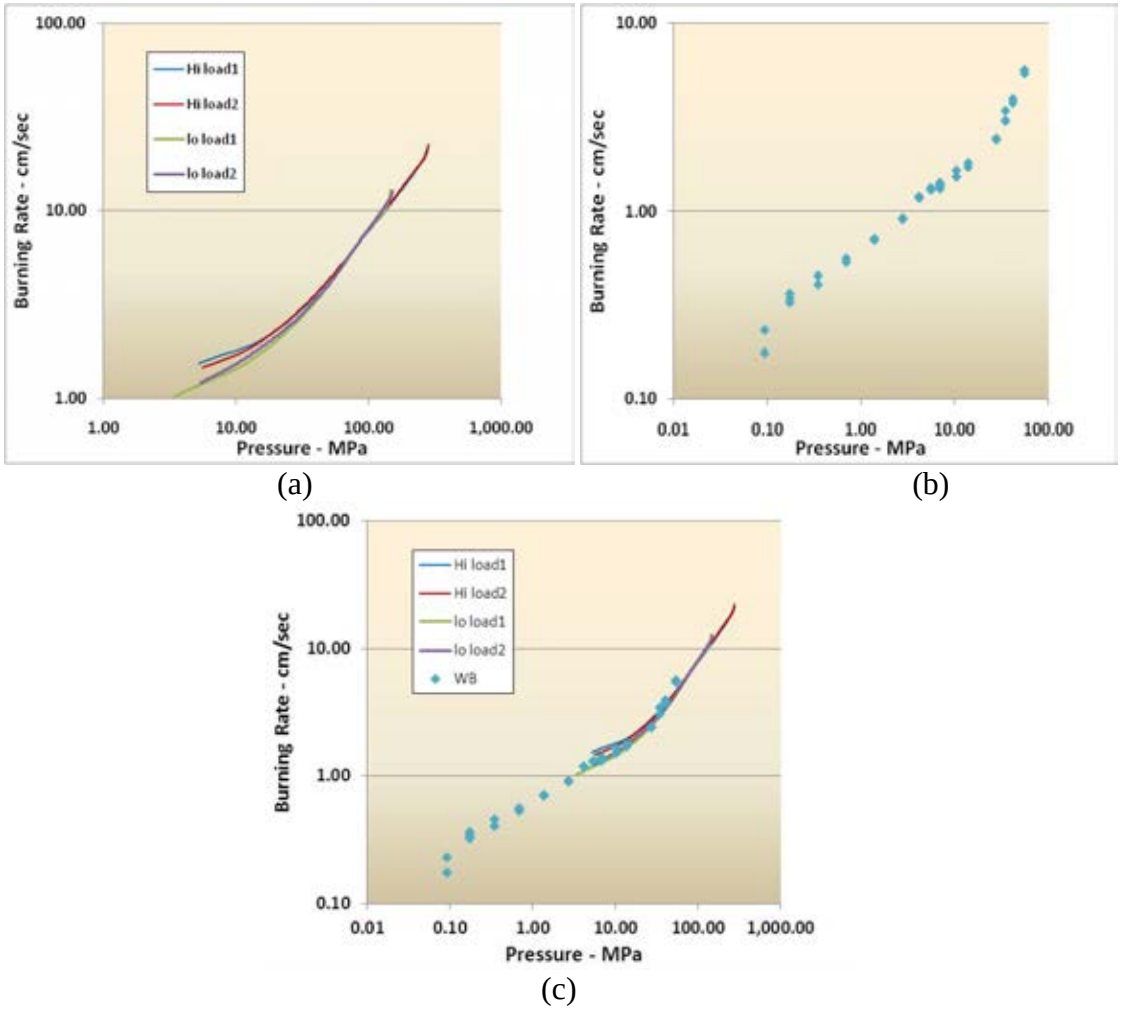

FIGURE C-24. Burning Rate Versus Pressure as Determined by (a) Closed Bomb, (b) Cinephotomicroscopy, and (c) Combined Data.

RESULTS

Closed bomb burning rate versus pressure data for three undamaged CompB (60 weight percent RCX) explosive samples are given in Figure C-25. It can be seen that the burning rates are not reproducible. The burning rate at 69 MPa (10,000 psi), for

example, ranges from 21.17 to 44.57 cm/s (8.33 to 17.55 in/s). It should also be noted that the burning rate pressure exponent is about unity.

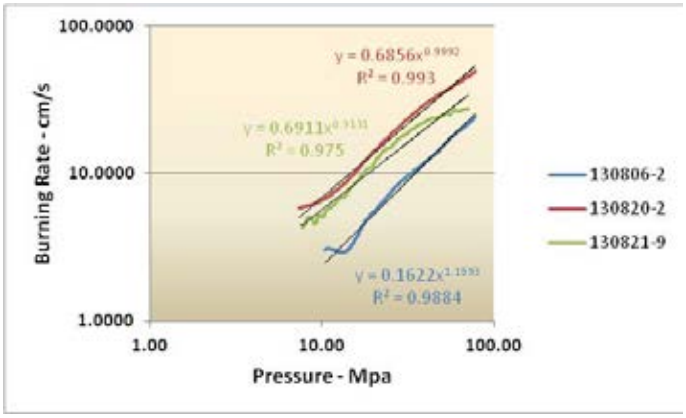

FIGURE C-25. CompB Burning Rate Versus Pressure as Determined from Closed Bomb.

Burning rate versus pressure data as determined with the LLNL high pressure strand burner are given in Figure C-26. Two CompB samples were tested in the high pressure strand vessel, one pressed and the other melt cast. The burning rate pressure exponent of the pressed pellets (~3.3) suggests a deconsolidation of the explosive grain during combustion. The closed bomb burning rates are included in the high pressure strand data; however, the large variation makes their use in analysis of the damaged surface area questionable. The closed bomb and strand data are compared in Figure C-27.

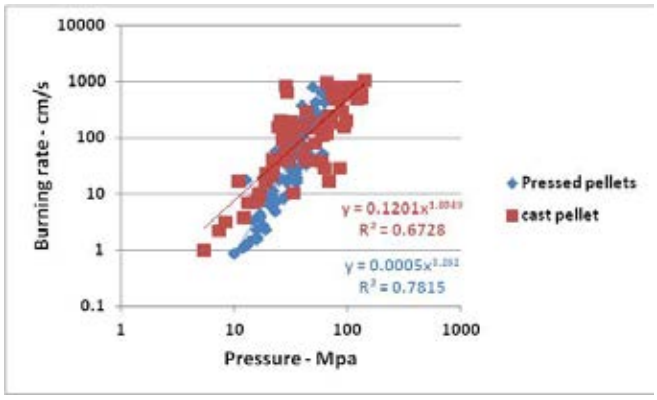

FIGURE C-26. CompB Burning Rate Versus Pressure as Determined from LLNL High Pressure Strand Burner.

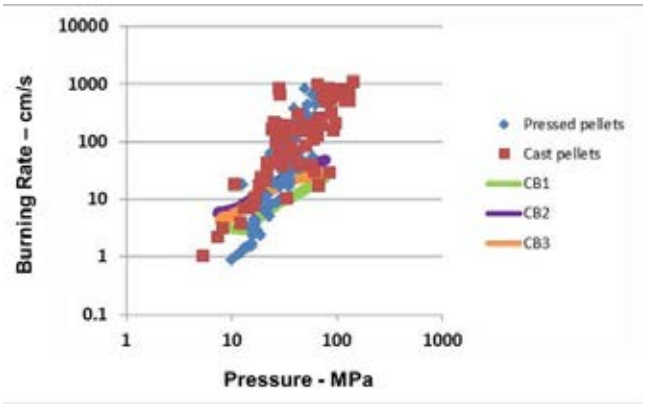

FIGURE C-27. Combined, High Pressure Strand and Closed Bomb CompB Burning Rate Data.

Photomicrography of the TNT and model CompB samples was employed in order to gain some understanding of the variations in data observed to date. It was believed that casting the samples in a thin sheet would remove the possible settling of RDX as a variable.

The burning rate versus pressure data for TNT are plotted in Figure C-28. The neat TNT would not self-deflagrate at pressures below 5.52 MPa (800 psia) under the conditions of this test. A frame from a typical burning sample is given in Figure C-29. An irregular orange flame and copious black smoke formation can be seen in the figure. A burning rate pressure exponent of ~0.35 was observed for the neat TNT at pressures from 5.52 to 55.17 MPa (800 to 8,000 psia). Combustion of the TNT samples was not smooth resulting in an irregular, "puffing," or periodic burning behavior.

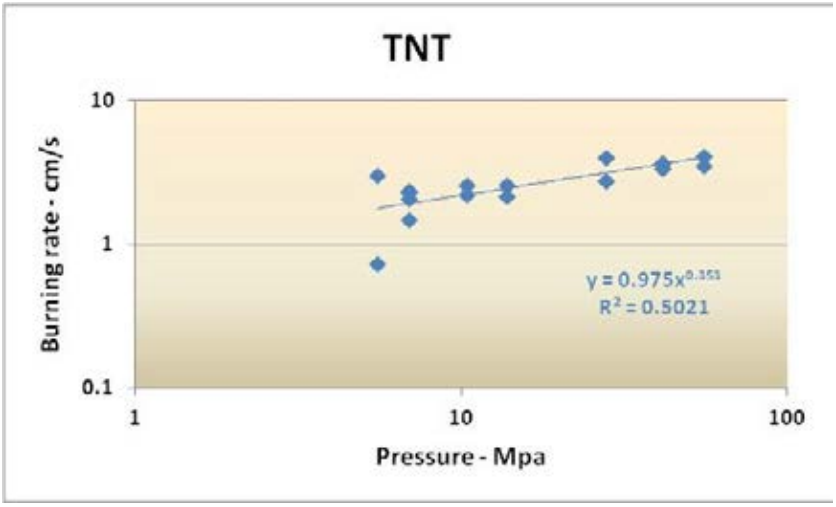

FIGURE C-28. Neat TNT Burning Rate Versus Pressure.

FIGURE C-29. TNT Burning Sample at 10.34 MPa (1,500 psia).

Neat RDX, in contrast, will self-deflagrate at pressures below 5.5 MPa (800 psia) as can be seen in the burning rate versus pressure plotted in Figure C-30 (Reference C-19).

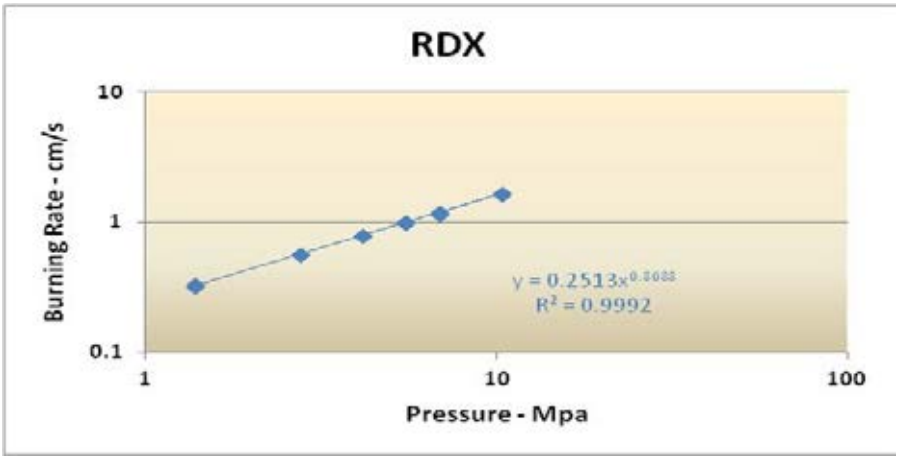

FIGURE C-30. Neat RDX Burning Rate Versus Pressure.

The burning rate versus pressure CompB and TNT data taken with the Window bomb are compared to neat RDX in Figure C-31. All of the CompB samples would burn at pressures as low as 1.38 MPa (200 psia) in this test. The addition of RDX to TNT appeared to increase the burning rate slightly, but not linearly with RDX addition. RDX burning rate data at higher pressures are needed to make a more compete comparison. No sample deconsolidation was observed in the conditions tested; however, irregular burning was again observed and at pressure below ~27.58 MPa (~4,000 psia) the periodicity, as observed in the neat TNT, was also seen. Small flamelets erupting from the surface of the propellant were observed in the CompB samples at pressures above ~27.58 MPa (~4,000 psia) as shown in Figure C-32.

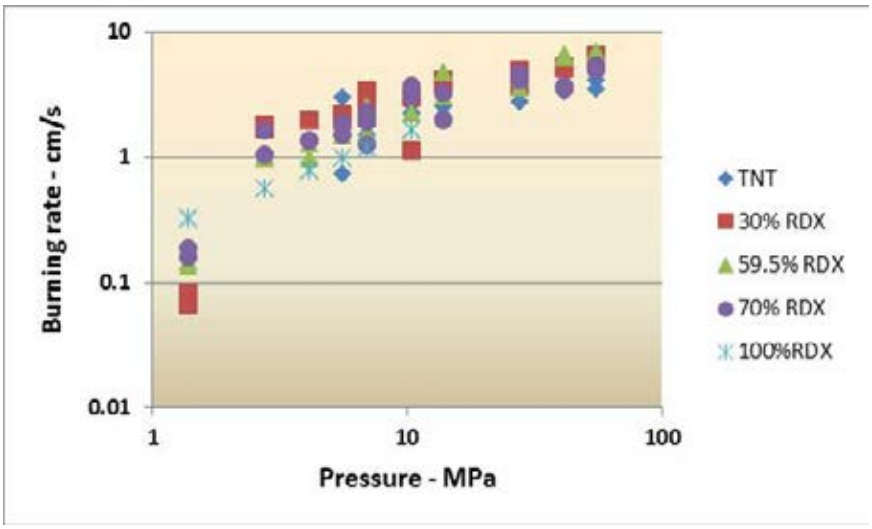

FIGURE C-31. A Comparison of RDX, CompB, and TNT Burning Rates.

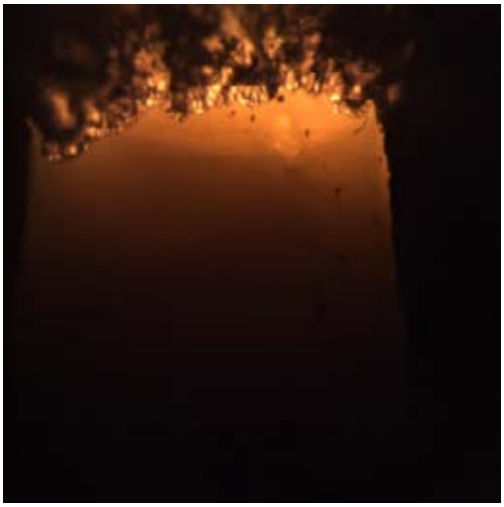

FIGURE C-32. Combustion of CompB at 55.17 MPa (8,000 psia).

A periodic shedding of plumes was observed at lower pressures in the CompB samples and at all of the pressures measured for TNT. A representative sequence of images is shown in Figure C-33 for TNT. A smoke cloud builds just above that surface as the burning surface regresses as seen in the dashed circle of $t=t_0$ and $t=t_0$ + 6 ms frames. Eventually, the cloud is observed to detach as seen in the dashed circle of $t=t_0$ + 12 ms and $t=t_0$ + 18 ms frame. The detachment process occurs at a regular frequency for each condition (e.g., pressure and sample composition). Although there were irregularities in the shapes of the burning surface and lifted plumes, the frequency of detachment was measured by recording the time of the first frame after the cloud was observed to lift off from the surface. A summary of these measurements is displayed in Table C-1.

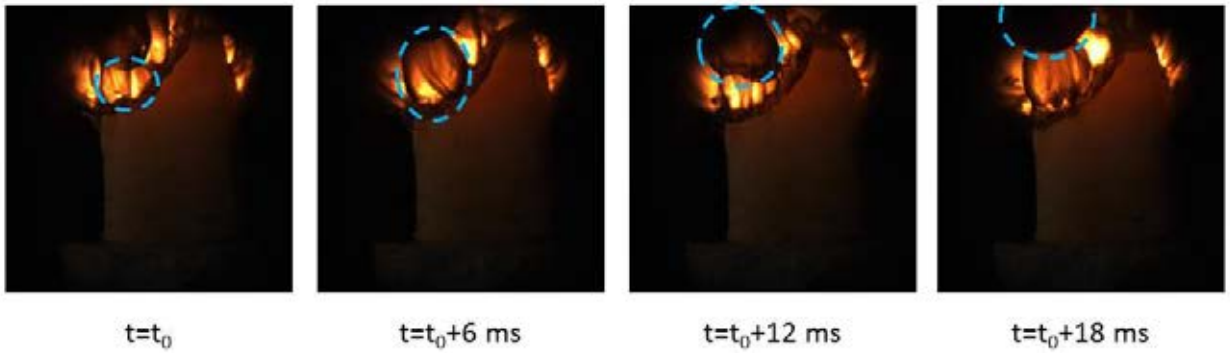

FIGURE C-33. Sequence of Images from Burning a 70% TNT/30% RDX Sample Under 800 psi. The blue circle highlights the formation and a detached cloud. The video was taken at a rate of 500 frames/sec.

TABLE C-1. Plume Detachment Frequency of TNT/RDX Samples.

RDX Content (%)	0	30	30	70	70
Pressure (psi)	1,500	800	1,500	800	1,500
Frequency (Hz)	58.3	57.4	80.4	47.2	70.3
Uncertainty (Hz)	12.9	7.3	14.1	7.4	13.5

A limited amount of tests were conducted and analyzed with this phenomenon; however, two trends were observed: (1) The measured frequency from the samples with 30 and 70% RDX decreased as pressure was lowered. (2) The size of the lifted cloud increased at the lower pressures, which made the phenomenon more evident at those pressures.

A comparison of photographic and closed bomb burning rates made for CompB is made in Figure C-34. The two techniques do not compare for this formulation in either the rate or pressure exponent.

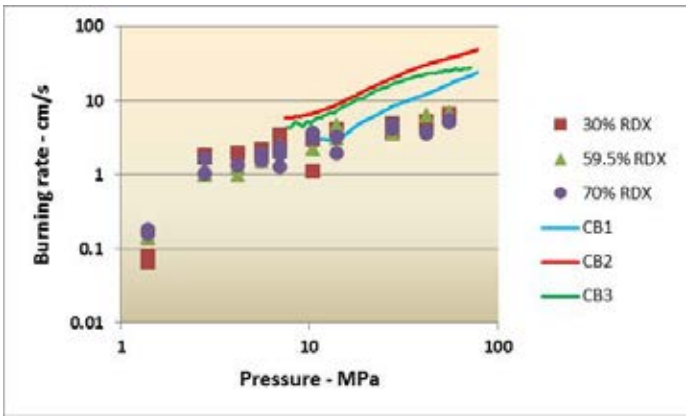

FIGURE C-34. A Comparison of Closed Bomb and Photographic Burning Rate Techniques.

CONCLUSIONS/RECOMMENDATIONS

A large variation in CompB burning rates was observed using three different burning rate measurement techniques: closed bomb, high pressure strand, and cinephotomicrography. The photographic technique allowed for the direct examination of the burning explosive. The CompB appeared to burn with a periodicity observed in neat TNT at low pressures and with small flamelet eruptions at higher pressures suggesting heterogeneous burning. The burning rate increase with addition of RDX was not linear and appeared to be dominated by the TNT in the formulation over the range of pressures tested.

The addition of RDX appears to have decreased the low pressure deflagration limit of the explosive as neat TNT would not self-deflagrate at pressures below 5.52 MPa (800 psia) nitrogen under the conditions of this study.

The variations in CompB burning have been observed by other investigators (References C-20 through C-22). Added scrutiny must be placed on the closed bomb results as the technique is not a direct measurement. Unlike previous investigators (Reference C-22), no distinct change regression rate (slope break) was observed in the closed bomb for the pressures tested in this study. The CompB burning observed in the photographic technique did indicate a change at about 27 MPa (4,000 psia) with the appearance of "flamelets," suggesting a change in the combustion mechanism. The observed irregular CompB burning can be explained as subsurface tunneling with RDX burning into the TNT matrix; as described by Birk, et al, (Reference C-22). The irregularity observed in the neat TNT may be due in part to the periodic burning (billowing).

Sample deconsolidation or breakup has been suggested as a possible cause of the differences seen in the high pressure LLNL strand and closed bomb data. The burning rate pressure exponent of the pressed pellets was higher than that of the melt cast (3.26 and 1.80, respectively), suggesting that the pressed formulation was not as rigid as the melt cast. The large amount of scatter together with the high burning rate pressure exponents of greater than unity is indicative of deconsolidation in both samples.

Sample deconsolidation was not observed for CompB with the photographic technique. Catastrophic deconsolidation does not appear to have occurred in the closed bomb as the burning rate exponents were lower than those observed with the high pressure strand technique but cannot be completely discarded.

RDX settling in the closed bomb samples may be a possible cause of the higher burning rates observed at the higher closed bomb pressures; however, the addition of up to 70% RDX in the photographic burning rate samples did not appreciably increase the rate. Higher pressure burning rate measurements of neat RDX should be made to compare to the neat TNT data.

A more careful examination of TNT thermochemistry should also be made. No TNT data were available in the BLAKE library, and it is not clear on the source of the data taken from PEP. Future plans call for additional examination of TNT thermochemistry used in the analysis of the closed bomb data. The thermochemistry differences do not explain the apparent sample to sample variation, but may explain some of the observed differences in burning rate pressure exponent.

REFERENCES

C-11. A. I. Atwood, I. Purifoy, and K. P. Ford, H. K. Springer. "Characterization of Explosive Brittle Fracture," *in Proceedings of the 2014 JANNAF Propulsion Systems Hazards Subcommittee Meeting, Albuquerque, New Mexico, 8-11 December 2014*, Columbia, Maryland, Chemical Propulsion Information Agency, 2011. Paper UNCLASSIFIED, publication UNCLASSIFIED.

C-12. George P. Sutton. *Rocket Propulsion Elements, An Introduction to the Engineering of Rockets*, John Wiley & Sons, 1986, 266 pp.

C-13. A. I. Atwood, K. P. Ford, and C. J. Wheeler. "High Pressure Burning Rate Studies of Solid Rocket Propellants," *in Proceedings of the 4th European Conference for Aerospace Sciences (EUCASS)*, St. Petersburg, Russia, 2011. Paper UNCLASSIFIED.

C-14. A. I. Atwood, K. P. Ford, D. T. Bui, P. O. Curran, and T. M. Lyle. "Assessment of Mechanically Induced Damage in Solid Energetic Materials," *Seventh International Symposium on Special Topics in Chemical Propulsion (7-ISICP) Advancements in Energetic Materials & Chemical Propulsion*, Kyoto, Japan, September 2007. (Also published in *International Journal of Energetic Materials and Chemical Propulsion*, Begell House, Redding, Connecticut, Vol. 8, No. 5, pp. 391-410, December 2009.) Publication UNCLASSIFIED.

C-15. Army Ballistic Research Laboratory. *BLAKE – A Thermodynamics Code Based on TIGER: User's Guide and Manual*, by E. Freedman. Aberdeen Proving Ground, Maryland, BRL, July 1982. (BRL-TR-02411, publication UNCLASSIFIED.)

C-16. Army Ballistic Research Laboratory. *A Versatile User-Oriented Closed Bomb Data Reduction Program (CBRED)*, by C.F. Price and A. Juhasz. Aberdeen Proving Ground, Maryland, BRL, September 1977. (BRL R2018, publication UNCLASSIFIED.)

C-17. Naval Weapons Center. *Theoretical Computations of Equilibrium Compositions, Thermodynamic Properties, and Performance Characteristics of Propellant Systems*, by D. R. Cruise. China Lake, California, NWC, November 1991. (NWC TP 6037, Revision 1, publication UNCLASSIFIED.)

C-18. E. A. Glascoe, P. C. Hsu, and H. K. Springer. "The Role and Importance of Porosity in the Deflagration of HMX-based Materials," *Proceedings for the JANNAF 26th Propulsion Systems Hazards Subcommittee, Crystal City, VA, April 2011*, Columbia, Maryland, Chemical Propulsion Information Agency, 2011. Paper UNCLASSIFIED, publication UNCLASSIFIED.

C-19. A. I. Atwood, T. L. Boggs, P. O. Curran, T. P. Parr, and D. M. Hanson-Parr. "Burning Rate of Solid Propellant Ingredients, Part 1: Pressure and Initial Temperature Effects," *Journal of Propulsion and Power*, Volume 15, Number 6, November-December 1999. Publication UNCLASSIFIED.

C-20. U.S. Army Armament Research and Development Command. "A Method to Evaluate the Burning Behavior of Secondary Explosives – Composition B," by R. W. Velicky. Dover, New Jersey, ARLDC, June 1983. (ARLDC-TR-83030, publication UNCLASSIFIED.)

C-21. R. W. Velicky and J. Hershkowitz. "Anomalous Burning Rate Characteristics of Composition B and TNT," *Seventh Symposium (International) on Detonation*, 1981. Paper UNCLASSIFIED.

C-22. A. Birk, P. Baker, D. E. Kooker, R. Lieb, S. Stegall, and J. Delaney. "Nondetonative Explosions and Burning of Composition-B Explosive," *2002 Symposium (International) on Detonation*. Paper UNCLASSIFIED.

INITIAL DISTRIBUTION

1 Defense Technical Information Center, Fort Belvoir, VA
4 Lawrence Livermore National Laboratory, Livermore, CA
Reaugh, J. (2)
Springer, H. K. (2)

ON-SITE DISTRIBUTION

2 Code 4G0000D (Scientific and Technical Library Branch, archive copies)
2 Code 4G0000D (Technical Communication Office, file copies)
10 Code 474200D
Atwood, A. (2)
Kalman, J. (2)
Purifoy, I. (2)
Wheeler, C. (2)
Woods, E. (2)